2008

Mesoporous Nb and Ta Oxides: Synthesis, Characterization and Applications in Heterogeneous Acid Catalysis

Yuxiang (Tony) Rao
University of Windsor

Mesoporous Nb and Ta Oxides: Synthesis, Characterization and Applications in Heterogeneous Acid Catalysis

By

Yuxiang(Tony) Rao

A Dissertation
Submitted to the Faculty of Graduate Studies through the Department of Chemistry and Biochemistry in Partial Fulfillment of the Requirements for the Degree of Doctor of Philosophy at the
University of Windsor

Windsor, Ontario, Canada

2008

Your file Votre référence
ISBN: 978-0-494-82072-8
Our file Notre référence
ISBN: 978-0-494-82072-8

Declaration of Co-Authorship / Previous Publication

I. Co-Authorship Declaration

I hereby declare that this thesis incorporates material that is result of joint research, as follows:

This thesis incorporates the outcome of a joint research undertaken in collaboration with Tom F. Kemp and Professor Mark E. Smith at University of Warwick related to ^{17}O and ^{93}Nb solid-state NMR studies in Chapter 2 and Chapter 8. This thesis also incorporates the work undertaken in collaboration with Dr. Michel Trudeau at Hydro-Quebec Research Institute related to research in TEM, SEM studies. The collaboration research work with Dr. Boris O. Skadtchenko and Dr. Junjie Kang under the supervision of Professor David M. Antonelli is covered in Chapter 2 and Chapter 4 of the thesis. In all cases, the key ideas, primary contributions, experimental designs, data analysis and interpretation, were performed by the author.

I am aware of the University of Windsor Senate Policy on Authorship and I certify that I have properly acknowledged the contribution of other researchers to my thesis, and have obtained written permission from each of the co-author(s) to include the above material(s) in my thesis.

I certify that, with the above qualification, this thesis, and the research to which it refers, is the product of my own work.

II. Declaration of Previous Publication

This thesis includes 7 original papers that have been previously published/submitted for publication in peer-reviewed journals, as follows:

Thesis Chapter	Publication title/full citation	Publication status
Chapter 2	A Solid-State ^{17}O NMR study of Local Order and Crystallinity in Amine-Templated Mesoporous Nb Oxide, *Angewandte Chemie International Edition*, **2007**, *46*, 2635-2638	*Published*
Chapter 3	Sulfated and Phosphated Mesoporous Nb Oxide in the Benzylation of Anisole and Toluene by Benzyl Alcohol, *Journal of the American Chemistry Society*, **2006**, *128*, 13996-13997	*Published*
Chapter 4	Sulfated Mesoporous Tantalum Oxides in the Shape Selective Synthesis of Linear Alkyl Benzen, *Angewandte. Chemie. International. Edition.* **2008**, *47*, 4896-4899	*Published*
Chapter 5	1-Hexene Isomerization over Sulfated Mesoporous Ta Oxide: The Effects of Active Site and Confinement, *Journal of the American Chemistry Society*, **2008**, *130*, 394-395	*Published*
Chapter 6	Investigation of the catalytic activities of sulfated mesoporous Nb and Ta oxides in 1-hexene isomerization, *Journal of Materials Chemistry*, **2008**	*Submitted for publication*
Chapter 7	Mesoporous transition metal oxides: applications in heterogeneous catalysis, *Journal of Materials Chemistry*, **2008**	*Submitted for publication*
Chapter 8	^{17}O and ^{15}N Solid State NMR Studies on Ligand-Assisted Templating and Oxygen Coordination in the Walls of Mesoporous Nb, Ta and Ti Oxides, *Journal of the American Chemistry Society*, **2008**	*published*

I certify that I have obtained a written permission from the copyright owner(s) to include the above-published material(s) in my thesis. I certify that the above material describes work completed during my registration as a graduate student at the University of Windsor.

I declare that, to the best of my knowledge, my thesis does not infringe upon anyone's copyright nor violate any proprietary rights and that any ideas, techniques, quotations, or any other material from the work of other people included in my thesis, published or otherwise, are fully acknowledged in accordance with the standard referencing practices. Furthermore, to the extent that I have included copyrighted material

that surpasses the bounds of fair dealing within the meaning of the Canada Copyright Act, I certify that I have obtained a written permission from the copyright owner(s) to include such material(s) in my thesis.

I declare that this is a true copy of my thesis, including any final revisions, as approved by my thesis committee and the Graduate Studies Office, and that this thesis has not been submitted for a higher degree to any other University of Institution.

ABSTRACT

In this work, a series of mesoporous Niobium and Tantalum oxides with different pore sizes (C_6, C_{12}, C_{18}, ranging from 12Å to 30 Å) were synthesized using the ligand-assisted templating approach and investigated for their activities in a wide range of catalytic applications including benzylation, alkylation and isomerization. The as-synthesized mesoporous materials were characterized by nitrogen adsorption, powder X-ray diffraction, transmission electron microscopy (TEM), scanning electron microscopy (SEM), thermo gravimetric analysis (TGA), differential scanning calorimetry (DSC), and solid-state Nuclear magnetic resonance (NMR) techniques.

In order to probe into the structural and coordination geometry of mesoporous Nb oxide and in efforts to make meaningful comparisons of mesoporous niobia prepared by the amine-templating method with the corresponding bulk sol-gel prepared Nb_2O_5 phase, ^{17}O magic-angle-spinning solid-state NMR studies were conducted. The results showed a very high local order in the mesoporous sample. The oxygen atoms are coordinated only as ONb_2 in contrast with bulk phases in which the oxygen atoms are always present in a mixture of ONb_2 and ONb_3 coordination environments.

To enhance their surface acidities and thus improve their performance as solid acid catalysts in the acid-catalyzed reactions mentioned above, pure mesoporous Nb and Ta oxides were further treated with 1M sulfuric acid or phosphoric acid. Their surface acidities before and after acid treatment were measured by Fourier transform infraRed (FT-IR), amine titration and temperature programmed desorption of ammonia (NH_3-TPD).

Results obtained in this study showed that sulfated mesoporous Nb and Ta oxides

materials possess relative high surface areas (up to 612 m^2/g) and amorphous wormhole structure. These mesoporous structures are thus quite stable to acid treatment. It was also found that Brønsted (1540 cm^{-1}) and Lewis (1450 cm^{-1}) acid sites coexist in a roughly 50:50 mixture on the surfaces of the parent pristine materials. However, the acid-treated Nb and Ta materials both exhibited a strong dominance of Brønsted acid sites, which is believed to be responsible for their higher catalytic activities with respect to the untreated materials.

Although Ta samples (C_6, C_{12}, C_{18}) have relatively lower surface areas than the Nb samples, they always show much higher catalytic activity as well as selectivity. For instance, in the isomerization of 1-hexene and alkylation of benzene with bulky olefins, the best results were achieved using C_{12} H_2SO_4 mesoporous Ta oxide, which has a BET surface area of 292.19 m^2/g, far less than its sulfated C_{12} Nb counterpart (413.97 m^2/g). This demonstrates that the catalytic performance of these materials does not only depend on their surface areas, but is also influenced by the pore size and surface acidity. To investigate this unusual phenomenon, ammonia TPD was used to precisely measure the surface acidities of the Nb and Ta samples and show that the Ta materials have a much greater concentration of Brønsted acid sites than the Nb materials. This explains the observed higher activities.

ACKNOWLEDGEMENTS

First of all, I would like to express my sincere appreciation to my supervisor Dr. David M. Antonelli for his academic and generous financial support, guidance, encouragement and help during the course of my Ph.D. study.

I am extremely grateful to Dr. Michel Trudeau for his collaboration work on the TEM and SEM analysis of samples. Dr. Mark Smith and Mr. Thomas Kemp are acknowledged for their help with solid-state NMR experiments. Dr. S.H. Eichhorn is thanked for his great assistant in X-Ray powder diffraction measurement and thermal analysis including TG-DTA and DSC. I also would like to thank Dr. James Green for his suggestion and assistance on setting up and operating the gas chromatograph.

Many thanks are given to my committee member Dr. Jichang Wang, Dr. Derek Northwood for their valuable advice and discussion of the results. In addition, I would like to thank other past and present members of our group: Dr. Boris Skadtchenko, Dr. Longhui Qiu, Dr. Junjie Kang, Dr. Xin Hu, Mr. Chaoyang Yue, Mr. Ahmad Hamaed and Mr. Tuan Hoang for their advice and making my graduate years enjoyable and memorable.

Finally, last but not least, my deep gratitude and appreciation go to my wife Mrs.Lu Wang, my parents and other family members for their constant love, encouragement and forever support throughout my life.

TABLE OF CONTENTS

Chapter 9 Conclusion and Future Work

LIST OF TABLES

Table **Description** **Page**

LIST OF FIGURES

Figure **Description** **Page**

LIST OF SCHEMES

Scheme **Description** **Page**

LIST OF ABBREVIATIONS AND SYMBOLS

Three-Dimensionally Ordered Macroporous 3DOM

Brunauer-Emmett-Teller ..... BET

Barret-Joyner-Halenda ..... BJH

Density Functional Theory ..... DFT

Differential Scanning Calorimetry ..... DSC

Differential Thermal Analysis ..... DTA

Elemental Analysis ..... EA

Fourier Transform Infra-Red Spectroscopy ..... FT-IR

Folded Sheets Mesoporous Silica ..... FSM

Family of Silica Based Mesoporous Materials M41S

Gas Chromatography-Mass Spectrometry ..... GC-MS

Horvath-Kowazoe ..... HK

High-Resolution Transmission Electron Microscopy ..... HRTEM

International Union of Pure and Applied Chemistry ..... IUPAC

Linear alkylbenzenes ..... LAB

Ligand Assisted Template ..... LAT

Liquid Crystal Template ..... LCT

Magic-Angle-Spinning ..... MAS

Mobil Composition of Matter-41, Hexagonal Mesoporous Phase MCM-41

Mobil Composition of Matter-48, Cubic Mesoporous Phase MCM-48

Mobil Composition of Matter-50, Lamellar Mesoporous Phase MCM-50

Michigan State University Material ..... MSU

Mesoporous Niobium Oxide Nb-TMS1

Mesoporous Tantalum Oxide Ta-TMS1

Mesoporous Titanium Oxide Ti-TMS1

Mesoporous Transition Metal Oxides ..... TMS

Mesoporous Nb Oxide Synthesized by Hexylamine Template ..... C6 Nb

Mesoporous Nb Oxide Synthesized by Dodecylamine Template ..... C12 Nb

Mesoporous Nb Oxide Synthesized by Octadecylamine Template ..... C18 Nb

Mesoporous Ta Oxide Synthesized by Hexylamine Template ..... C6 Ta

Mesoporous Ta Oxide Synthesized by Dodecylamine Template ..... C12 Ta

Mesoporous Ta Oxide Synthesized by Octadecylamine Template ..... C18 Ta

Nuclear Magnetic Resonance ..... NMR

Powder X-ray Diffraction ..... PXRD

Periodic Mesoporous Organosilicas ..... PMOs

Rotor Assisted Population Transfer ..... RAPT

Rotational-Echo Adiabatic Passage Double Resonance ..... REAPDOR

Structure-Directing Agent ..... SDA

Scanning Electron Microscopy ..... SEM

Strong Metal-Support Interaction ..... SMSI

Thermogravimetric Analysis ..... TGA

Temperature Programmed Desorption ..... TPD

Temperature Programmed Reduction ..... TPR

Ultraviolet-Visible Spectrophotometry ..... UV/ Vis

X-ray Absorption Near-Edge Structure ..... XANES

X-ray Photoelectron Spectroscopy ..... XPS

Asymmetry Parameter ..... η

Acid Strength ..... Ho

Absolute Temperature ..... T

Actual Vapor Pressure ..... P

Brønsted-Acid Site ..... B

Equilibrium Constant ..... K_{eq}

Gas Constant ..... R

Isotropic Chemical Shift ..... δ_{iso}

Lewis-Acid Site L

Molar Volume ..... Vm

Quadrupole Coupling Constant ..... χ_Q

Radius of the Droplet ..... r

Standard Gibbs Energy Change of Reaction ..... ΔG_Θ

Saturated Vapor Pressure ..... P_0

Surface Tension ..... γ

Chapter 1

Introduction

1.1 Brief Overview of Porous Materials.

Porous materials are defined as solids possessing cavities, channels or interstices and have been intensively studied with regard to technical applications as catalysts, catalyst supports, sorption and separation [1,2]. According to the IUPAC (International Union of Pure and Applied Chemistry) definition [3], porous materials are divided into three class; microporous (pore size < 2nm), mesoporous (pore size in the range of 2~50nm), and macroporous (> 50nm).

Examples of porous materials include zeolites, zeotypes, activated carbon (microporus), aerogels, pillared layered clays, M41S (mesoporous) and glass (macroporous) [4]. Among the family of microporous materials, the best-known members are zeolites, which have a narrow and uniform micropore size distribution due to their crystallographically defined pore system. Zeolites are the most widely used catalysts in

industry for oil refining, petrochemistry, and organic synthesis for the production of fine and specialty chemicals, particularly when dealing with molecules having kinetic diameters below 10 Å [5]. The reason for their success in catalysis is related to their very high surface area, high thermal and hydrothermal stability, high and controllable adsorption capacity, and well-defined pore structure.

Despite these catalytically desirable properties of zeolites they are ineffective using reactants with sizes above the dimensions of the pores in applications. The rational approach to overcome such a limitation is to maintain the porous structure, which is responsible for the benefits described above, but to increase its diameter into the mesoporous region. Unfortunately, their ring structure has prevented zeolites from expanding beyond the 15 Å thresholds.

Periodic mesoporous silicates (MS41) were first synthesized by Mobil scientists in 1992 [6,7]. These mesoporous (alumino) silicate materials, possess well-defined pore sizes of 15~100 Å and thus break past the pore-size constraint (<15 Å) of microporous zeolites. The extremely high surface areas (>1000m^2/g, up to 1600 m^2/g) and precise tuning of pore sizes are among the many desirable properties that have made these materials the focus of much research. In the family of MS41 mesoporous silicates, three sub-categories have been classified: MCM-41, MCM-48, and MCM-50 (Figure 1.1). The first two phases are stable to template removal, while MCM-50 collapses on calcination. MCM-41 features a hexagonally packed array of unidimensional pore, while MCM-48 possesses a structure with three-dimensional pore architecture. MCM-50 has a lamellar mesostructure in the non-calcined form, but removal of the mesoporous pillared layers appeared on the removal of the surfactant causes the layers to collapse.

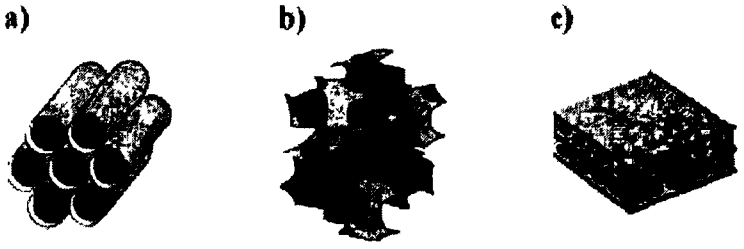

Figure 1.1 Illustrations of mesoporous M41S materials: a) MCM-41, b) MCM-48, and c) MCM-50 [8]

MCM-41-type mesoporous materials are of great interest to scientists due to their unique physical properties such as large pore size and surface area over volume, and long range ordering of the pore structure. Such properties are important in a large number of industrial and environmental applications such as heterogeneous catalysts, gas sorption, selective absorption of heavy metal ions [6].

Periodic three-dimensional macroporous samples (3DOM) titania, zirconia, and alumina samples with narrow macropore size distribution have also been fabricated using latex spheres as templates [9,10,11] instead of conventional methods involving mixing metal oxide particles with some type of binder. This is because by using the latter method, it is difficult to control the shape of the pore and thus broad pore size distribution and low porosity are frequently encountered. These novel macroporous metal oxides can be used as filtration and separation materials [12,13], catalyst supports [14], carriers for cell immobilization [15], battery materials [16], and thermal insulators [17].

1.2 Synthesis of ordered mesoporous materials

The discovery of ordered mesoporous solids of the MCM-41 type and related materials in the early 1990s was a breakthrough in materials engineering [6,7], and since then there has been great progress in the development of many new mesoporous solids based on the templating mechanisms used for the original MCM-41 synthesis. In general, the presence of self-assembled surfactant micelles in a solution is necessary to guide the formation of the inorganic mesostructure from the solubilized inorganic precursors (Scheme 1.1).

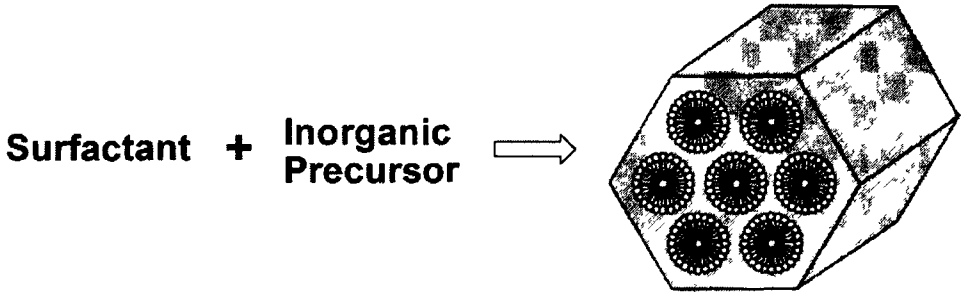

Scheme 1.1 Schematic representation of the general formation of MCM-41 from inorganic precursors and organic surfactants. [4]

Depending on the synthesis conditions, the silica source or the type of template surfactant used for synthesis, the interaction of the inorganic species with the organic template molecules, the synthesis of mesoporous materials can be classified into the following pathways (Table 1.1).

Table 1.1 Possible pathways for the synthesis of mesoporous materials [18].

Template	Interaction		Synthesis Condition	Examples
Ionic Surfactant	Ionic Bond (Direct)	I^-S^+ I^+S^-	Basic Neutral-basic	M41S, FSM-16 Aluminum oxides, AMS
	Ionic Bond (Intermediated)	$I^+X^-S^+$ $I^-X^+S^-$	Acidic Basic	SBA-1 (2,3), HMS, TLCT Aluminum, Zinc oxides
Non-Ionic Surfactant	Hydrogen Bond	I^0S^0	Acidic	HMS, MSU, SBA-15, TLCT
	Covalent Bond	I--S	Neutral-acidic	Nb-TMS, Ta-TMS

(S = Surfactant, I = Inorganic species, X = counter ions)

The first ordered mesoporous silica and aluminosilicate materials were introduced by the Mobil research group by using an ionic surfactant template in basic conditions and an ionic assembly mechanism schematically represented as I^-S^+ [6,7]. The formation of the inorganic-organic composite is based on electrostatic interactions between the positively charged surfactants and the negatively charged silicate species in solution. This mechanism was further extended by Stucky and co-workers to a whole series of electrostatic assembly mechanisms, including reversed S^-I^+ and counter-ion mediated $I^+X^-S^+$ and $I^-X^+S^-$ pathways [19,20,21,22,23,24].

Pinnavaia et al introduced the non-ionic surfactant method for the synthesis of mesoporous materials by using neutral surfactants. This method is mainly based on hydrogen bonding and self-assembly of non-ionic primary amines such as hexadecyl

amine or polyethylene oxide (EO) surfactants with neutral oligomeric silica precursors S^0I^0 to prepare HMS (hexagonal mesoporous silica) [25,26] and MSU (Michigan State University material) [27], respectively. The pore systems of the latter silicas have been shown to have wormhole structures rather than long-range ordered hexagonal arrays, which are characteristic for MCM-41 [28,29]. Hydrogen bonding is thought to be the driving force for the formation of the mesophases in this case. Because of this, the surfactant can be recovered by extraction instead of calcination, which is advantageous both from an economical and an environmental point of view.

Later, Stucky and co-workers introduced a new synthesis route involving amphiphilic di- and tri-block copolymers as organic structure directing agents [30,31,32,33] These materials, exemplified by hexagonal (p6mm) SBA-15, have long range order, large monodispersed mesopores (up to 50nm) and thicker walls (3~9 nm) which make them more thermally and hydrothermally stable than the previous materials, although the surface areas are usually less than 100 m^2/g. Also, due to the very weak interactions between polypropylene oxide (PO) block copolymers and the inorganic surface, it is easier to remove the surfactant from the composite than in the case of ionic surfactants. For example, the decomposition temperature of $PEO_{20}PPO_{70}PEO_{20}$ (Pluronic 123) is 270 °C, this temperature is much lower compared with that of cationic surfactants around 360 °C.

1.2.1 Mesoporous Silica Based Materials (M41S)

The preparation of M41S materials involves an ionic surfactant, best exemplified by cetyltrimethyl ammonium bromide (CTAB), as a structure directing agent. For example,

Aluminosilicate M41S was synthesized by the addition of an aluminum source to the synthesis mixture. The mixture was aged at elevated temperatures (≥ 100°C) for 24 to 144 hours, which resulted in a solid precipitate. The organic-inorganic mesostructured product was filtered, washed with water, and air-dried. The product was calcined at about 500°C under flowing air to burn off the surfactant, yielding the mesoporous material. A liquid crystal templating mechanism (LCT) in which surfactant liquid crystal structures serve as organic templates has been proposed for the formation of these materials. The negatively charged inorganic components first interact with the positively charged ammonium head groups of the surfactants and then condensed into a solid, continuous framework. The as-synthesized organic-inorganic mesostructure can be viewed as a hexagonal array of surfactant micellar rods embedded into a silica matrix. Finally, the surfactants need to be removed by calcinations at high temperature to produce the mesoporous MCM-41 framework. (Scheme 1.2)

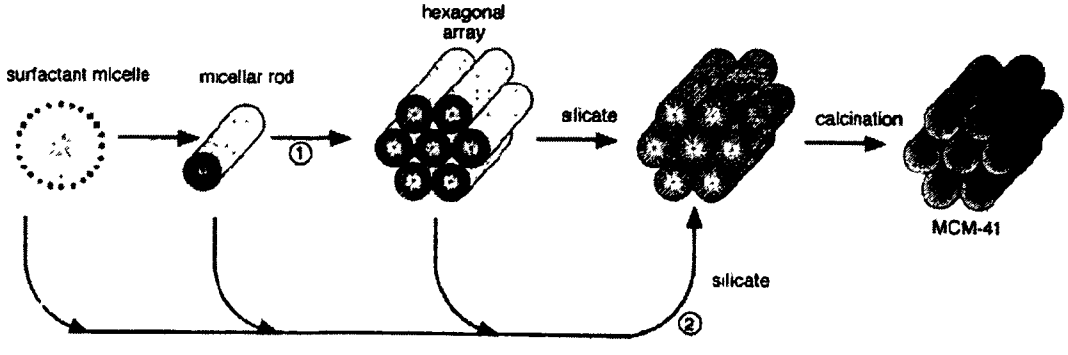

Scheme 1.2 Possible mechanistic pathways for the formation of MCM-41: (1) liquid crystal initiated and (2) silicate anion initiated [6,7]

It was also observed that the surfactant to silica ratio has a substantial impact on the

composite structure obtained. This is given in the following table (Table 1.2).

Table 1.2 Mesophase and their type [34].

Name	Mesophase	Parameter
MCM-41	Hexagonal	[Surfactant/Silica]<1
MCM-48	Cubic	[Surfactant/Silica]= 1~1.5
MCM-50	Lamellar	[Surfactant/Silica]= 1.5~2

It is worth to mention here that the pore sizes (or interlayer distances) of M41S materials are easily adjustable from ca. 20 to about 100Å. This can be achieved in three different ways: (i) by changing the length of the alkyl chain of the surfactant molecule [6,7], (ii) by adding swelling agents such as 1,3,5-trimethylbenzene [6,7,35] which dissolve in the hydrophobic region of the micelles, thus increasing their size, or (iii) by aging a sample prepared at low temperature (e.g., 70 °C) in its mother liquor at higher temperature (e.g., 150 °C) for different periods of time [36].

1.2.2 Mesoporous non-siliceous ordered mesoporous materials

Since the discovery of silica or aluminumsilicate ordered mesoporous materials FSM-16 [37] and MCM-41 [6] in 1992, much work has been devoted to the study of the synthesis, properties, and possible uses of such materials. These topics are covered in several comprehensive recent reviews [4,5,38]. In 1993, it was suggested that it should be possible to synthesize non-siliceous materials following similar pathways mechanism [39]. In the following year, Stucky and co-workers reported the first examples of mesostructured non-siliceous metal oxides, such as oxides of Sb, Fe, Zn, Pb, W and Mo

[40,41] through a generalized electrostatic approach. However, for these materials it was not possible to remove the template without structure collapse and thus only mesostructured, but not mesoporous materials, could be obtained. This was due to the lack of complete condensation of the inorganic framework.

Compared to stable silica and aluminum silicates, non-siliceous compositions are often more susceptible to hydrolysis, redox reactions or phase transitions accompanied by thermal breakdown of the mesostructure, making it much more difficult to remove the templates and create porous materials from these substance. However, if this problem can be resolved, the potential of the non-silica compositions seems to be higher than that of the classical silica MCM-41, FSM-16 or SBA-15, especially for transition metal oxides since they have variable oxidation states and higher surface acidity, which gives them potential in catalysis.

The first successful examples of stable mesoporous non-siliceous frameworks were provided by Antonelli et al. in the case of Nb oxide [42, 43], from which rapid development ensued. The synthesis was achieved via the condensation of an organometallic precursor in which the propagating niobium alkoxide moiety is chemically linked through an Nb-N covalent bond to a long-chain amine surfactant molecule. As depicted in Scheme 1.3, the initial reaction between the amine and $Nb(OEt)_5$ was conducted in the absence of water to ensure that a covalent bond between the Nb and the surfactant is formed prior to condensation of the inorganic species. The resultant complex was then allowed to hydrolyze and condense in the present of water, leading to a thermally stable, hexagonally packed mesoporous niobium oxide (denoted Nb-TMS1).

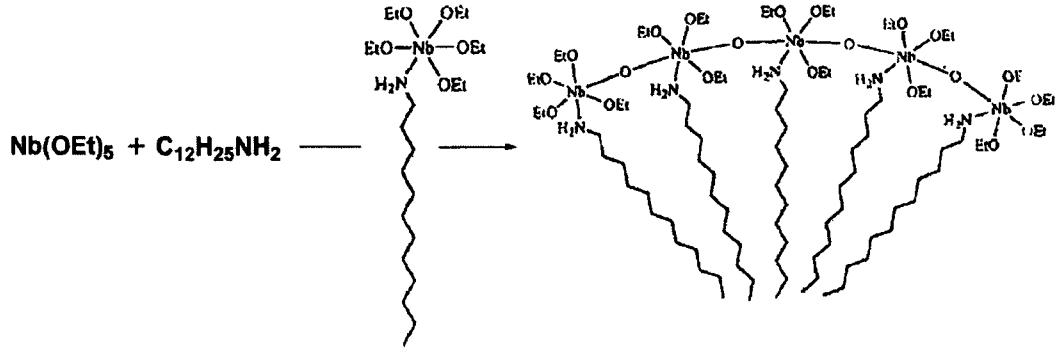

Scheme 1.3 Schematic representations of possible pathways for the synthesis of mesostructured niobium oxide under a ligand-assisted templating mechanism [43].

However, the field of non-siliceous ordered mesoporous materials has garnered considerably less attention as compared to that of mesostructured silica, and only few reviews are available which focus exclusively on non-siliceous materials [44,45]. The main reason for that is because mesoporous transition metal oxides are considered more exotic and are somewhat less thermally stable than M41S materials [46,47,48].

Although non-siliceous ordered mesoporous materials have some drawbacks as stated above, the extension of MCM-41-like structures into the realm of pure transition metal oxides still represents an important development from both the catalytic and electronic standpoints, because the variable oxidation states of transition metal oxides are useful in tailoring their catalytic, conductive, and magnetic properties.

1.3 Characterization of Mesoporous Molecular Sieves

The main techniques used for the characterization of mesoporous materials are Physical gas adsorption, Powder X-ray diffraction (PXRD), ^{27}Al, ^{29}Si and ^{17}O MAS NMR,

transmission electron microscopy (TEM), Scanning Electron Microscopy (SEM), infrared spectroscopy of adsorbed pyridine and temperature-programmed desorption (TPD) of ammonia.

1.3.1 Physical gas adsorption

When a gas comes into contact with a solid surface, molecules of the gas will adsorb to the surface in quantities that are a function of the partial pressure of the gas over the solid. The measurement of the amount of gas adsorbed over a range of partial pressure at a single temperature results in a graph known as an adsorption isotherm. These isotherms can have very different shapes depending on the type of adsorbents and adsorbate, and intermolecular interactions between the gas and the surface. The first systematic attempt to interpret adsorption isotherms for gas-solid equilibria was introduced by Brunauer, Deming, Deming, and Teller (BDDT) in 1940 [49]. These authors classified isotherms into five types. These BDDT isotherms and an additional one introduced much later by Sing has become the core of the modern IUPAC classification of adsorption isotherms and illustrated in Figure 1.2

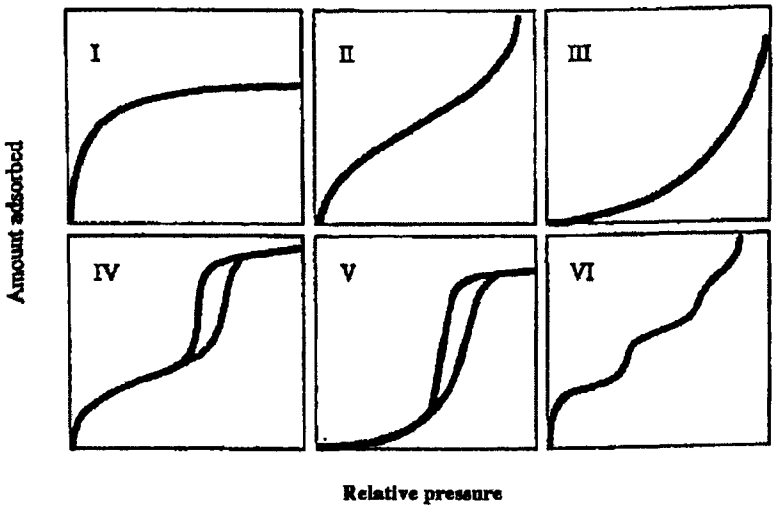

Figure 1.2 The IUPAC classification for adsorption isotherms

Type I isotherms characterize microporous adsorbents. Type II and III describe adsorption on macroporus adsorbents with strong and weak adsorbate-adsorbent interactions, respectively. Type IV and V represent adsorption isotherms with hysteresis, which is the characteristic of mesoporous adsorbents with strong and weak affinities, respectively. Finally, type VI has steps, and only occurs in rare idealized cases.

The physical gas adsorption technique also accurately determines the amount of gas adsorbed on a solid material, which is a direct measure for the porous properties and structure. In addition, this technique is relatively fast and is accomplished with a relative ease of operation of the equipment. The isotherm obtained from these adsorption measurements provides information on the surface area, pore volume, and pore size distribution [50,51,52]. Different probe gases including N_2, Ar, and CO_2 are frequently used as adsorptives, depending on the nature of the material (adsorbent) and the information required. N_2 adsorption at 77 K and at sub-atmospheric pressures has

remained pre-eminent and can be used for routine quality control, as well as for investigation of new materials. If applied over a wide range of relative pressures (P/P_0), N_2 adsorption isotherms provide information on size distributions in the micro-, meso- and macroporosity range (approximately 0.5~200 nm). The Kelvin equation is widely used for determination of pore size distribution of a porous medium using adsorption porosimetry, especially for materials in micropore range (<2nm). The Kelvin equation may be written in the form

$$\ln\frac{p}{p_0} = \frac{2\gamma V_m}{rRT}$$

Where P is the actual vapor pressure, P_0 is the saturated vapor pressure, γ is the surface tension, Vm is the molar volume, R is the universal gas constant, r is the radius of the droplet, and T is temperature. The classical pore size model developed by Barret, Joyner and Halenda (BJH) in 1951, which is based on the Kelvin equation and corrected for multilayer adsorption, is most widely used for calculations of the pore size distribution over the mesopore and part of the macropore range [53].

Barret-Joyner-Halenda scheme for calculation of mesopore distribution from nitrogen adsorption data may be summarized in the formula:

$$v_{ads}(x_k) = \sum_{i=1}^{k} \Delta V_i(r_i \le r_c(x_k)) + \sum_{i=k+1}^{n} \Delta S_i t_i(r_i > r_c(x_k))$$

In this formula, $v_{ads}(x_k)$ is the volume of (liquid) adsorbate [cm^3/g] at relative pressure x_k (calculated from the value of adsorption expressed in [cm^3/g STP] by $v_{ads}(x) = 0.0015468$

a(x)), pore volume V is given in [cm^3/g], S is surface area [m^2/g] and t is the thickness of adsorbed layer (in appropriate units). This formula says, that the adsorbed amount at k-th point of adsorption isotherm may be divided into 2 distinct parts:

1st is a volume in condensate in all pores smaller than some characteristic size depending on current relative pressure, $r_c(x_k)$

2nd is a volume of adsorbed film on all larger pores, calculated a sum of terms: Σ (pore surface) (thickness of film in pore).

1.3.2 Powder X-ray Diffraction

The Bragg formulation of X-ray diffraction (also referred to as Bragg diffraction) was first proposed by William Lawrence Bragg and William Henry Bragg in 1913 in response to their discovery that crystalline solids produced surprising patterns of reflected X-rays. They found that in these crystals, for certain specific wavelengths and incident angles, intense peaks of reflected radiation (known as Bragg peaks) were produced. Bragg's law can be expressed by

$$n\lambda = 2d\sin\theta$$

Where

- n is an integer determined by the order given
- λ is the wavelength of x-rays, and moving electrons, protons and neutrons
- d is the spacing between the planes in the atomic lattice
- θ is the angle between the incident ray and the scattering planes

PXRD patterns of mesoporous phases are dominated by a limited number of low angle peaks, which can be indexed to a specific crystalline phase. (Figure 1.3) HMS,

MSU-n and some"MCM-41" silicates exhibit only the (100) peak either because of too small scattering domain sizes or poorly ordered pore systems.

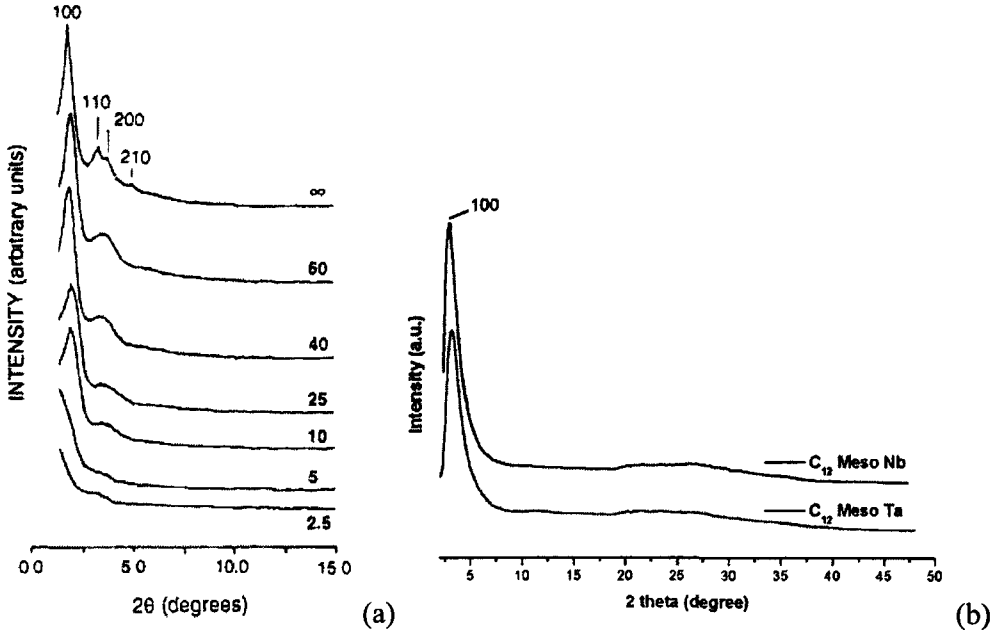

Figure 1.3 X-ray diffraction patterns of Al-MCM-41 samples(a) and Mesoporous Nb and Ta samples (b) [54]. The numbers on the right-hand side indicate the Si/Al ratios.

1.3.3 ^{27}Al, ^{29}Si and ^{17}O MAS NMR

^{27}Al and ^{29} Si MAS NMR is by far the most widely used technique to distinguish between "framework" and extraframework aluminum and silica. Luan et al. [54] studied a series of non-calcined samples with Si/Al ratios in the range 2.5-60 prepared using aluminum sulfate. They found a linear relationship between the absolute intensity of the ^{27}Al NMR peak and the Al content. ^{17}O MAS NMR was less popular than ^{27}Al and ^{29} Si MAS NMR. However, its large chemical shift has high sensitivity to even subtle difference in the structure in both amorphous and crystalline solids [55,56]. Recently, our group reported

the application of ^{17}O NMR in exploring the degree of local ordering in atomic-scale structure and crystallinity in amine-templated mesoporous Nb oxide [57].

1.3.4 TEM and SEM

Transmission electron microscopy (TEM) is an imaging technique whereby a beam of electrons is transmitted through a specimen, then an image is formed, magnified and directed to appear either on a fluorescent screen or layer of photographic film, or to be detected by a sensor such as a CCD camera. The first practical transmission electron microscope was built by Albert Prebus and James Hillier at the University of Toronto in 1938 using concepts developed earlier by Max Knoll and Ernst Ruska.

The TEM is used heavily in both material science/metallurgy and the biological sciences. In both cases the specimens must be very thin and able to withstand the high vacuum present inside the instrument. The HRTEM (High Resolution Transmission electron microscopy) technique allows the direct observation of crystal structure and therefore has an advantage over other methods in that there is no displacement between the location of a defect and the contrast variation caused in the image. However, it is not always possible to interpret the lattice images directly in terms of sample structure or composition. This is because the image is sensitive to a number of factors (specimen thickness and orientation, objective lens defocus, spherical and chromatic aberration), and although quantitative interpretation of the contrast shown in lattice images is possible, it is inherently complicated and may require extensive simulation of the images. The ability to determine the positions of atoms within materials has made the HRTEM an indispensable tool for nanotechnology research and development in many fields,

including heterogeneous catalysis and the development of semiconductor devices for electronics and photonics.

There are a number of drawbacks to the TEM technique. Many materials require extensive sample preparation to produce a sample thin enough to be electron transparent, which makes TEM analysis a relatively time consuming process with a low throughput of samples. The structure of the sample may also be changed during the preparation process. Also the field of view is relatively small, raising the possibility that the region analyzed may not be characteristic of the whole sample. There is potential that the sample may be damaged by the electron beam, particularly in the case of biological materials.

The scanning electron microscope (SEM) is a type of electron microscope capable of producing high-resolution images of a sample surface by scanning an electron beam over the surface of an object and measures how many electrons are scattered back. Due to the manner in which the image is created, SEM images have a characteristic three-dimensional appearance and are useful for judging the surface structure of the sample.

The spatial resolution of the SEM depends on the size of the electron spot that in turn depends on the magnetic electron-optical system, which produces the scanning beam. The resolution is also limited by the size of the interaction volume, or the extent to which the material interacts with the electron beam. The spot size and the interaction volume both might be large compared to the distances between atoms, so the resolution of the SEM is not high enough to image individual atoms, as is possible in the transmission electron microscope (TEM). The SEM has compensating advantages, though, including

the ability to image a comparatively large area of the specimen; the ability to image bulk materials (not just thin films or foils); and the variety of analytical modes available for measuring the composition and nature of the specimen. Depending on the instrument, the resolution can fall somewhere between less than 1 nm and 20 nm. In general, SEM images are easier to interpret than TEM images.

Transmission electron microscopy (TEM) and scanning Electron Microscopy (SEM) techniques are widely used [37, 58] to study mesoporous materials on the nanometer scale since they can provide information on the surface morphology, structural and textural properties, especially for measuring the particle size, wall thickness and diameter of pore channels.

For example, Schuth et al. successfully observed a highly ordered hexagonal structure using TEM on a calcined hexagonally ordered zirconium-based mesostructure [37] (Figure 1.4). Templer and co-workers also obtained accurate information about the particle size, pore size (around 3nm) and wall thickness of mesoporous Pt metals by using SEM combined with TEM techniques [55].

Figure 1.4 TEM of a calcined hexagonally ordered zirconium oxophosphate. [37]

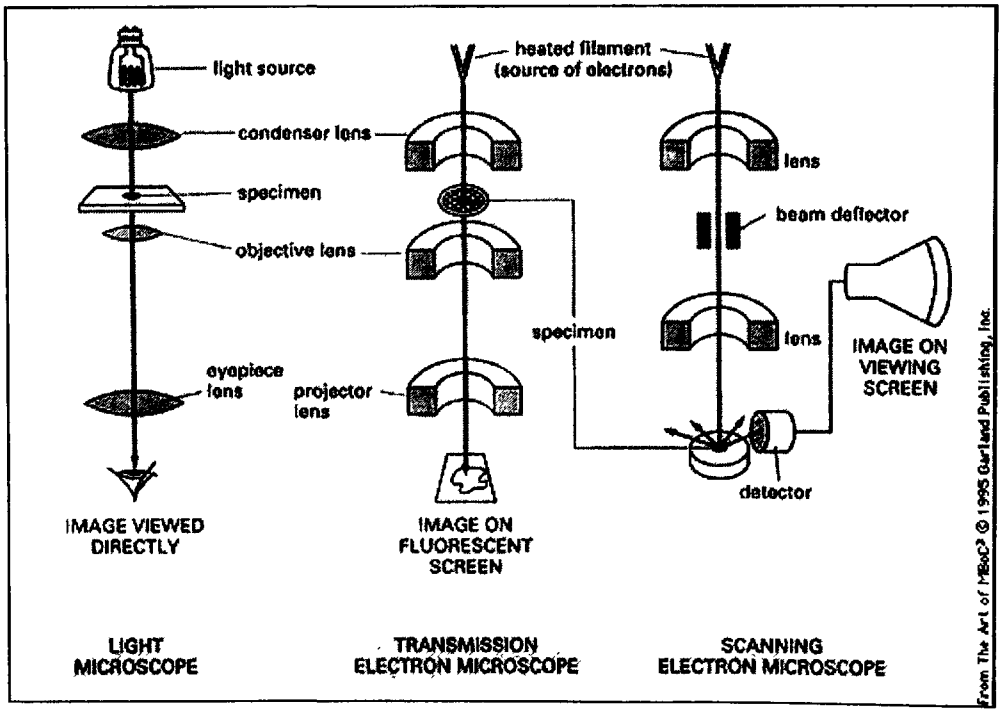

Scheme 1.4 Principle of light microscope, Transmission electron microscope and scanning electron microscope.

1.3.5 FT-IR and TPD of Ammonia

Infrared spectroscopy of adsorbed pyridine and temperature-programmed desorption (TPD) of ammonia are the two most commonly used techniques for characterizing the surface acid properties of mesoporous materials while acid concentration and strength are measured by studying the interaction of an acid with a base. For instance, pyridine-IR and NH_3-TPD permit acidity to be characterized by the pyridine N-H vibration and NH_3 desorption activation energy on the acid sites, respectively. Usually, there are two types of acid sites on the surface sorption sites of solid acids, namely Brønsted acid site and Lewis acid site. In general, the bands at 1545 and 1455 cm^{-1} can be assigned due to B- and L-sites, respectively, whereas the band at 1495 $cm^{-1}$is normally attributed to a combination band associated with both B- and L- sites [59].

Table 1.3 IR spectroscopy correlation table of vibrational modes used for the analysis by the pyridine technique.

Bond	Type of bond	Specific type of bond	Absorption peak	Appearance
N-H	Primary amines	Any	3400–3500 cm^{-1}	Strong
		Any	1560–1640 cm^{-1}	Strong
	Secondary amines	Any	>3000 cm^{-1}	Weak to medium
	Ammonium ions	Any	2400–3200 cm^{-1}	Multiple broad peaks
C-N	Aliphatic amines	Any	1020–1220 cm^{-1}	Overlapped
	C=N	Any	1615–1700 cm^{-1}	Similar conjugation effects to C=O
	C≡N (nitriles)	Unconjugated	2250 cm^{-1}	Medium
		Conjugated	2230 cm^{-1}	Medium
	R–N–C (isocyanides)	Any	2165–2110 cm^{-1}	
	R–N=C=S	Any	2140–1990 cm^{-1}	

TPD of ammonia is a widely used method for characterization of site densities and strength in solid acids due to the simplicity of the technique. The desorption of ammonia peaks at high temperature corresponding to strong acid sites while weak acid sites always show peaks at relative low temperature due to their low binding energy with ammonia. The acid concentrations information can be easily obtained by measuring the peak areas. However, ammonia often overestimates the quantity of acid sites. Its small molecular size allows ammonia to penetrate into all pores of the solid where larger molecules commonly found in cracking and hydrocracking reactions only have access to large micropores and mesopores. Also, ammonia is a very basic molecule that is capable of titrating weak acid sites, which may not contribute to the activity of catalysts. The strongly polar adsorbed ammonia is also capable of adsorbing additional ammonia from the gas phase.

Larger non-reactive amines such as pyridine and t-butyl are often preferable alternatives to ammonia because their size permits access to the pore size range required for catalytic cracking reactions and they titrate only the strong and moderate acid sites. The most common application for these probes is the characterization of pyridine adsorption by infrared spectroscopy. However, the determination of extinction coefficients is difficult and IR of pyridine is typically used in a qualitative manner, rather than as a measurement of site densities.

FT-IR spectroscopy of adsorbed pyridine is a useful technique used for discernment of Brønsted and Lewis acid sites. The adsorbed pyridine probe molecules couple with aprotic (Lewis) and/or protonic (Brønsted) catalytic centers through the nitrogen lone-pair electrons and hence can be detected by monitoring their ring vibrations.

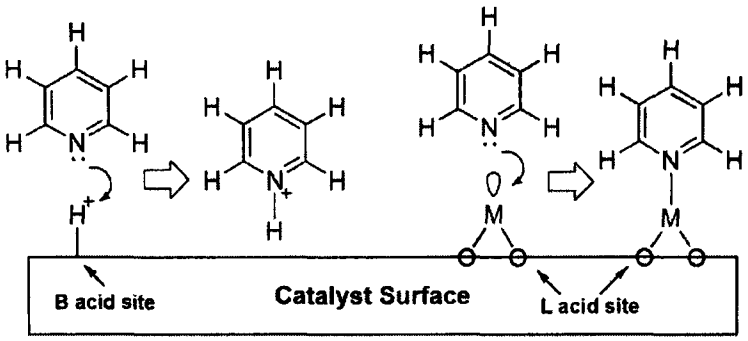

Scheme 1.5 Cartoons of pyridine attached to Lewis acid and Brønsted acid sites of Nb or Ta oxides. (M=Nb or Ta)

However, acidity characterization by the pyridine-IR technique is limited in that it is only capable of providing qualitative information on types of acid sites. As such, it is normally combined with NH_3-TPD, which can provide additional qualitative information regarding to the overall concentration and strength of the acid sites. Determining the quantity and strength of the acid sites on alumina, amorphous silica-alumina, and zeolites is crucial to understanding and predicting the performance of a catalyst. For several significant commercial reactions (such as n-hexane cracking, xylene isomerization, propylene polymerization, methanol-to-olefins reaction, toluene disproportionation, and cumene cracking), all reaction rates increase linearly with Al content (acid sites) in H-ZSM-5. The activity depends on many factors, but the Brønsted-acid site density is usually one of the most crucial parameters. For example, by using the TPD of ammonia technique, Ramoa Ribeiro and co-workers studied the relationship between the acidity and the catalytic activity of HZSM-5 catalysts for n-hexane cracking. The results showed a linear relationship between the enthalpy of the reaction and the activation energy for the desorption of ammonia [60].

1.4 Application of Mesoporous Molecular Sieves in Heterogeneous Catalysis

As stated above, mesoporous molecular sieves such as the M41S family of materials possess extremely high specific surface areas, high thermal and hydrothermal stability, large and uniform pore size (relative to that of microporous zeolites) These unique physical properties of MMS have made them highly desirable for catalytic applications. Mesoporous materials with narrow pore size distribution may eventually replace zeolite catalysts in some commercial applications. In many research applications they already have a comparable or superior performance with respect to conventional microporous zeolites or amorphous silica-alumina catalysts. In the following section, we will focus on some catalytic applications of siliceous and non-siliceous ordered mesoporous materials.

1.4.1 Catalysis by siliceous ordered mesoporous materials

Mesoporous materials have been extensively investigated with regard to their use in cracking and hydrocracking reactions. Unfortunately, the disadvantage of low acid strength of MCM-41 catalysts is a counterbalance to the advantage of the accessibility of the pores even for larger molecules. Nevertheless, MCM-41 catalysts show substantial cracking activity for bulky substances such as palm oil and asphaltene [61,62].

The pore diameter of mesoporous silica or aluminum silicate materials is too large to expect any shape selectivity in conversions of small hydrocarbons [63]. However, one may expect shape selectivity for very large substrates in certain conversions. For example, in benzene alkylation of linear 1-olefins with a chain length of C_6 to C_{16} by $AlCl_3$-grafted

MCM-41 (pore diameter of 3.34 nm), selectivity to mono-substituted alkyl benzene was increased and the formation of multi-substituted products decreased with increasing alkyl chain length of the olefin [64] (Table 1.4)

Table 1.4. Selectivities for the alkylation of benzene with 1-alkenes over homogeneous (free $AlCl_3$) and heterogeneous ($AlCl_3$-grafted MCM-41) catalysts [60].

Alkene	Catalyst[a]	Selectivity toward alkylbenzenes[b]		
		Mono-[c]	Di-	Tri-
1-Hexene	Homog	88.6	31.1	10.3
	Heterog	79.9	20.1	
1-Octene	Homog	66.0	24.3	9.7
	Heterog	79.7	20.3	
1-Decene	Homog	68.5	22.5	9.0
	Heterog	91.1	8.9	
1-Dodecene	Homog	72.5	27.5	d
	Heterog	96.2	3.8	
1-Tetradecene	Homog	70.1	29.9	d
	Heterog	98.5	1.5	
1-Hexadecene	Homog	77.5	22.5	d
	Heterog	>99.0	<1.0	

a Homog.: homogeneous catalysis with $AlCl_3$ (0.15 mmol); heterog. over $AlCl_3$-MCM-41 (Dp = 3.34nm, 0.15g of catalyst containing 0.15mmol of AlClx).

b Determined by GC of the product mixture.

c Exclusively linear alkyl benzenes.

d Nonvolatile product, not analyzed by GC.

Although the inherent weakness of the acid sites in mesoporous silica or aluminumsilicate materials restricts their applicability in many petrochemical reactions, there still is potential for their use in reactions that require a lower level of acidity, such as the Friedel-Crafts alkylation of electron rich aromatic compounds. For instance, Al-MCM-41 with a pore diameter of 3.0 nm is active in the Friedel-Crafts alkylation of 2,4-di-tert-butylphenol with cinnamyl alcohol. The yield over Al-MCM-41 (35%) was much higher than over HY zeolite (<1%), suggesting that diffusion restrictions of the bulky substrate exist in the zeolite. Furthermore, Al-MCM-41 also gave a much higher yield of dihydrobenzopyran than conventional catalysts, such as H_2SO_4 (12%) and

amorphous silica-alumina (6%) catalysts. These results clearly indicate the potential offered by mesoporous materials in fine chemical synthesis with bulky substrates.

1.4.2 Catalysis by non-siliceous ordered mesoporous materials

Surfactant templating has provided a breakthrough methodology for the preparation of non-siliceous mesoporous materials. Through a number of alternative surfactant-assisted synthesis approaches, non-silicate mesoporous metal oxides were achieved using low molecular weight surfactants, eg. titania [42,65,66,67,68 , niobia [43, 69], tantalum [70 , 71 , 72], manganese [73 , 74], zirconia [75,76,77,78,79,80,81,82,83,84,85,86], vanadium [87,88] For all of the above non-silica materials prepared using low molecular weight surfactants, the resulting mesoporous materials had small pore sizes (~ 4 nm) and their channel walls were exclusively amorphous. Most of the above syntheses were carried out in aqueous solution using metal alkoxides as inorganic precursors. Several reviews [4,89,90] have already been devoted to these materials.

Although price could be a serious obstacle for commercialization, MMS type materials composed of transition metal oxides are attractive heterogeneous catalysts, catalyst supports and nanocomposite host materials for a wide range of applications. For example, mesoporous CeO_2 and ZrO_2 were found to be effective catalyst supports in vapor phase phenol hydrogenation [91]. The hydrogenation catalyst was palladium, which was loaded by a deposition–precipitation method into the mesopores of CeO_2 and ZrO_2. Hydrogen sorption experiments confirmed that palladium was present in the catalyst in the form of nanoparticles. The resulting Pd/CeO_2 (3wt%) showed a phenol

conversion of 81.4% at 180 °C with selectivity to cyclohexanone, cyclohexanol and cyclohexane of 46.2%, 34.8% and 19.0%, respectively. Another example of catalytic applications of (semi) conducting mesoporous transition metal oxides is mesoporous titanium and niobium oxides in photocatalysis, although they have extremely low quantum yields as compared to standard titania catalysts [67,71]. It was also reported by our group that mesoporous low-valent niobium oxide [43] coated with niobium by the deposition of bis(toluene) niobium could react with molecular nitrogen and form nitride species at room temperature [92]. In a similar way, mesoporous titanium oxide treated with bis(toluene) Ti was prepared and tested by experiments with isotope labeled nitrogen; the results confirmed that the source of nitrogen was from the reaction atmosphere [93].

Since Nb and Ta oxides possess high acidities, especially in their sulfated or phosphated form, the potential applications of mesoporous Nb and Ta oxides to acid catalyzed hydrocarbon couplings and rearrangement reactions seems promising, especially due to the failure of mesoporous aliminosilicates in this area. This thesis is thus devoted to the study of the mesoporous Nb and Ta oxides in acid catalysis and the exploration of the structure of their oxide walls, which could have an impact on their activities in this area.

1.5 References

1 A. Stein, *Adv. Mater.* **2003**, *15*, 763

2 M. E. Davis, *Nature*, **2002**, *417*, 813

3 J. Rouquerol, *Pure Appl. Chem.* **1994**, *66*, 1739.

4 J.Y. Ying, C.P. Mehnert, M.S. Wong, *Angew. Chem. Int. Ed.* **1999**, *38*, 56

5 A. Corma, *Chem. Rev.* **1997**, *97*, 2373

6 C.T. Kresge,, M.E. Leonowicz, W.J. Roth,, J.C. Vartuli, J.S. Beck, *Nature* **1992**, *359*, 710

7 J.S. Beck, J.C. Vartuli, W.J. Roth, M.E. Lernowicz, C.T. Kresge, K.D. Schmitt, C.T.W. Chu, D.H. Olson, E.W. Sheppard, S.B. Mccullen, J.B. Higgins, J.C. Schlenker, *J. Am. Chem. Soc.* **1992**, *144*, 10834

8 J. C. Vartuli, C. T. Kresge,W. J. Roth, S. B. McCullen, J. S. Beck, K. D. Schmitt, M. E. Leonowicz, J. D. Lutner, E. W. Sheppard in *Advanced Catalysts and Nanostructured Materials: Modern Synthesis Methods* (Ed.: W. R. Moser), Academic Press, New York, **1996**, pp. 1-19.

9 B. T. Holland, C. F Blanford and A. Stein, *Science*, **1998**, *281*, 538

10 C. F. Blanford, H. Yan, R. C. Schroden, M. Al-Daousand A. Stein, *Adv. Mater.* **2001**, *13*, 401

11 H. W. Yan,C. F. Blanford, B. T. Holland, W. H. Smyrl and A. Stein, *Chem. Mater.*, **2000**, *12*, 1134

12 Sarrade, S. J.; Rios, G. M.; Carles, M. *Sep. Purif. Technol.* **1998**, *14*, 19

13 Nakanishi, K.; Minakuchi, H.; Soga, N.; Tanaka, N. *J. Sol-Gel Sci. Technol.* **1998**, *13*, 163

14 P. Diddams, *Inorganic Supports and Catalysts*; K. Smith, Ed.; Ellis Horwood: New York, **1992**; pp 3-39.

15 A. Aivasidis, C. Wandrey, W. Kiefer, U.S. Patent 5 096 814, **1992.**

16 T. J. Clough, U.S. Patent 5 895 732, **1999**.

17 E. Litovsky, M. Shapiro, A. Shavit, *J. Am. Ceram. Soc.* **1996**, *79*, 1366

18 A. Taguchi, F. Schuth, *Micropor. Mesopor. Mat.* **2005**, *77*, 1

19 G.D. Stucky, A. Monnier, F. Schueth, Q. Huo, D.I. Margolese, D. Kumar, M. Krishnamurty, P. Petroff, A. Firouzi, M. Janicke, B.F. Chmelka, *Mol. Cryst. Liq. Cryst.***1994**, *240*, 187

20 U. Ciesla, D. Demuth, R. Leon, P. Petroff, G.D. Stucky, K.Unger, F. Schueth, *J. Chem. Soc., Chem. Commun.* **1994**,1387

21 L. Bull, D. Kumar, S.P. Millar, T. Besier, M. Janicke, G.D. Stucky, B.F. Chmelka, *Stud. Surf. Sci. Catal.* **1994**, *84*, 429

22 Q. Huo, R. Leon, P. Petroff, G.D. Stucky, *Science* **1995**, *268*,1324

23 A. Firouzi, D. Kumar, L.M. Bull, T. Besier, P. Sieger, Q. Huo, S.A. Walker, J. Zasadzinski, A.G. Glinka, J. Nicol, D. Margolese, G.D. Stucky, B.F. Chmelka, *Science* **1995**, *267*, 1138

24 Q. Huo, D.I. Margolese, G.D. Stucky, *Chem. Mater.* **1996**, *8*, 1147

25 P.T. Tanev, T.J. Pinnavaia, *Science* **1995**, *267*, 865

26 P.T. Tanev, M. Chibwe, T.J. Pinnavaia, *Nature* **1994**, *368*, 321

27 S. A. Bagshaw, E. Prouzet, T.J. Pinnavaia, *Science* **1995**, *269*,1242.

28 T.R. Pauly, Y. Liu, T.J. Pinnavaia, S.J.L. Billige, T.P. Rieker, *J. Am. Chem. Soc.* **1997**, *121*, 8835

29 E. Prouzet, T.J. Pinnavaia, *Angew. Chem. Int. Ed.* **1997**, *36*, 516

30 D. Zhao, J. Feng, Q. Huo, N. Melosh, G.H. Fredrickson,B.F. Chmelka, G.D. Stucky, *Science* **1998**, *279*, 548

31 D. Zhao, Q. Huo, J. Feng, B.F Chmelka, G.D. Stucky, *J. Am. Chem. Soc.* **1998**, *120*, 6024

32 G.D. Stucky, D. Zhao, P. Yang, W. Lukens, N. Melosh, B.F. Chmelka, *Stud. Surf. Sci. Catal.* **1998**, *117*, 1

33 G.D. Studky, B.F. Chmelka, D. Zhao, N. Melosh, Q. Huo, J. Feng, P. Yang, D. Pine, D. Margolese, W. Lukens, G.H. Fredrickson, P. Schmidt-Winkel, Int. Patent WO99/37705 (July **1999**)

34 B. Viswanathan, S. Sivasanker, A. V. Ramaswamy, *Catalysis: Principles And Applications*, CRC Press, **2002**, Page 88

35 Q.Huo, D. I. Margolese, U. Ciesla, D. G.. Demuth, P. Feng, T. E. Gier, P. Sieger, A. Firouzi, B. F Chmelka, F. Schuth, G. D. Stucky, *Chem. Mater.* **1994**, *6*, 1176

36 D. Khushalani, A. Kuperman, G. A. Ozin, K. Tanaka, J. Garce´s, M. M.Olken, N.Coombs, *Adv. Mater.* **1995**, *7*, 842

37 T. Yanagisawa, T. Shimizu, K. Kuroda, C. Kato, *Bull. Chem. Soc. Jpn.* **1990**, *63*, 988

38 U.Ciesla, F. Schuth, *Micropor. Mesopor. Mater.* **1999**, *27*,131

39 A. Monnier, F Schuth, Q. Huo, D. Kumar, D. Margolese, R. S. Maxwell, G. D. Stucky, M. Krishnamurty, P. Petroff, A.Firouzi, M.Janicke, B. Chmelka, *Science* **1993**, *261*, 1299

40 Q. Huo, D. Margolese, U. Ciesla, P. Feng, T.Gier, P. Sieger, R. Leon, P. Petroff, F. Schuth, G. D. Stucky, *Nature* **1994**, *368*, 317

41 Q. Huo, D.I. Margolese, U. Ciesla, D.G. Demuth, P. Feng, T.E. Gier, P. Sieger, A. Firouzi, B.F. Chmelka, F. Shüth, G.D. Stucky, *Chem. Mater.* **1994**, *6*, 2317

42 D.M. Antonelli, J. Y.Ying, *Angew. Chem. Int. Ed. Engl.* **1995**, *34*, 2014

43 D.M. Antonelli, J.Y. Ying, *Angew. Chem. Int. Ed. Engl.***1996**, *35*, 426

44 A. Sayari, P. Liu, *Micropor. Mater.* **1997**, *12*, 149

45 F. Schuth, *Chem. Mater.* **2001**, *13*, 3184

46 V. Luca, J.M. Hook, *Chem. Mater.* **1997**, *9*, 2731

47 G. Pacheco, E. Zhao, A. Garcia, A. Sklyarov, J.J. Fripiat, *Chem. Commun.* **1997**, 491

48 G. Pacheco, E. Zhao, A. Garcia, A. Sklyarov, J.J. Fripiat, *J. Mater. Chem.* **1998**, *8*, 219

49 S. Brunauer, L. Deming, W. Deming, E. Teller, *J. Am. Chem. Soc.* **1940**, *62*, 1723

50 S.J. Gregg, K.S.W. Sing, *Adsorption Surface Area and Porosity*, second ed., Academic Press, London, **1982**, p. 303.

51 F. Rouquerol, J. Rouquerol, K.S.W. Sing, *Adsorption by Powders and Porous Solids*, Academic Press, London, **1999**, p. 467.

52 S. Lowell, J.E. Shields, *Powder, Surface Area and Porosity*, third ed., Chapman and Hall, London, **1991**, p. 250.

53 E.P. Barret, L.G. Joyner, P.H. Halenda, *J. Am. Chem. Soc.* **1951**, *73*, 373

54 Z. Luan, C. F.Cheng, W. Zhou, J. Klinowski, *J. Phys. Chem.* **1995**, *99*, 1018

55 K. J. D. MacKenzie, M. E. Smith, *Multinuclear Solid State NMR of Inorganic Materials*, Pergamon, Oxdord, **2002**.

56 S. E. Ashbrook, M. E. Smith, *Chem. Soc. Rev.* **2006**, *35*, 718

57 B.O. Skadtchenko, Y. Rao, T.F. Kemp, P. Bhattacharya, P.A. Thomas, M. Trudeau, M.E. Smith, D.M. Antonelli, *Angew. Chem. Int. Ed.* **2007**, *46*, 2635

58 G. S. Attard, C. G. Goltner, J. M. Corker, S. Henke, R. H. Templer, *Angew. Chem., Int. Ed. Engl.* **1997**, *36*, 1315

59 F. Babou, G. Coudurier, J.C. Vedrine, *J. Catal.* **1995**, *152*, 341

60 P. Borges, R. Ramos Pinto, M.A.N.D.A. Lemos, F. Lemos, J.C. Vedrine, E.G. Derouane, F Ramoa Ribeiro, *J. Mol. Catal. A. Chem* **2005**, *229*, 127

61 F.A. Twaiq, A.R. Mohamed, S. Bhatia, *Micropor. Mesopor. Mater.* **2003**, *64*, 95

62 E. Byambajav, Y. Ohtuska, *Fuel* **2003**, *82*, 1571

63 G. Seo, N.H. Kim, Y.H. Lee, J.H. Kim, *Catal. Lett.* **1999**, *57*, 209

64 X. Hu, M.L. Foo, G.K. Chuah, S. Jaenicke, *J. Catal.* **2000**, *195*, 412

65 H. Fujii, Ohtaki, K. Eguchi, *J. Am. Chem. Soc.* **1998**,*120*, 6832

66 R.L. Putnam, N. Nakagawa, K.M. McGrath, N. Yao, I.A. Aksay, S.M. Gruner, A. Navrotsky, *Chem. Mater.* **1997**, *9*, 2690

67 V.F. Stone Jr., R.J. Davis, *Chem. Mater.* **1998**, *10*, 1469

68 D. Trong On, *Langmuir* **1999**, *15*, 8561

69 D.M. Antonelli, A. Nakahira, J. Ying, *Inorg. Chem.* **1996**, *35*, 3126

70 D.M. Antonelli, J.Y. Ying, *Chem. Mater.* **1996**, *8*, 874

71 Y. Takahara, J.N. Kondo, T. Takata, D. Lu, K. Domen, *Chem. Mater.* **2001**, *13*, 1194

72 J.N. Kondo, Y. Takahara, D. Lu, K. Domen, *Chem. Mater.* **2001**, *13*, 1200

73 Z-R. Tian, W. Tong, J.-Y. Wang, N.-G. Duan, V.V. Krishnan, S.L. Suib, *Science*, **1997**, *276*, 926

74 J. Luo, S.L. Suib, *Chem. Commun.* **1997**, 1031

75 M.J. Hudson, J.A. Knowles, *J. Mater. Chem.* **1996**, *6*, 89

76 J.S. Reddy, A. Sayari, *Catal. Lett.* **1996**, *38*, 219

77 U. Ciesla, S. Schacht, G.D. Stucky, K.K. Unger, F. Schüth, *Angew. Chem. Int. Ed. Engl.* **1996**, *35*, 541

78 U. Ciesla, M. Fröba, G.D. Stucky, F Schüth, *Chem. Mater.* **1999**, *11*, 227

79 Y.-Y. Huang, T.J. McCarthy, W.M.H. Sachtler, *Appl. Catal.* **1996**, *148*, 135

80 M.S. Wong, D.M. Antonelli, J.Y. Ying, *Nanostr. Mater.* **1997**, *9*,165

81 M.S. Wong, J.Y. Ying, *Chem. Mater.* **1998**, *10*, 2067

82 R.A. Boyse, E.I. Ko, *Catal. Lett.* **1996**, *38*. 225

83 A. Kim, P. Bruinsma, Y. Chen, L.-Q. Wang, J. Liu, *Chem. Commun.* **1997**, 161

84 G. Pacheco, E. Zhao, A. Garcia, A. Sklyarov, J.J. Fripiat, *Chem. Commun.* **1997**, 491

85 E. Zhao, S.E. Hardcastle, G. Pacheco, A. Garcia, A.L. Blumenfeld, J.J. Fripiat, *Micropor. Mesopor. Mater.* **1999**, *31*, 9

86 G. Pacheco, J.J. Fripiat, *J. Phys. Chem. B* **2000**, 11906

87 M.E. Spahr, P. Bitterli, R. Nesper, M. Müller, F. Krumeich, H.U. Nissen, *Angew. Chem. Int. Ed.* **1998**, *37*, 1263

88 V. Luca, J.M. Hook, *Chem. Mater.* **1997**, *9*, 2731

89 S. Biz, M.L. Occelli, *Catal. Rev.-Sci. Eng.* **1998**, *40*, 329

90 Y. Ma, W. Tong, H. Zhou, S.L. Suib, *Micropor. Mesopor.Mater.* **2000**, *37*, 243

91 S. Velu, M.P. Kapoor, S. Inagaki, K. Suzuki, *Appl. Catal. A: Gen.* **2003**, *245*, 317

92 M. Vettraino, X. He, M. Trudeau, J.E. Drake, D.M. Antonelli, *Adv. Func. Mater.* **2002**, *12*, 174

93 M. Vettraino, M. Trudeau, A.Y.H. Lo, R.W. Schurko, D. Antonelli, *J. Am. Chem. Soc.* **2002**, *124*, 9567

Chapter 2

A Solid-State ^{17}O NMR Study of Local Order and Crystallinity in Amine-Templated Mesoporous Nb Oxide

This chapter is organized based on a paper published in Angewandte Chemie International Edition, by Boris O. Skadtchenko, **Yuxiang Rao**, Tom F. Kemp, Prodipta Bhattacharya, Pamela A. Thomas, Michel Trudeau, Mark E. Smith, and Dave M. Antonelli

2.1 Introduction

The study and modification of materials on the nanoscale has attracted a great deal of attention from a wide variety of scientific disciplines ranging from medicine to physics [1, 2]. One of the most important classes of nanoscale materials is those with repeat and

regular pore structure on the nanometer scale [3, 4]. The discovery of M41Smesoporous silica in 1992 led to new techniques of fabrication of highly ordered, high-surface-area mesoporous materials, especially those of metal oxides [5]. The first synthesis of mesoporous Ti oxide was reported in 1995 [6], followed by mesoporous niobia material [7], which displayed pore sizes in the range 2~5 nm and surface areas up to 1200 m^2g^{-1} The advantage of these mesoporous transition-metal oxides over the traditional silica-based materials is that these oxides are capable of existing in various oxidation states. Recent advances showed that such mesoporous oxides can act as stoichiometric electron acceptors, which allowing the fine tuning of electronic properties of the mesostructure and making them potential candidates for battery applications, fuel-cell fabrication [8], and hydrogen-storage materials [9]. Mesoporous sulfated niobia has also been shown to have very high activity for acid-catalyzed benzylation of anisole [10].

Despite the intriguing and promising properties of mesoporous transition-metal oxides, there is still very little detailed information concerning their atomic-scale structure. The degree of local ordering is extremely important for tailoring catalytic properties into porous materials. Although conventional analytical techniques such as X-ray diffraction (XRD) and X-ray photoelectron spectroscopy (XPS) have provided information on the degree of medium-range order and surface electronic states, respectively, in these materials, the local structure of the walls remains largely unknown. The lack of discrete high-angle reflections in the XRD pattern suggests that the structure is amorphous. Tatsumi and coworkers used XRD along with UV/Vis and X-ray absorption near-edge structure (XANES) spectroscopy to probe the structure of mesoporous Ti oxide [11]. The effectively amorphous structure was made up of coexisting TiO_5 and TiO_6 units according

to XANES. In V_2O_5 • n H_2O xerogels, conventional XRD revealed little, but analysis of the atomic-pair distribution function suggested that the lamellar structure was made up of bilayers of perfect V_2O_5 units in which the vanadium center is coordinated as VO_5 and the bilayers are separated by water [12]. Despite this recent progress, deeper insight into the local structure of mesoporous transition-metal oxides is still required.

Solid-state NMR spectroscopy has proved to be an extremely useful and informative tool in identifying and characterizing local environments in materials [13]. The large chemical-shift range of ^{17}O produces high sensitivity to even subtle differences in the structure in both amorphous and crystalline solids [13,14]. The major problem with ^{17}O NMR spectroscopy is the low natural abundance of ^{17}O (0.037 %) and subsequent poor sensitivity, which can be overcome by even modest enrichment of the material (e.g. by using 20 at % in the precursor material) [13, 14]. Solid-state ^{17}O NMR data are reported herein for both conventional sol–gel bulk niobia and mesoporous niobia. These data indicate that the wall in the latter has an unprecedented, highly ordered local structure about the oxygen site, with the oxygen exclusively present as ONb_2, unlike conventional Nb_2O_5, which is mixture of ONb_2 and ONb_3 environments. Static ^{93}Nb NMR data are also reported for the mesoporous sample.

^{17}O magic-angle-spinning (MAS) NMR spectra were collected from sol–gel-produced bulk Nb_2O_5 for comparison. The resonances observed in the Nb_2O_5 can be compared to data from previous study of hydrolyzed niobium ethoxide in the as-prepared sample [15,16], which were assigned on the basis of solution-state NMR spectroscopy of niobium-containing cluster compounds [17] as ONb_2 at δ= 540 ppm and ONb_3 at δ= 358

ppm (Figure 2.1, Table 2.1). The structural development of niobia gels is shown herein for the first time by means of ^{17}O MAS NMR spectroscopy. The peak at δ=540 ppm is more intense than the other peak. Upon heating the sample first to 250 °C for 4 h, the intensities of the two peaks become more comparable. After heating the sample to 500 °C for 4h, the peak at δ= 375 ppm is more intense than the peak at δ= 565 ppm, and there is also slight narrowing of the line at δ= 375 ppm (Table 2.1). After heating the sample to 750 °C, the peak at 565 ppm disappears almost completely and is replaced by much broader, less intense peak centered at δ= 617 ppm, which indicates that the material has undergone a significant structural change. After heating to 1000 °C, the material crystallized and had two peaks present at δ = 371 and 565 ppm, which were approximately 30% narrower than they were in the amorphous state. These ^{17}O NMR peaks can be assigned to ONb_3 and ONb_2 respectively, as expected for a niobium phase consisting of NbO_6 units sharing a mixture of edges and corners.

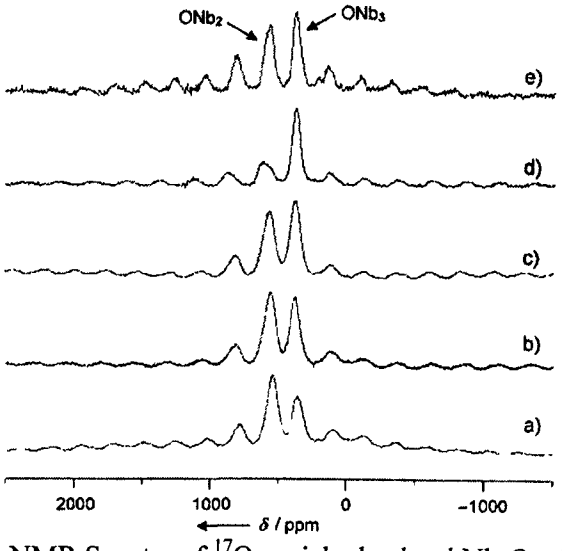

Figure 2.1 ^{17}O MAS NMR Spectra of ^{17}O-enriched sol-gel Nb_2O_5 a) as-formed, and after heating to b) 250 °C, c) 500 °C, d) 750°C, and e) 1000°C. (Main peaks identified, all others are spinning sidebands).

Table 2.1: Summary of NMR spectral characteristics of mesoporous niobia samples.[a]

Heat treatment	Mesoporous niobia				Bulk sol–gel-prepared niobia	
	^{93}Nb static NMR		^{17}O MAS NMR		^{17}O MAS NMR	
	δ_{peak}	Δ	δ_{peak}	Δ	δ_{peak}	Δ
	[(±5) ppm]	[(±3) kHz]	[(±0.2) ppm]	[(±10) Hz]	[(±1) ppm]	[(±80) Hz]
None	~1145	122	565.5	395	358	5540
					540	5320
250°C	~1145	171	559.3	320	374	4580
					556	5320
500°C	~1195	237	556.0	530	375	4630
					565	5060
750°C	~1660	341	589.0	250	372	3370
			556.3	275	617	6990
1000°C	n.m.	n.m.	n.m.	n.m.	371	3900
					565	4340

[a] δ_{peak} is the peak position without correction for any second-order quadrupole contribution to the peak position away from the chemical shift; D=full width at half maximum; n.m.=not measured.

The XRD (Figure 2.2) shows a relatively simple pattern from mesoporous niobia. With no heat treatment (and after treatment at 250 °C, not shown), only a very low angle reflection is observed at approximately 2.5° After further heat treatment, additional reflections are observed at approximately 22°, 28°, and 37° (2θ), and the main low-angle peak for the mesostructure gradually diminishes in intensity, which suggests a loss in pore structure as evidenced by a decrease in surface area from 700 m^2g^{-1} in the untreated material down to less than 5 m^2g^{-1} in the material heated to 750°C. These reflections can best be indexed, although not exactly, on the orthorhombic phase (JSCPDS 27-1313) of

niobia and not the usual room temperature form [18]. The trend of gradual crystallization can also be clearly followed in the TEM images (Figure 2.4 in the Supporting Information).

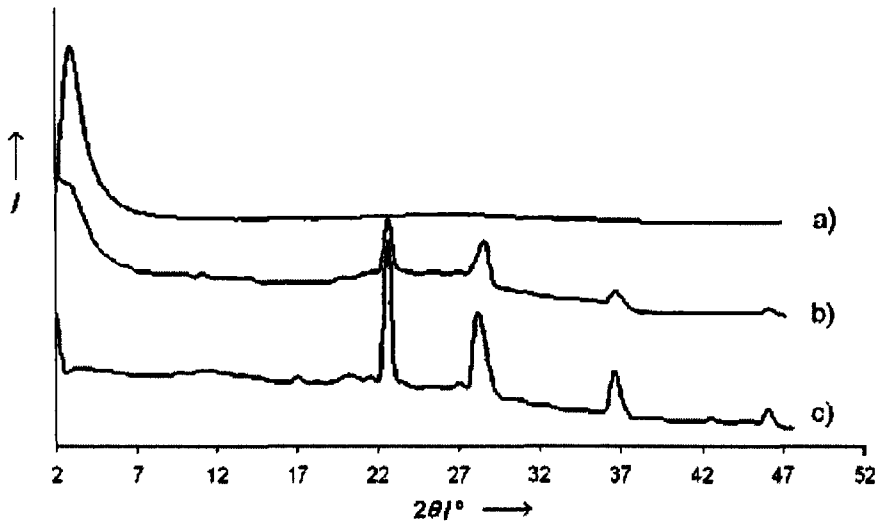

Figure 2.2 X-ray diffraction pattern of mesoporous Nb oxides a) at room temperature, and after heating for 2h at b) 500°C and c) 750°C.

^{93}Nb despite having a high nuclear spin of I= 9/2 can experience significant quadrupole broadening so that MAS is often ineffective in providing any line narrowing. Static ^{93}Nb NMR data collected on the as-synthesized sample showed a quite broad asymmetric spectrum (Figure 2.5 in the Supporting Information and Table 2.1). Up to 500°C, the peak position (note that the peak position is not the isotropic chemical shift [13], but the large shift range usually allows identification) does not change much, clearly indicating that niobium is present as NbO_6 throughout [19]. The increase in the line width suggests that there is some increase in the average interaction, probably as a result of the NbO_6 units becoming more distorted. After the sample was heated to 750 °C, there was a much larger

change in the spectrum: the peak shifted by approximately ~450 ppm. This shift is at the very extreme of the shift range of NbO_6 units [19], probably suggesting an unusual NbO_6 unit. The significant increase in line width also suggests that the site has become further distorted.

The ^{17}O MAS NMR spectra (Figure 2.3, Table 2.1) show some intriguing results. The spectrum of the as-synthesized oxide is dominated by a single sharp resonance at δ = 565.5 ppm, and some low-intensity spinning sidebands are also present, along with a hint of some much weaker features—broader underlying intensity and some very much smaller peaks (e.g. at $\delta \approx 500$ ppm), all in the chemical shift range for ONb_2. There is relatively little change in the line shape upon heat treatment other than a small decrease in the shift successively to δ = 559.3 and 556.0 ppm in the samples heated to 250 and 500 °C, respectively. On heating the sample to 750 °C, the peak at δ = 556 ppm remains, but a second narrow peak of almost equal intensity appears at δ= 589 ppm.

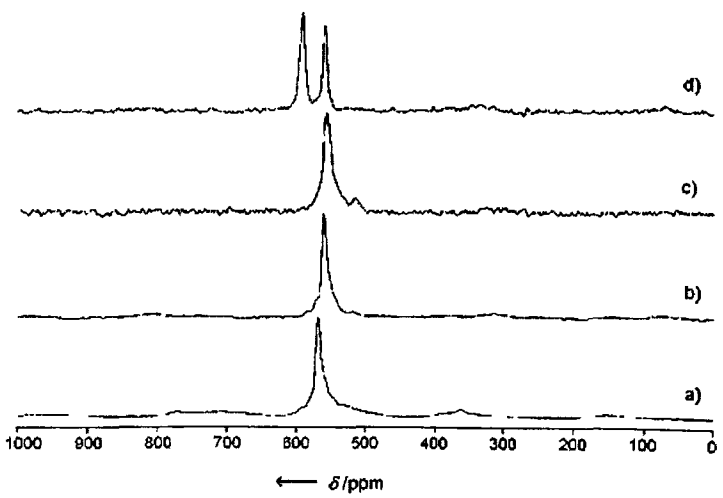

Figure 2.3 ^{17}O MAS NMR spectra of ^{17}O-enriched mesoporous niobia a) as-synthesized, and after heating to b) 250°C, c) 500°C, and d) 750 °C.

Hence it is very clear that the niobia walls in the sample are exclusively constructed of ONb_2 linkages, which is very unusual, as all other ^{17}O NMR data reported on niobia have shown a mixture of ONb_2 and ONb_3 environments. Perhaps even more surprising is the line width. In sol–gel-prepared Nb_2O_5, the line widths are about 5 kHz at a similar magnetic field, and even on crystallization there is only a modest decrease of width to around 4 kHz. Crystalline niobates tend to exhibit significantly broader resonances than, for example, chemically similar titanates [13,20], which is attributed to the generally observed relation that the quadrupole broadening depends on the electronegativity difference across the metal-oxygen bond [14]. This would suggest a typical quadrupole interaction (χ_Q) of 4 MHz for Nb-O, whereas on the basis of the small line width an upper estimate of χ_Q is only 2.5 MHz. Although XRD indicates that this mesoporous niobia has long-range order that resembles the orthorhombic phase, the local structure is different and consists of a single, highly symmetric oxygen site (only ONb_2 and no ONb_3). At 750 °C, the structure changes as two similar, but nonequivalent, ONb_2 sites appear, and the niobium probably remains as NbO_6, but with a large chemical shift, in a structure that is still very highly ordered locally.

These results show that the walls of the mesoporous Nb oxide are made up of NbO_6 units that are linked through corner-sharing ONb_2 arrangements in three dimensions with very few edge-sharing units and probably hydroxy groups on the inner and outer surfaces. Such hydroxy groups are often not observed in ^{17}O MAS NMR spectra [21], but they must be present, as previous work has shown that treatment of mesoporous niobium oxide with trimethylsilyl chloride leads to silicon incorporation in the materials [9]. ^{17}O NMR spectroscopy is shown herein to provide very clear information on the local order within

this material. Although the vast majority of the octahedra are linked at the corners, the flexibility about the ONb_2 unit must allow enough dislocations and twisting that the orientation of the NbO_6 units changes, thus decreasing medium-/long-range order and preventing discrete Bragg reflections in the XRD pattern. This structure is surprisingly well ordered relative to other samples of niobia gels, as well as samples of mesoporous titania and tantala prepared through the same route. On heat treatment of the samples, the local order (as indicated by the narrow ^{17}O NMR resonances) remains much higher than indicated by the broad Bragg reflections. A consequence of this situation is that there must be regular microporous channels in the walls running between the three-dimensional arrays of octahedra. The appearance of this structure is unprecedented in surfactant-templated mesoporous materials, although organically modified mesoporous silicas with aryl groups in the channels display regular stacking of these organic functionalities [22]. Appearance of any order in the walls of surfactant-templated mesoporous structures typically occurs by crystallization at elevated temperatures and leads to collapse of the mesopores and formation of nanocrystalline grains, although in some cases individual nanocrystals can be formed in the walls prior to complete collapse of the pore structure [23]. Crystalline walls are more common in lower surface-area polymer-templated structures with much thicker walls; however, surfactant-templated mesoporous germania and some Zintl salts possess a regular wall structure, but the template remains within the structure [24]. None of these oxide structures possess exclusively corner-shared octahedra and the order observed in the samples in this case is not related to crystallization. The reason that the walls of the mesoporous niobia adopt this highly ordered structure is presently unknown. The combination of a unique,

template-free highly ordered structure with a surface area of 700 m^2 g^{-1} and thermal stability up to around 400°C suggests a number of exciting applications. Furthermore, the suggested presence of regular microporous channels in the walls makes this material very interesting from the standpoint of gas separation and catalysis with small molecules (e.g. CH_4, CO, H_2O, and nitrogen oxides).

2.2 Experimental Section

2.2.1 Sample Preparation

Mesoporous niobia was prepared as described previously [7]. The ^{17}O enrichment was carried out by heating stoichiometric amounts of mesoporous metal oxide and [^{17}O] water (20 % enriched) together in a sealed vessel under an inert atmosphere at 140 °C for 24 h. The samples were subsequently heat treated under air at 250, 500, and 750 °C for 2 h at a time.

2.2.2 XRD experiment

XRD patterns were recorded with Cu_{Ka} radiation on a Siemens D500 θ/2θ diffractometer. TEM images were obtained on a Hitachi H9000 high-resolution transmission electron microscope operating at 200 kV.

2.2.3 NMR experiment

NMR experiments were carried out on a CMX Infinity 600 spectrometer equipped with a 14.1-T magnet for ^{93}Nb at an observation frequency of 146.7 MHz and a CMX

Infinity 360 spectrometer equipped with a 8.45-T magnet for ^{17}O at an observation frequency of 48.2 MHz. (Scheme 2.1) The ^{93}Nb NMR experiments used a solid echo pulse sequence on a Bruker 5-mm static probe with an echo time of 25 μs and a recycle delay of 3 s, and typically 1500 scans were coadded. A frequency of 12 kHz was employed for the ^{17}O MAS on a Varian-Chemagnetics Apex 4-mm probe with the echo time set to the reciprocal of the spinning period. A recycle time of 1 s was used and typically 10^4 acquisitions were coadded. The ^{93}Nb NMR spectra were referenced by using the highest shift singularity of well-crystallized $LiNbO_3$ at δ =-1016.3 ppm so that the shift is reported indirectly against the primary shift reference, whereas the ^{17}O NMR spectra were referenced against tap water at a shift of δ = 0 ppm.

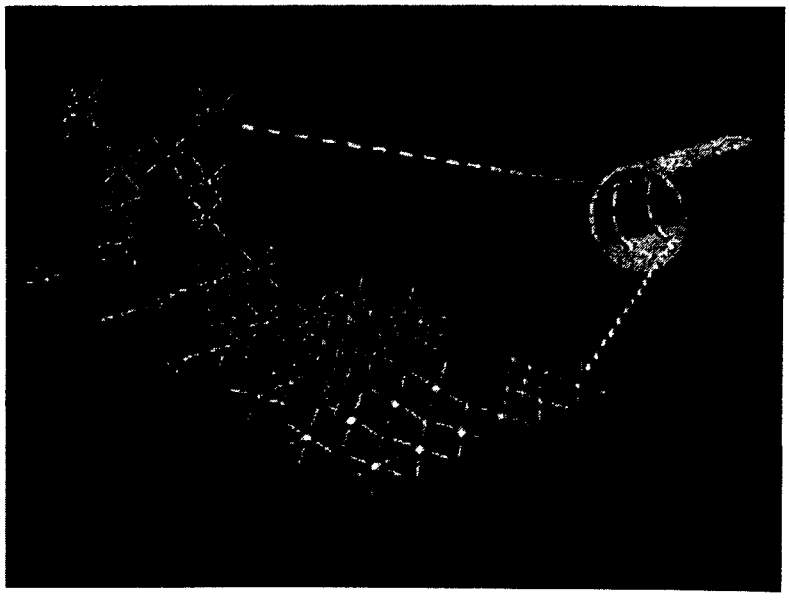

Scheme 2.1 Schematic representation of very high local order in the mesoporous Nb_2O_5 sample

2.3 Supporting Information

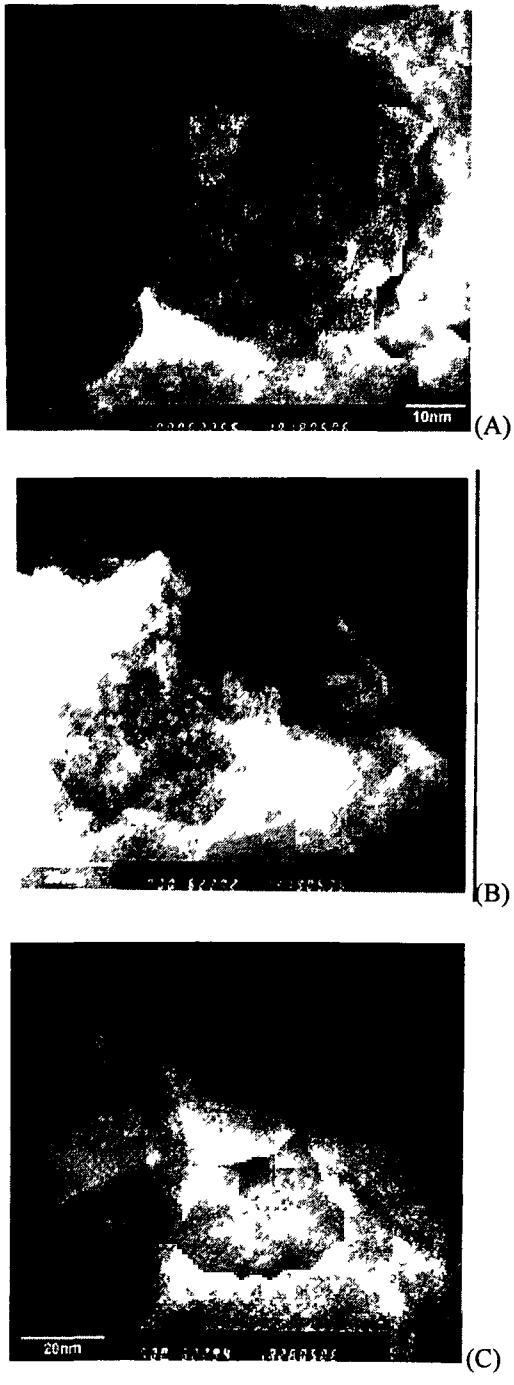

Figure 2.4. TEM images of mesoporous niobia (a) as-prepared; (b) heated at 500°C for 2 h; (c) heated at 750°C for 2 h.

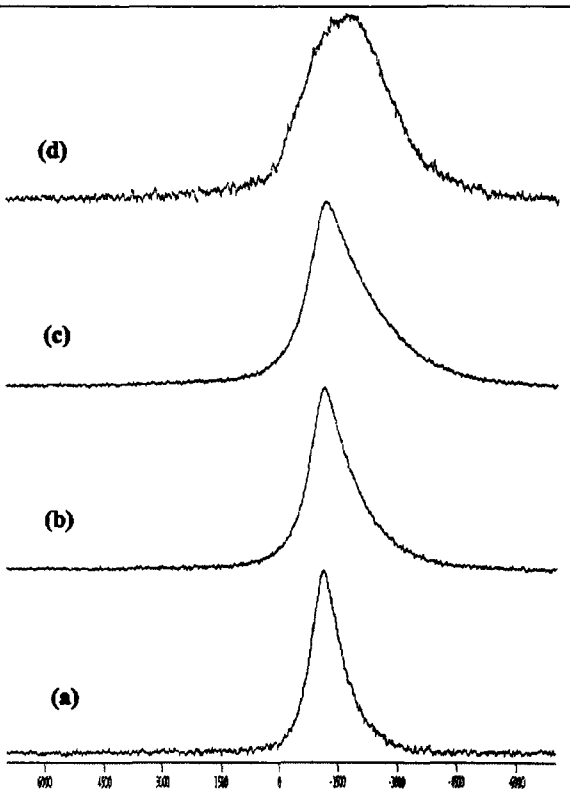

Figure 2.5. Static ^{93}Nb NMR spectra of mesoporous niobia that was as-synthesized (a) and subsequently heat treated to 250°C (b), 500°C (c) and 750°C (d).

2.4 References

1. M.C. Roco, W.S. Baindbridge, *Societal Implications of Nanoscience and Nanotechnology*, Kluwer, **2002**.
2. C. P. Collier, E. W. Wong, M. Belohradsky, F M. Raymo, J. F. Stoddart, P. J. Kuekes, R. S. Williams, J. R. Heath, *Science* **1999**, *285*, 391
3. B. T. Holland, C. F Blanford, A. Stein, *Science* **1998**, *281*, 538
4. Y. Huang, X. Duan, Q. Wei, C. M. Lieber, *Science* **2001**, *291*, 630
5. C. T. Kresge, M. E. Leonowicz, W. J. Roth, J. C. Vartulli, J. S. Beck, *Nature* **1992**,

359, 710

6. D. M. Antonelli, J. Y. Ying, *Angew. Chem.* **1995**, *107*, 2202; *Angew. Chem. Int. Ed. Engl.* **1995**, *34*, 2014
7 D. M. Antonelli, J. Y. Ying, *Angew. Chem.* **1996**, *108*, 461; *Angew. Chem. Int. Ed. Engl.* **1996**, *35*, 426
8. M. Vettraino, M. Trudeau, D. M. Antonelli, *Adv. Mater.* **2000**,*12*, 337
9. X. Hu, B. O. Skadtchenko, M. Trudeau, D. M. Antonelli, *J. Am. Chem. Soc.* **2006**,*128*, 11740
10. Y. Rao, M. Trudeau, D. M. Antonelli, *J. Am. Chem. Soc.* **2006**, *128*, 13996
11. H. Yoshitake, T. Sugihara, T. Tatsumi, *Chem. Mater.* **2002**, *14*, 1023
12. V. Petkov, P. N. Trikalitis, E. S. Bozin, S. L. Billinge, T. Vogt, M. G. Kanatzidis, *J. Am. Chem. Soc.* **2002**, *124*, 10157
13. K. J. D. MacKenzie, M. E. Smith, *Multinuclear Solid State NMR of Inorganic Materials*, Pergamon, Oxdord, **2002**.
14. S. E. Ashbrook, M. E. Smith, *Chem. Soc. Rev.* **2006**, *35*, 718
15. B. JuliMn, C. Gervais, E. Cordoncillo, P. Escribano, F. Babonneau, C. Sanchez, *Chem. Mater.* **2003**, *15*, 3026
16. B. Julian, C. Gervais, M. N. Rager, J. Maquet, E. Cordoncillo, P. Escribano, F. Babonneau, C. Sanchez, *Chem. Mater.* **2004**, *16*, 521
17. M. Filowitz, R. K. C. Ho, W. G. Klemperer, W. Shum, *Inorg. Chem.* **1979**, *18*, 93
18. J. L. Waring, R. S. Roth, H. S. Parker, *J. Res. Natl. Bur. Stand. Sect. A* **1973**, *77*, 703
19. O. B. Lapina, D. F. Khabibulin, K. V. Romanenko, Z. H. Gan, M. G. Zuev, V. N. KrasilNnikov, V. E. Fedorfov, *Solid State Nucl. Magn. Reson.* **2005**, *28*, 204

20. T. J. Bastow, P. J. Dirken, M. E. Smith, H. J. Whtifield, *J. Phys. Chem.* **1996**, *100*, 18539

21. E. R. H. van Eck, M. E. Smith, S. C. Kohn, *Solid State Nucl. Magn. Reson.* **1999**, *15*, 181

22. S. Inagaki, S. Guan, T. Ohsuna, O. Terasaki, *Nature* **2002**, *416*, 304

23. M. Mamak, N. Coombs, G. A. Ozin, *J. Am. Chem. Soc.* **2000**, *122*, 8932

24. X. Zou, T. Conradsson, M. Klingstedt, M. S. Dadchov, M. O'Keefe, *Nature* **2005**, *437*, 716

Chapter 3

Sulfated and Phosphated Mesoporous Nb Oxide in the Benzylation of Anisole and Toluene by Benzyl Alcohol

This chapter is organized based on a communication paper published in Journal of the American Chemistry Society, by **Yuxiang Rao**, Michel Trudeau and Dave M. Antonelli

3.1 Introduction

Acid catalyzed conversions of hydrocarbons have been studied for several decades. Because of the environmental hazards associated with the use of liquid acids, much effort has been put into developing more environmentally friendly solid acids to perform the same function. Solid acids are mineral oxides such as sulfated zirconia that contain both Lewis and Brønsted acid sites. These materials are used in the isomerization of alkanes and other petrochemical processes such as alkylation of aromatics and hydrocarbon

cracking. Isomerization of linear hydrocarbons is performed commercially using solid Pt/chlorided Al_2O_3 catalysts in the case of n-butane (UOP Butamer process or BP process), and Pt/mordenite zeolite (Shell Hysomer) in the case of C5/C6 alkanes [1]. Trace amounts of transition metals such as Fe, Mn, or Pt [2] can promote isomerization by sulfated zirconia to the extent that the catalyst performs at room temperature or lower, rivaling the performance of liquid acid agents. [2] Despite this high activity, sulfated zirconia has two major problems. These are (a) the low surface area and porosity of the material and (b) rapid deactivation owing to build up of carbonaceous deposits on the oxide surface. Thus, a higher surface area transition metal oxide catalyst with larger pores, resistant to blockage by carbonaceous deposits, is required. While the tailoring of super acidity into mesoporous silica has been thwarted by deactivation and instability to acids, MCM-41 has been used as a support for sulfated zirconia [3], although extension to more active Fe/Mn doped systems has not yet been reported. Al-Daous et al. [4] described the synthesis 3-d ordered macroporous sulfated zirconia with 120 m^2/g surface area that shows catalytic activity for n-butane isomerization. Mesoporous phosphated zirconias with high surface acidity have also been studied by Wong and Ying, although competing layered phases were observed under the conditions of study [5]. Because of the ease of preparation, enormous surface areas (400-900 m^2/g), controlled pore sizes, and accessible variable oxidation states, amine-templated mesoporous Nb (Nb-TMS1) and Ta oxides (Ta-TMS1) [6] are ideal catalyst materials [6]. Nb and Ta oxides exhibit special properties such as high stability, strong metal support interaction (SMSI), and potential for the formation of unique mixed metal oxides, as well as variable acidic properties, crucial to alkane isomerization and alkylation reactions [7]. Hydrated Nb and Ta oxides are highly acidic in the amorphous form [8], while partially hydrated Nb oxide, calcined at moderate

temperatures, is an effective solid acid catalyst. These properties can be maintained even in the presence of water [9]. Nb oxides pretreated with phosphoric or sulfuric acid are solid acid catalysts with a high ratio of Lewis acidity to Brønsted acidity [10,11]. Generally, Lewis acidity is found in all of the supported Nb oxide systems, while Brønsted acid sites are only detected in niobia supported on alumina and silica [12]. Precious metal dopants improve the activity of Nb and Ta oxides in many hydrocarbon reactions while maintaining their high selectivity [13]. Herein we provide a report of the synthesis, characterization, and catalytic properties of mesoporous sulfated and phosphated Nb oxides. The catalytic activity in the benzylation of anisole is studied and compared to standard Nb phosphate and sulfate acid catalysts.

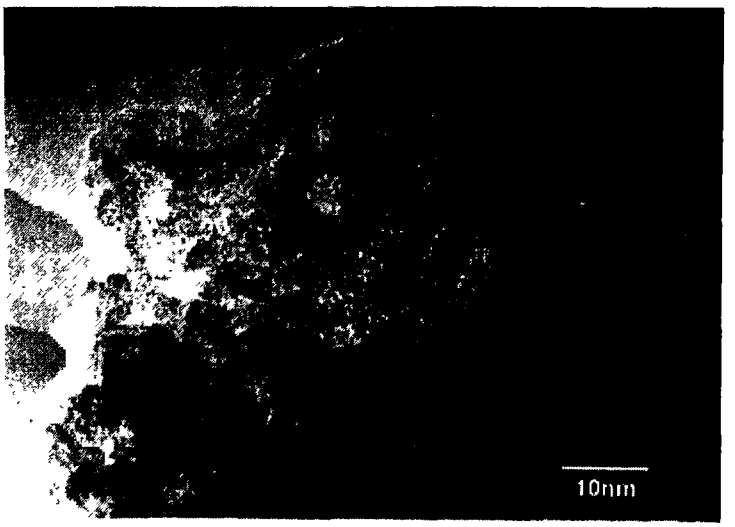

Figure 3.1 TEM image of sulfated mesoporous Nb oxide synthesized with a dodecylamine template.

The synthesis of niobium oxide molecular sieve (Nb-TMS1) was successfully achieved by using the ligand-assisted liquid crystal templating approach; the optimized ratio of dodecylamine-to-Nb-$(OEt)_5$ used was 0.3:1 [6]. The as-synthesized samples were

further treated with 1 M sulfuric acid or phosphoric acid (in methanol solution) separately to obtain mesoporous sulfated and phosphated Nb oxides. Elemental analyses showed that the samples were 1.15 wt % P and 2.03 wt % S for the phosphated and sulfated samples, respectively.

Figure 3.3 shows the XRD patterns of pure Nb oxide and sulfated and phosphated Nb oxides. The strong reflection at d= 32Å in all samples demonstrates the retention of the mesoporous structures after acid treatment. Nitrogen adsorption/desorption measurements (Figure 3.4) show a typical type IV isotherm for the sulfated and phosphated materials, further confirming that the mesoporous structure was retained. This stability to acid is surprising considering that mesoporous silica and alumina lose their pore structure under these conditions. Figure 3.1 shows a transmission electron micrograph (TEM) of mesoporous Nb oxide treated with sulfuric acid, clearly illustrating the wormhole pore structure of this material. It can be estimated from the image that the average pore size of H_2SO_4/Meso Nb is around 20 Å.

The FTIR (Fourier transform infrared, Figure 3.5) analysis of the spectra of pyridine adsorption show that Brønsted (1540 cm^{-1}) and Lewis (1450 cm^{-1}) acid sites coexist in a roughly 50:50 mixture on the surfaces of the parent material and that the sulfated and phosphated materials exhibit a strong dominance of Brønsted sites. This distribution of acid sites is unusual from the standpoint of bulk niobia (see above) [12] and demonstrates the unique nature of the inner surface of the Nb oxide mesostructure. To further probe the surface acidity of these mesoporous Nb oxides, the Hammett acidity and n-butylamine titration methods [14] were employed.

Commercially available bulk niobium pentoxides were used here as standards to gauge the effect of the mesoporous structure on acidity (Table 3.1, 3.2). From these data it is clear that bulk niobia possesses only very weak acidic sites on the surface (pK_a =+3.3), even for the sulfated and phosphated samples (pK_a = -3.0).

In contrast, pure mesoporous Nb oxide has a surprising high surface acidity *Ho*< -6.6, and after being treated with 1 M sulfuric or phosphoric acid, its *Ho* value can reach as low as -8.2, equal to 90% sulfuric acid [14]. Table 3.2 shows the n-butylamine titration data for these materials. The sulfated mesoporous material possesses 10 times more total Lewis and Brønsted acid sites (31.78 mmol/g) than the parent (2.478 mmol/g) or phosphated (3.086 mmol/g) oxides, and almost 100 times more acid sites than the bulk samples (0.024-0.338 mmol/g). The higher BET surface areas (Table 3.3) of the mesoporous materials can account for some of this difference, although it is also clear that sulfate is more effective than phosphate in generating surface acid sites.

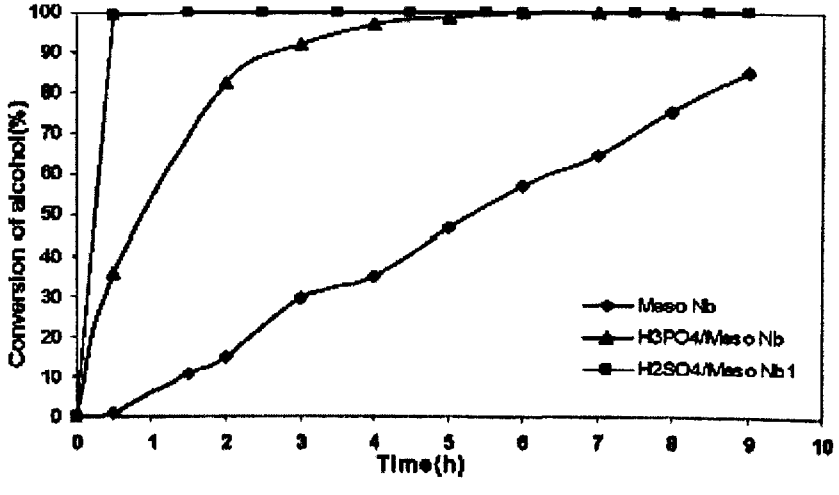

Figure 3.2. Percent conversion of benzyl alcohol in benzylation of anisole catalyzed by different mesoporous Nb oxides.

The catalytic activities of these mesoporous Nb oxide materials and bulk Nb oxides were evaluated in the benzylation of anisole with benzyl alcohol in liquid phase at reflux temperature of the mixture [10a] (Figure 3.2, Scheme 3.1). These relatively bulky substrates were used to illustrate the diffusion advantages of the mesoporous system. Bulk Nb_2O_5 show moderate catalytic activities similar to those reported by Morais et al. [10a] (Figure 3.6). The untreated mesoporous Nb oxide has an activity of ca. 8 times (80% in 9 h) that of the sulfated bulk material (10% in 9 h), while the phosphated mesoporous sample possesses an activity almost 20 times higher than this value. The best results were achieved with the sulfated mesoporous oxide, which showed 100% conversion in only 30 min. This activity is ca. 200 times greater than that of the sulfated bulk oxide, and can be attributed to the higher acid strengths, greater number of acid sites, and more ideal diffusion properties in the mesoporous sample. Since the phosphated and sulfated materials possess a similar strength and distribution of acid sites, the greater activity of the latter over the former is likely due to the greater number of acid sites in the sulfated material. This material also showed > 50 times greater activity than the phosphated or parent mesoporous sample in the benzylation of toluene (Figure 3.7). A mixture of products was obtained in all cases, and surface areas of catalyst ca. 10 m^2/g after reactions and > 12 wt % C indicated that rapid polymerization of the neat reactants may have occurred over the course of the reaction, resulting in pore blockage. This excess C could not be washed out. The S content dropped in the used catalyst to ca. 0.5%, and the catalyst could not be reused. To offset the effects of sulfate leaching and formation of polymers, further optimization of reaction conditions is obviously necessary.

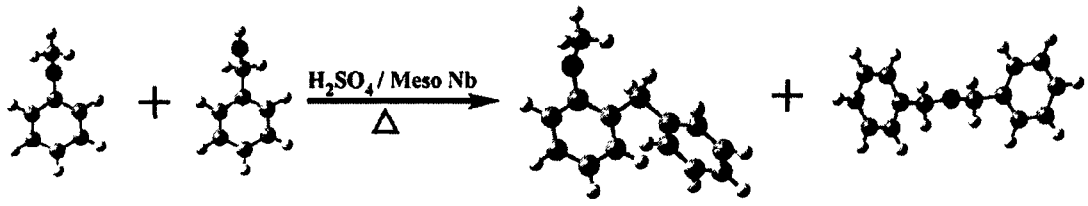

Scheme 3.1 Graphic illustration of anisole reaction with benzyl alcohol over mesoporous Nb oxides.

Amberlyst 15 and MCM-41 were chosen as standards to compare the catalytic activities in this study. The results showed that Amberlyst 15 possesses roughly 1.5 times higher activity than sulfated mesoporous Nb oxide, while MCM-41 has no activity at all. Our catalyst is also three times more active in this reaction than SiO_2-Si-SCF_3 [15]. Since our material has tunable pores in the 15~30 Å range, it is anticipated that it may find applications in size and shape selective acid-catalyzed reactions for molecules too large to fit in zeolite pores, yet small enough that the macroporous (200~300Å) structure of Amberlyst 15 would have no effect on the steric profile of the reaction.

3.2 Conclusion

In summary, a series of high surface area mesoporous niobium oxide materials with a range of acidity of *Ho* value from -6.6 to -8.2 were prepared and screened for activity in the acid-catalyzed benzylation of anisole. The sulfated material showed the highest activity, almost 200 times greater than bulk sulfated standard. The high activities were attributed to the mesoporosity and increased concentration of Brønsted sites on the surface of the mesoporous channels.

3.3 Supporting Information

3.3.1 Synthesis of mesoporous niobium oxide materials

In a typical preparation, niobium ethoxide (50g, 157.1mmol) was warmed with dodecylamine (8.7372g, 47.13mmol) using a heat gun until a homogeneous colorless solution was obtained. To this solution was added 1L of distilled water with stirring. A white gelatinous precipitates formed immediately. After precipitation occurred, hydrochloric acid (0.1743g, 4.713mmol) was added directly to the solution before the white solid was allowed to sit at room temperature overnight. The mixture was heated at 40°C for 2 days, 60°C for 2 days, 80°C for 2 days, and 95°C for 4 days. After filtration, the solid was dried in an oven at 95°C for 1~2 hours, sealed in a tube, and heated to 120°C for 2 days and 140°C for 2 days. The product was then collected and washed five times with methanol to remove the surfactant. Each washing cycle was conducted for 24 h in a large beaker with vigorous stirring followed by filtration. For the first wash, p-toluene sulfonic acid (9.8615g, 51.843mmol) was added to the solution with 200ml diethyl ether. For the second wash, 0.8965g p-toluene sulfonic acid was added to methanol solution. The solid was then collected and dried for 24 h at 120°C. The template-free samples were then treated with 1M sulfuric acid or phosphoric acid (in methanol) and filtered to obtain the mesoporous sulfated or phosphated Nb oxides.

3.3.2 Characterization

X-ray powder diffraction data were recorded on a Siemens D5000-2θ diffractometer using Cu Kα radiation. Nitrogen adsoption and desorption data were collected on a

Micromeritics ASAP 2010. High-resolution transmission electron microscopy (TEM) images were obtained by using a H9000 HR-TEM operated at 300 kV. FTIR experiments were performed on Bruker Vector 22 FT-IR spectrometer. Elemental analyses were performed by Galbraith lab (Knoxville, TN) for P and S, and locally at the University of Windsor for C, H, and N on a Perkin Elmer Series II Analyzer 2400.

3.3.3 Catalytic Runs

A 100 mL round-bottom 3-neck flask provided with a reflux condenser was used as a stirred batch reactor to test the catalytic activities of the materials. Nitrogen was introduced into the flask through one of the gas inlets. The second inlet was equipped with a septum for sample removal. 50ml of Anisole or Toluene and 5 ml of Benzyl alcohol were added to the reactor with 0.5g catalysts at each run. The reactant mixture was refluxed with stirring at atmospheric pressure and constant temperature (controlled oil bath temperatures of 170°C for anisole and 130°C for toluene). Samples of the reaction mixture were periodically withdrawn and analyzed by using a Varian CP-3800 gas chromatograph equipped with a hydrogen flame ionization detector system and capillary column CP-SIL 5CB (15 m, 0.25 mm ID), the temperature was programmed from 50 to 300 °C (10°C/min) with H_2 1ml/min as carrier gas. The results from GC identify the o- and p- benzylation products and benzyl ether as the main products of these reactions. Activities were calculated on the basis of percentage conversion benzyl alcohol in the starting mixture.

Table 3.1. Distribution of the acidic strength with Hammett indicators

Indicator	pKa	Nb_2O_5	H_2SO_4 /Nb_2O_5	H_3PO_4 /Nb_2O_5	Meso Nb	H_2SO_4 /Meso Nb	H_3PO_4 /Meso Nb
Methyl red	+5.0	+	+	+	+	+	+
Methyl yellow	+3.3	+	+	+	+	+	+
Crystal Violet	+0.8	-	+	+	+	+	+
Dicinnamalacetone	-3.0	-	+	+	+	+	+
2,4-Dinitroaniline	-4.4	-	-	-	+	+	+
Benzalacetophenone	-5.6	-	-	-	+	+	+
2-Bromo-4,6-dinitroanil	-6.6	-	-	-	+	+	+
9,10-Anthraquinone	-8.2	-	-	-	-	+	+
3-Nitrotoluene	-11.99	-	-	-	-	-	-
1-chloro-4-Nitrobenzen	-12.70	-	-	-	-	-	-
2,4-Dinitrofluorobenzen	-14.52	-	-	-	-	-	-

+": color changed "-": color unchanged

Table 3.2. The amount of acids as mmol/g, as calculated from n-butylamine titration

Indicator	Nb_2O_5	H_2SO_4/ Nb_2O_5	H_3PO_4/ Nb_2O_5	Meso Nb	H_2SO_4/ Meso Nb	H_3PO_4/ Meso Nb
Methyl yellow	0.024	0.338	0.317	2.478	31.784	3.086

Table 3.3.The internal structure and surface properties of catalysts before and after reaction

Sample	BET surface area (m^2/g)	Volume (cm^3/g)	BJH Pore size (A)
Nb_2O_5	3.63	N/A	N/A
H_2SO_4/Nb_2O_5	5.29	N/A	N/A
H_3PO_4/Nb_2O_5	2.96	N/A	N/A
Meso Nb	612.63	0.3956	22.7
*Meso Nb (Anisole)	587.90	0.3123	20.6
*Meso Nb (Toluene)	386.04	0.2088	20.6
H_2SO_4/Meso Nb	519.10	0.3408	20.6
*H_2SO_4/Meso Nb (Anisole)	84.71	0.1409	37.2
*H_2SO_4/Meso Nb (Toluene)	3.35	0.004	51.1
H_3PO_4/Meso Nb	502.81	0.3286	20.7
*H_3PO_4/Meso Nb (Anisole)	76.38	0.0932	39.5
*H_3PO_4/Meso Nb (Toluene)	6.41	0.0146	47.0

* Denotes surface areas after reaction with substrate in bracket.

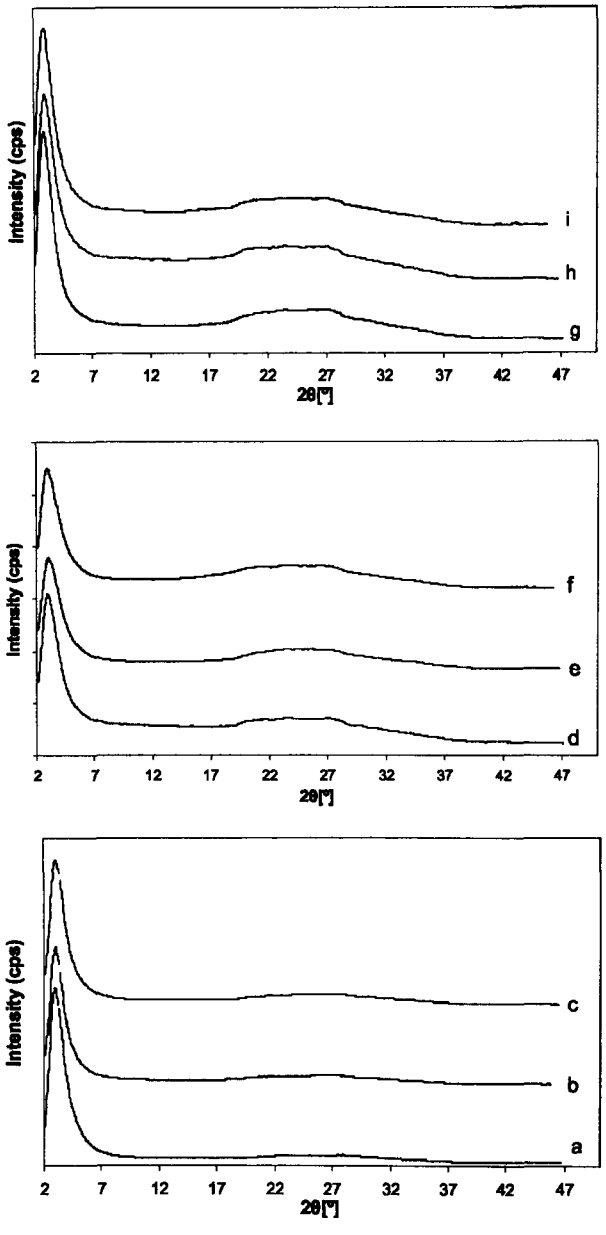

Figure 3.3 X-ray diffraction patterns of Nb-TMS samples. a) meso Nb oxide, b) meso Nb oxide after reaction with anisole, c) meso Nb oxide after reaction with toluene, d) H_2SO_4/meso Nb oxide, e) H_2SO_4/meso Nb oxide after reaction with anisole, f) H_2SO_4/meso Nb oxide after reaction with toluene, g) H_3PO_4/meso Nb oxide, h) H_3PO_4/meso Nb oxide after reaction with anisole, i) H_3PO_4/meso Nb oxide after reaction with toluene

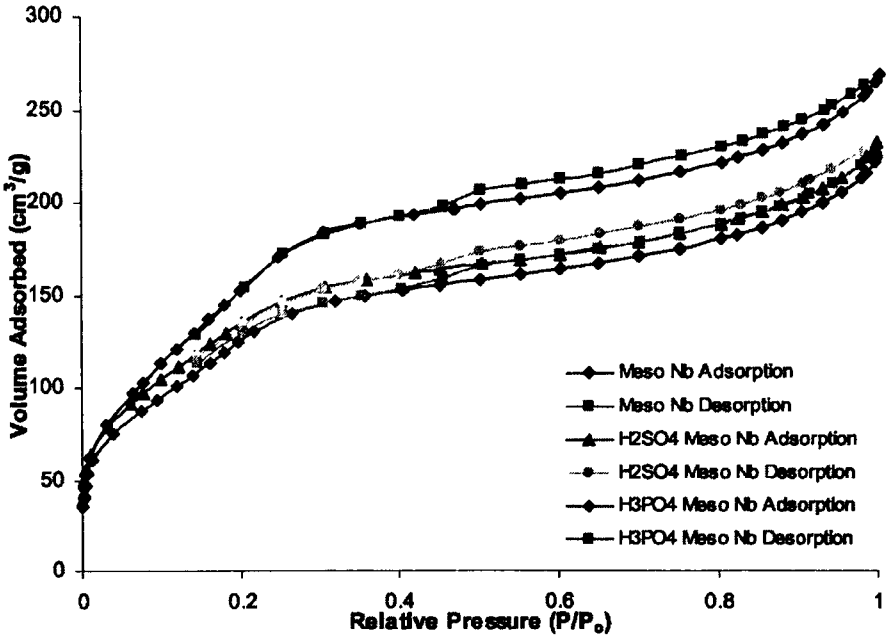

Figure 3.4. Nitrogen adsorption/desorption isotherms of pure and sulfated mesoporous Nb oxides synthesized with n-dodecylamine

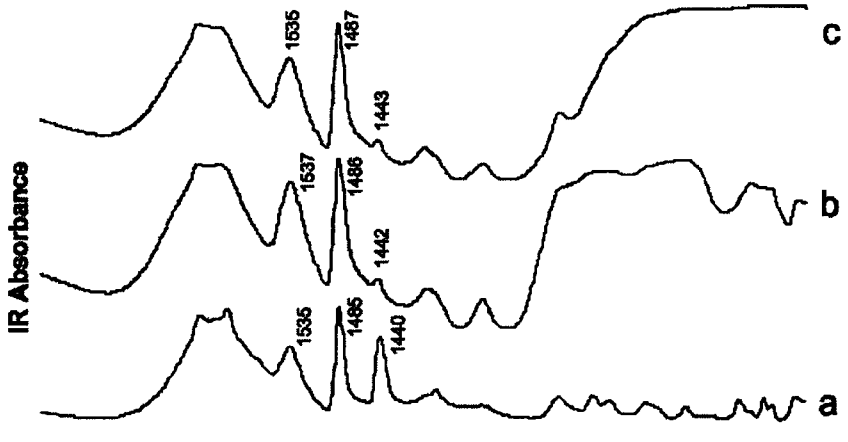

Figure 3.5. The FTIR spectra of different meso Nb oxides after pyridine vapor adsorption. a) Meso Nb, b) H_2SO_4/Meso Nb, c) H_3PO_4/Meso Nb

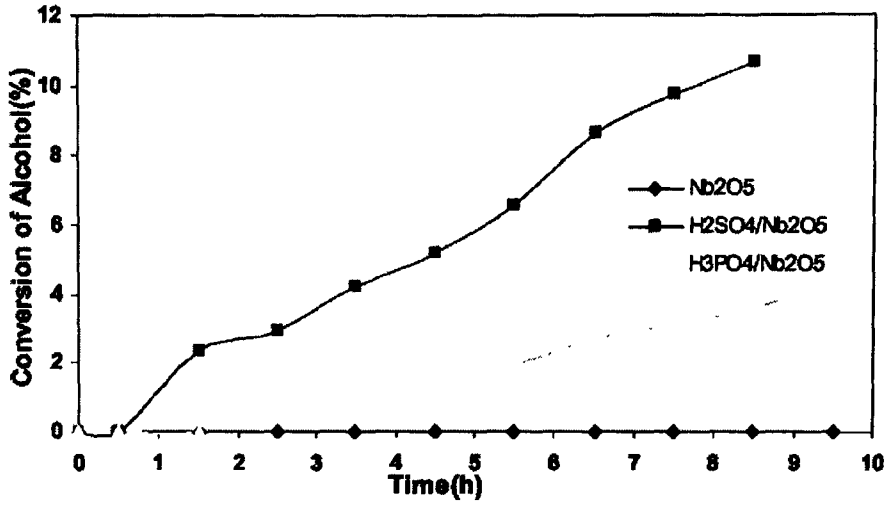

Figure 3.6 Percent conversion of benzyl alcohol in the benzylation of anisole catalyzed by different bulk Nb oxides

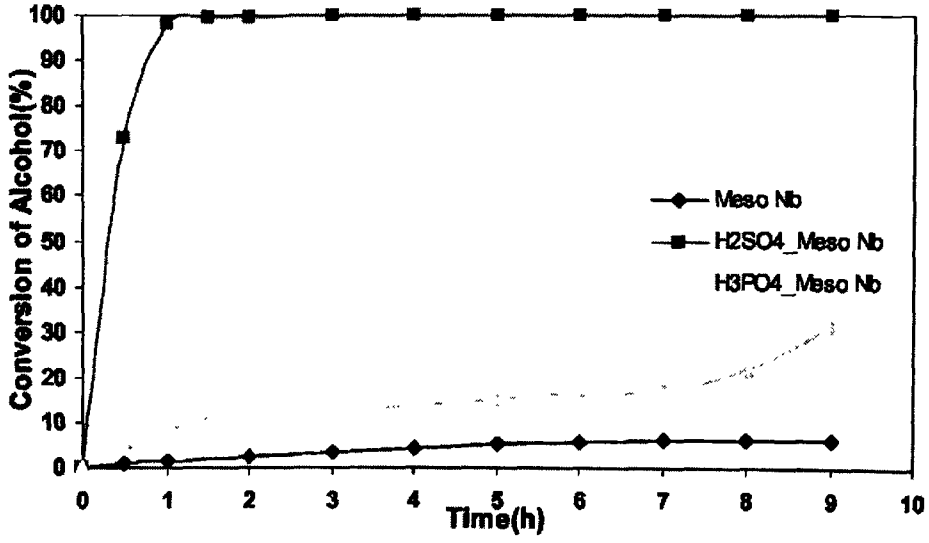

Figure 3.7 Percent conversion of benzyl alcohol in the benzylation of toluene catalyzed by different mesoporous Nb oxides

3.4 References

1. (a) M. Guisnet, F Alvarez, G. Giannetto, G. Perot, *Catal. Today*, **1987**, *1*, 415. (b) B. T. Carvill, B. A. Lerner, B. J. Adelman, D. C. Tomczak, W. M. Sachtler, *J. Catal.* **1993**, *144*, 1.
2. (a) M. Hino, K. Arata, *Chem. Lett.* **1979**, 1259 (b) M. Hino, K. Arata, *J. Chem. Soc. Chem. Commun.* **1980**, 851 (c) M. Hino, K. Arata, *J. Chem. Soc. Chem. Commun.* **1979**, 1148
3. Q.H. Xia, K. Hidajat, S. Kawi, *J. Chem. Soc. Chem. Commun.* **2000**, 2229
4. M. A. Al-Daous, A. Stein, *Chem. Mater.* **2003**, *15*, 2638
5. M. S. Wong, J. Y. Ying, *Nanostruct. Mater.* **1997**, *9*, 165
6. (a) D. M. Antonelli, J. Y. Ying, *Angew. Chem., Int. Ed. Engl.* **1996**, *35*, 426 (b) D. M. Antonelli, A. Nakahira, J. Y. Ying, *Inorg. Chem.* **1996**, *35*, 3126
7. (a) M. Ziolek, *Catal. Today* **2003**, *78*, 47 (b) I. Nowak, M. Ziolek, *Chem. Rev.* **1999**, *99*, 3603 (c) T. Ushikubo, *Catal. Today* **2003**, *78*, 79.
8. (a) T. Ushikubo, K. Wada, *Appl. Catal.* **1990**, *67*, 25. (b) T. Ushikubo, K. Wada, *Chem. Lett.* **1988**, 1573
9. M. Moraes, W. de S. F. Pinto, W. A. Gonzalez, L. M. P. M. Carmo, N. M. R. Pastura, E. R. Lachter, *Appl. Catal.* A **1996**, *138*, L7.
10. (a) M. Morais, E. F. Torres, L. M. P. M. Carmo, N. M. R. Pastura, W. A. Gonzalez, A. C. B. dos Santos, E. R. Lachter, *Catal. Today* **1996**, *28*, 17 (b) C. Guo, Z. Qian, *Catal. Today* **1993**, *16*, 379
11. (a) J.M. Jehng, I. E. Wachs, *Catal. Today* **1993**, *16*, 417 (b) I. E. Wachs, Y. Chen, J.M. Jehng, L. E. Briand, T. Tanaka, *Catal. Today* **2003**, *78*, 13

12. J. Datka, A. M. Turek, J. M. Jehng, I. E. Wachs, *J. Catal.* **1992**, *135*, 186

13. D. A. G. Aranda, A. L. D. Ramos, F. B. Passos, M. Schmal, *Catal. Today* **1996**, *28*, 119

14. M. Yurdakoc, M. Akcay, Y. Tonbul, K. Yurdakoc, *Turk. J. Chem.* **1999**, *23*, 319

15. D.Q. Zhou, J.H. Yang, G.M. Dong, M.Y. Huang, Y. Y. Jiang, *J. Mol. Catal. A. Chem* **2000**, 159, 85

Chapter 4

Sulfated Mesoporous Tantalum Oxides in the Shape Selective Synthesis of Linear Alkyl Benzene

This chapter is organized based on a paper published in Angewandte. Chemie. International. Edition, by Junjie Kang, **Yuxiang Rao**, Michel Trudeau and Dave M. Antonelli

4.1 Introduction

Linear alkylbenzenes (LAB), the primary intermediates in detergent industry, are commercially manufactured by the alkylation of benzene with C_{10-14} n-alkenes [1–3]. Among LAB isomers, 2-phenyl isomers are the most favorable starting materials for the production of ecofriendly domestic and industrial detergents because of their high solubility and biodegradability [4]. The development of catalysts with a high selectivity to

2-phenyl isomers in benzene alkylation is an area of great interest. The alkylation of benzene with olefins proceeds through a carbonium ion mechanism [5]. The relative stability of the formed carbonium ions increase with the carbon number towards the center of olefin chains. When homogeneous catalysts such as HF or $AlCl_3$ are used, a thermodynamic mixture of LAB isomers is always obtained. In addition to their low selectivity to the desired 2-phenyl isomers, the use of highly corrosive and toxic HF or $AlCl_3$ poses disposal problems. Considerable efforts have been made to carry out alkylation reactions over environmentally friendly solid acid catalysts [6–11]. Strength, distribution and number of acid sites, surface area, pore size, geometry and pore size distribution, and hydrogenation/dehydrogenation ability of solid acid catalysts are the key factors that determine their activity and selectivity in alkylation reactions. Studies on the alkylation of benzene with 1-dodecene over FAU, BEA and EMT zeolites showed that the selectivity towards the least bulky 2-phenyldodecane increased with an increase of porous constraints, while activity decreased due to diffusion limitation in the channels [12]. The very low activity of H-ZSM5 indicated that its channels did not provide enough space for the formation of the potential bulky LAB isomers. The larger pore openings of H-USY improved the diffusion of reactants and products, leading to 100 % conversion, but lower 2-phenyldodecane selectivity (25.5 %) [13].

Mesoporous materials exhibiting surface areas from 300-2000 m^2/g and controlled pore sizes offer high reaction rates and overall efficiency because of a greater number of available surface sites per gram of catalyst and better diffusion rates. Furthermore, the selectivity to desired products can be tuned by optimizing the pore size of mesoporous catalysts. The monoalkylation selectivity for benzene alkylations was significantly

enhanced to 89.9 % when $AlCl_3$ was grafted onto mesoporous molecular sieves [14]. Shape selective synthesis of LAB has been carried out over AlMCM-41/Beta zeolite composites, which combined the advantages of both microporous and mesoporous materials [15]. Though a high 2-phenyldodecane selectivity (76%) was achieved, the upper conversion limit was only 48 % even at 120 °C after 2 h.

Nb and Ta oxides exhibit special properties such as high stability, variable oxidation states useful in tailoring catalytic properties, as well as variable acidic properties crucial to acid catalyzed reactions. For example, niobic acid is an active catalyst for the alkylation of benzene with methanol and the catalytic activity is markedly enhanced when the catalyst was treated with a dilute phosphoric acid solution [16,17]. Because of their high surface area (400~900 m^2/g) and controlled pore sizes (20~100Å) [18–20], mesoporous Nb and Ta oxide could be potential catalysts for alkylation reactions and rival those of non-porous Nb and Ta oxides. In recent studies from our group, sulfated mesoporous Nb oxide showed extremely high catalytic activity, almost 200 times greater than sulfated bulk oxide in the benzylation of anisole with benzyl alcohol [21]. Mesoporous Ta oxide is more thermally stable [22] and thus shows even greater promise as a catalyst than its Nb counterpart. Herein, we report the catalytic properties of sulfated mesoporous Ta oxides for the alkylation of benzene with bulky olefins.

Mesoporous C_{12}-Ta oxide was prepared using the ligand-assisted templating approach with 1-dodecylamine surfactant. The sulfated samples were produced by treating the template free Ta oxides with sulfuric acid. The (100) reflection in the XRD pattern of sulfated mesoporous C_{12}-Ta oxide demonstrates the retention of the mesoporous structure after sulfuric acid treatment. The type IV N_2 adsorption/desorption

isotherms further confirmed the confined mesoporous structure in the sulfated sample. The BET surface area was found to be reduced from 582.7 m^2/g to 292.2 m^2/g by sulfuric acid treatment.

The Hammett acidity and acid amounts of Ta catalysts are summarized in Table 4.1. Sulfuric acid treatment leads to the increase in both acid strength and acid amount of mesoporous C_{12}-Ta oxide, which are essential to alkylation reactions. The FT-IR spectrum in Figure 4.1 shows that the sulfated mesoporous C_{12}-Ta oxide possesses mainly Brønsted-acid sites (1538 cm^{-1}) with a smaller number of Lewis-acid sites (1448 cm^{-1}), while Lewis-acid sites are dominant on H-Y and H-ZSM5 zeolites.

Table 4.1: Hammett acidity and acid amount of solid acid catalysts.

Catalyst	H_0	Acid amount [mmol/g]
Meso C_{12}-Ta	-6.6	0.40
Meso SO_4^{2-}/C_{12}-Ta	-8.2	19.8
Meso C_{12}-Nb	-6.6	2.48
Meso SO_4^{2-}/C_{12}-Nb	-8.2	31.78
H-Y zeolite	-6.6	1.55
H-ZSM5	-4.4	16.1

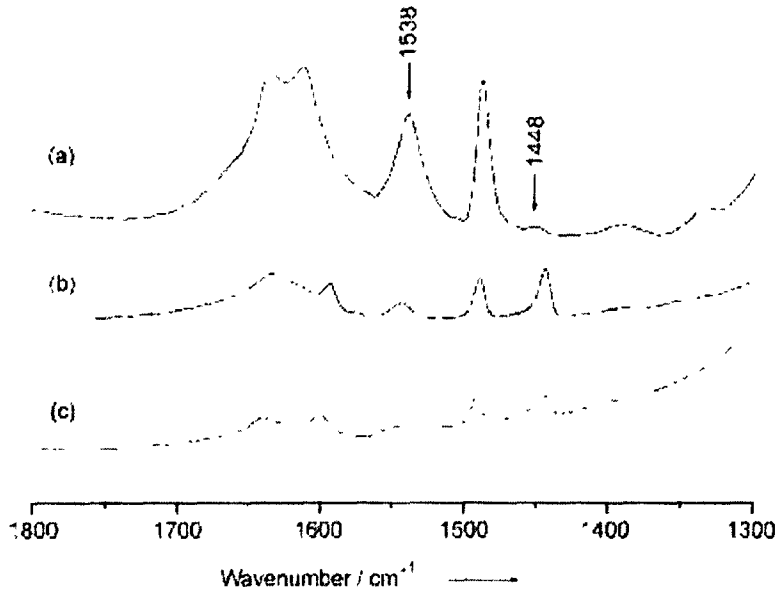

Figure 4.1 FT-IR spectra of pyridine adsorbed on a) sulfated mesoporous C_{12}-Ta oxide, b) H-Y and c) H-ZSM5 zeolites

The catalytic properties of sulfated mesoporous C_{12}-Ta oxide were evaluated in terms of olefin conversion and the selectivity towards 2-phenyl isomers (Scheme 4.1). At 80 °C and a benzene/ olefin molar ratio of 10:1, no oligomerization of 1-dodecene was observed and only monoalkylated phenyldodecanes were detected. As shown in Figure 4.2, 100 % 1-dodecene conversion was achieved within 0.5 h. However, the conversion was only 1.2 % over sulfated mesoporous C_{12}-Nb at 0.5 h, despite of larger number of relatively strong acid sites. The reason for this is not understood, and cannot be rationalized by the acid strength data in Table 4.1. Recent work in our group on the ^{17}O NMR of mesoporous Nb oxide showed a much more highly ordered crystal structure in the walls of this material than its Ta counterpart, which may account for the observed difference in catalytic behavior [23]. The alkylation reaction is dependent on the

chemisorption of reactants, surface reaction and desorption of products on the internal pore surface of solid acid catalysts, which are determined by their pore structures and sizes. GC results showed that all possible phenyldodecane isomers were formed. In contrast to homogeneous catalysts, the non-attainment of thermodynamic equilibrium over solid acid catalysts leads to a more favorable isomer distribution. As shown in Figure 4.3, the selectivity towards phenyldodecane isomers remains unchanged even after 6.0 h when sulfated mesoporous Ta oxide was employed as catalyst. This suggests that it is difficult for the reaction system to reach thermodynamic equilibrium due to the limited diffusion of bulky phenyldodecane isomers in the mesoporous channels.

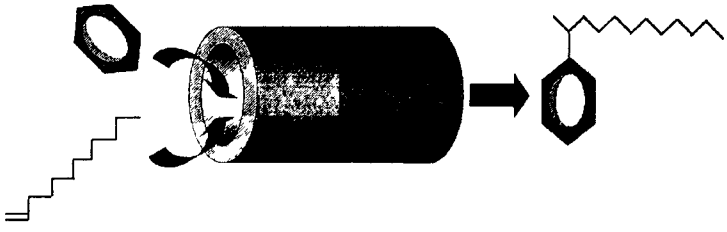

Scheme 4.1 Schematic representations of olefin conversion and the selectivity towards 2-phenyl isomers.

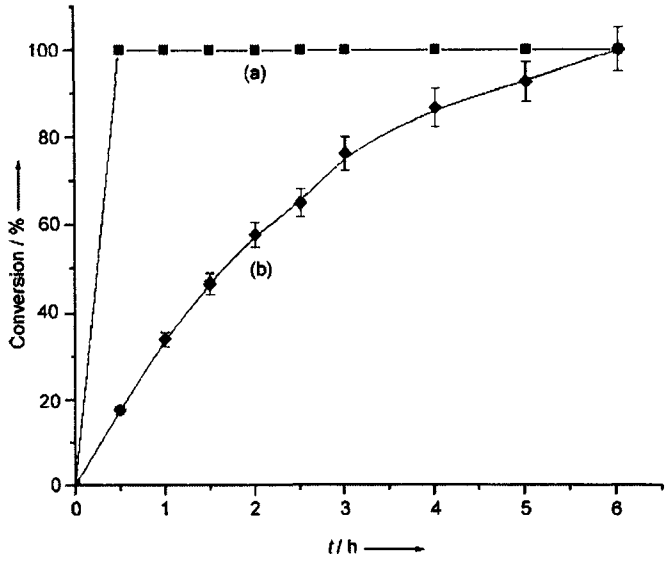

Figure 4.2. Olefin conversion in the alkylation of benzene with a) 1-dodecene and b) 1-tetradecene over sulfated mesoporous C_{12}-Ta oxide

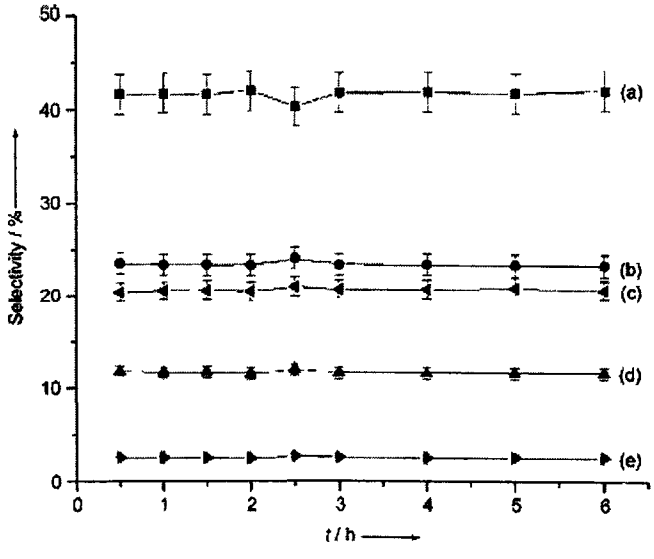

Figure 4.3. Distribution of phenyldodecane isomers over sulfated mesoporous C_{12}-Ta oxide as a function of reaction time. a) 2-phenyldodecane, b) 3-phenyldodecane, c) 5-phenyldodecane, d) 4-phenyldodecane, and e) 6-phenyldodecane. Reaction conditions: 80°C, catalyst loading = 4.0 wt.%.

Figure 4.4 shows the effect of catalyst loading on 1-dodecene conversions and 2-phenyldodecane selectivity over sulfated mesoporous C_{12}-Ta oxide. When catalyst loading was increased from 0.5 to 4.0 wt. %, 1-dodecene conversion increased from 28.8 % to 100 %, whereas the selectivity to 2-phenyldodecane decreased from 52.9 to 41.6 % at the reaction time of 0.5 h. With increased catalyst loading, the greater number of acid sites leads to higher activity, while the kinetic availability of external surface acid sites is increased relative to internal sites resulting in a decrease in the 2-phenyldodecane selectivity. Further increase in catalyst loading to 6.0 wt. % had no obvious effect on 2-phenyldodecane selectivity.

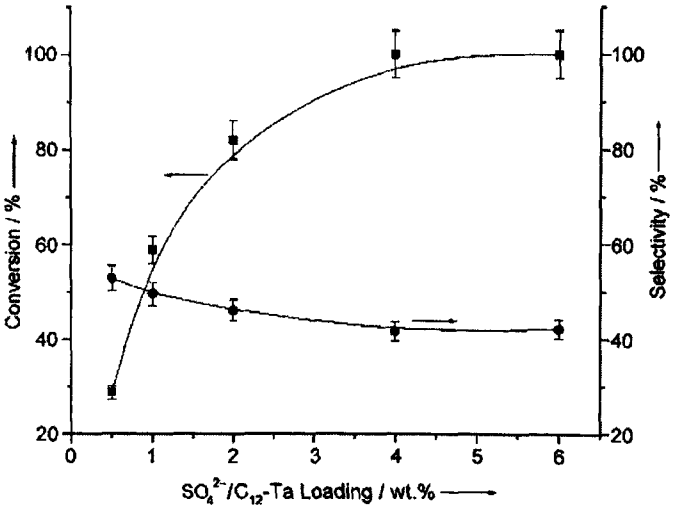

Figure 4.4 1-Dodecene conversion and 2-phenyldodecane selectivity as a function of catalyst loading (Reaction conditions: 80°C, 0.5 h)

The effect of the bulkiness of the olefin on the conversion over mesoporous C_{12}-Ta oxide was studied (Figure 4.2). When bulkier 1-tetradecene was used, olefin conversions at 0.5 h decreased greatly to 17.5 %. The longer the olefin chain, the more difficult for the olefin molecules to access to the active sites in mesopores. Therefore, activity decreased

with an increase in olefin chain length. In order to further clarify the effect of pore structure on activity, the alkylation reaction was carried out over sulfated mesoporous C_6-Ta and C_{18}-Ta oxide prepared by using 1-hexylamine and 1-octadecylamine as templates. The catalytic activity data is given in Table 4.2. The lower activity of C_6-Ta oxide is attributed to the strong diffusion resistance offered by the pore blocking in smaller pores [24]. Despite its larger pore size, sulfated C_{18}-Ta oxide showed very low activity. The low 1-dodecene conversion offered by sulfated C_{18}-Ta oxide may be caused by its relatively low surface area and extremely low pore volume, but may also be related to relative optimization of the reaction transition state by the two pore sizes. The large C_{18} pores are less effective at bringing the benzene and alkyl cation together than the intermediate C_{12} pores, while the small C_6 pores cause diffusion hindrances. Although more study may be necessary to fully elucidate this effect, a similar trend in pore size versus activity was observed in the isomerization of 1-hexene over sulfated mesoporous Ta oxide [25].

Table 4.2: Catalytic properties of solid acid catalysts in alkylation reactions

Catalyst	Olefin	Conversion [%][a]
SO_4^{2-}/C_6-Ta	1-dodecene	46.9
SO_4^{2-}/C_{12}-Ta	1-dodecene	100
SO_4^{2-}/C_{18}-Ta	1-dodecene	2.3
SO_4^{2-}/C_{12}-Nb	1-dodecene	1.2
H-Y zeolite	1-dodecene	100
H-ZSM5	1-dodecene	0
Amberlyst	1-dodecene	13.5

[a] 0.5 h at 80°C, catalyst loading=4.0 wt.%.

As one of the best solid acid catalysts for benzene alkylations,[5] H-Y zeolite (Zeolyst, Si/Al = 80) was tested for comparison. This material gave 100 % 1-dodecene conversions at 80°C within 0.5h. Though the acid amount on H-ZSM5 zeolite is comparable to that on sulfated mesoporous C_{12}-Ta oxide, no alkylation reaction was detected over H-ZSM5 at 80 °C. This can be rationalized by the diffusion limitation in the channels with smaller openings [12]. An alkylation reaction was conducted over Amberlyst 15 ion exchange resin (Aldrich). Despite the presence of strong acid sites, Amberlyst resin showed lower catalytic activity for the alkylation reaction, due to its lower surface area (55.1 m^2/g) and thus smaller amount of active sites on the internal surface of pores.

The selectivity towards the 2-phenyldodecane isomer were compared at the same conversion and summarized in Table 4.3. The selectivity over sulfated mesoporous C_{12}-Ta oxide, H-Y zeolite, and Amberlyst resin at 1-dodecene conversion of ca. 60% were 49.19%, 25.31 %, and 38.31 %, respectively. The high selectivity of sulfated mesoporous C_{12}-Ta oxide can be attributed to "confinement effects", which indicates that selectivity as well as conversion rate are pore size dependent [26]. Jaenicke et al. reported the shape-selective catalysts prepared by immobilizing $AlCl_3$ onto a series of MCM-41 mesoporous silica with different pore sizes [27]. They found that the selectivity towards monoalkylation product in the synthesis of linear alkyl benzenes can be controlled by changing the pore size of the MCM-41 supports. The mesoporous structure in our sulfated Ta oxide may offer a similar confined space for the establishment of shape selective reactions.

Table 4.3 2-Phenyldodecane selectivity over solid acid catalysts

Catalyst	Conversion [%]	Selectivity [%]
SO_4^{2-}/C_{12}-Ta	60.0	49.19
H-Y zeolite	61.1	25.31
Am berlyst	60.4	38.31

In order to examine the reusability of sulfated mesoporous C_{12}-Ta oxide, the catalyst was separated by filtration after the first run and then dried at 120 °C for 12h. The reaction was repeated under the same conditions using the recovered catalyst. The XRD pattern and N_2 adsorption/desorption isotherm after the first run confirmed the retention of mesoporous structure. However, the catalyst lost 17.4 % of its initial surface area after the first run. The catalyst used in the second run gave a 1-dodecene conversion of 26.8% at 0.5 h. The deactivation of the catalyst could be due to the blockage of the mesoporous pore by the accumulation of bulky phenyldodecane isomers during previous runs, or a small loss of sulfate by leaching as observed for the sulfated mesoporous Nb oxide in the benzylation of anisole and toluene [21]. Elemental analysis showed that the sulfur content in the sulfated mesoporous C_{12}-Ta oxide was 4.18 %, while the sulfur content was slightly decreased to 4.06 % after alkylation reaction. Therefore, the deactivation is not related to sulfate loss. The deactivated catalyst could not be regenerated by the treatment with sulfuric acid.

4.2 Conclusion

In summary, mesoporous Ta oxides were prepared and employed as solid acid catalysts in the alkylation of benzene with bulky olefins. The catalysts with optimal pore

size displayed comparable activity to H-Y zeolite, but much higher selectivity towards the desired isomer. Because of this ideal balance between high activity and selectivity, it is anticipated that this catalyst may see applications in industrial acid catalyzed reactions.

4.3 Experimental Section

Mesoporous Ta and Nb oxides were prepared as described previously [18]. The sulfated oxides were produced by stirring the template free oxides with 1 M sulfuric acid for 12 h.

Powder X-ray diffraction (XRD) patterns were recorded on a Siemens D5000-2 diffractometer using Cu Ka radiation. Nitrogen adsorption/desorption data were collected on Micromeritics ASAP 2010. FT-IR experiments were performed on Bruker Vector 22 FT-IR spectrometer. The Hammett acidity and acid amounts were measured according to literatures [28,29]. Elemental analysis was conducted in Galbraith Laboratories, Inc.

Before reaction, H-Y and H-ZSM5 zeolites were activated at 500 °C for 3 h in air, whereas sulfated mesoporous Ta and Nb oxides were dried at 120°C for 12 h. The liquid-phase alkylation reactions were carried out in a 100 mL 3-neck round-bottom flask with a reflux condenser, a nitrogen inlet and a septum. The reactant mixture was refluxed at atmospheric pressure in an oil bath. Samples were periodically withdrawn and analyzed using a Varian CP-3800 gas chromatograph.

4.4 Supporting Information

The selective synthesis of alkylbenzene is an area of great interest in detergent

industry. Because of rapid deactivation and low selectivity, the application of microporous solid acid catalysts in the alkylations involving bulky substrates was limited. In this work, mesoporous Ta oxides were treated with 1.0 M sulfuric acid and evaluated for their catalytic activity and selectivity to 2-phenyl isomers in the alkylation of benzene with bulky olefins.

The acid strength of the solid acids was determined by the color change of the indicators adsorbed on the surface of solid acid powders. Acid form of the indicators indicates that the acid strength of the solid acid is equal to or higher than that of the indicators. To show the color changes, the indicators were adsorbed on the surface of solid acids by mixing 0.2 g dried solid acids with 2.0 mL solution of indicators in benzene (0.5 wt.%). The pKa of the indicators, the corresponding wt.% of H_2SO_4 solution and color changes were summarized in Table 4.6.

The acid amounts of the solid acids were measured by the amine titration method using methyl yellow as indicator. Before titration, H-Y and H-ZSM5 zeolites were activated at 500 °C for 3h in air, whereas sulfated mesoporous Ta and Nb oxides were dried at 120 °C for 12 h. The dried samples (0.2 g) were mixed with 3.0 mL indicator solution (0.2 mg methyl yellow per 100 mL benzene) to form the red acidic state of the indicator. Then, 0.1 M n-butylamine solution in benzene was added drop wise until the end point at which the red color disappeared. The acid amounts were calculated from the amounts of n-butylamine used for the neutralization of the acid sites on solid acids.

XRD and nitrogen adsorption/desorption results demonstrated that the mesostructure was retained during acid treatment. The sulfated mesoporous Ta oxide showed comparable activity to H-Y zeolite, one of the best solid acid catalysts ever reported for

liquid-phase alkylation of benzene with olefins, but higher selectivity towards the desired isomer (2-phenyldodecane) under mild reaction conditions. The high activity and selectivity was rationalized by the eased diffusion of bulky reactants in the mesoporous frames.

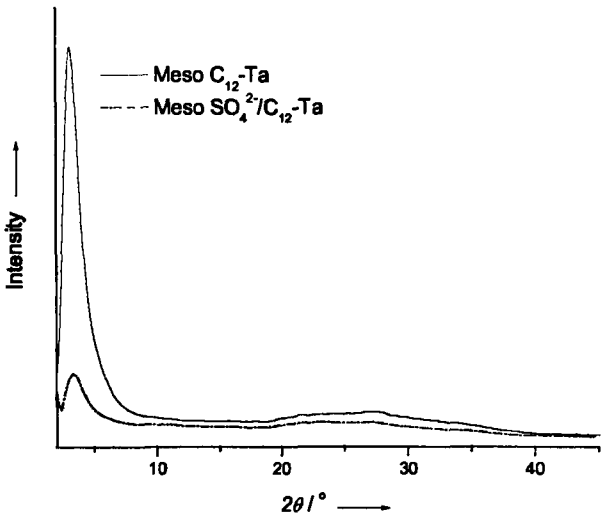

Figure 4.5 X-ray diffraction patterns of (a) mesoporous C_{12}-Ta oxide and (b) sulfated mesoporous C_{12}-Ta oxide

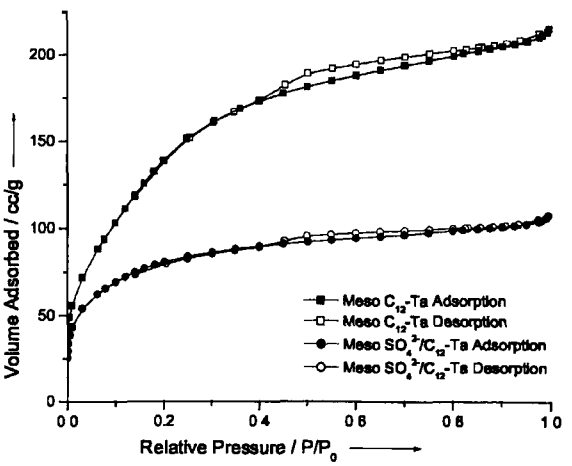

Figure 4.6 N_2 adsorption/desorption isotherms of (a) mesoporous C_{12}-Ta oxide and (b) sulfated mesoporous C_{12}-Ta oxide.

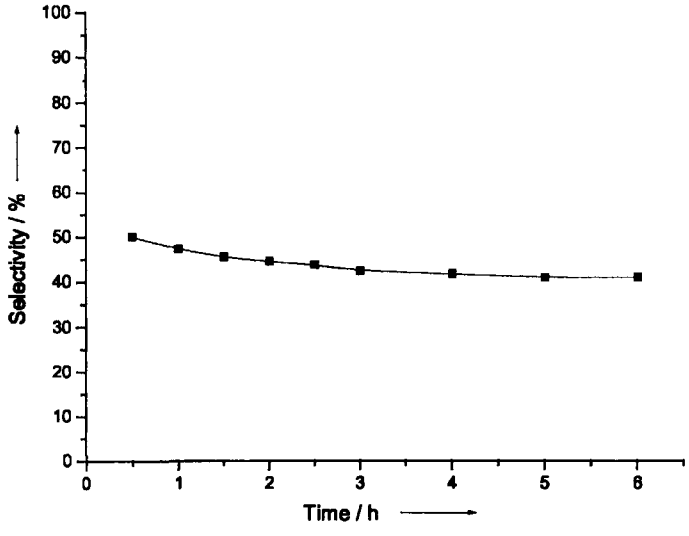

Figure 4.7 Selectivity to 2-phenyltetradecane over sulfated mesoporous C_{12}-Ta oxide. Reaction conditions: 80 °C, catalyst loading = 4.0 wt.%.

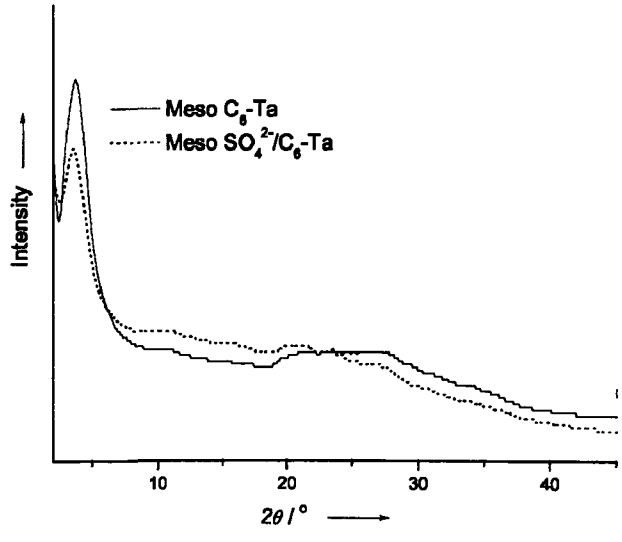

Figure 4.8 X-ray diffraction patterns of (a) mesoporous C_6-Ta oxide and (b) sulfated mesoporous C_6-Ta oxide

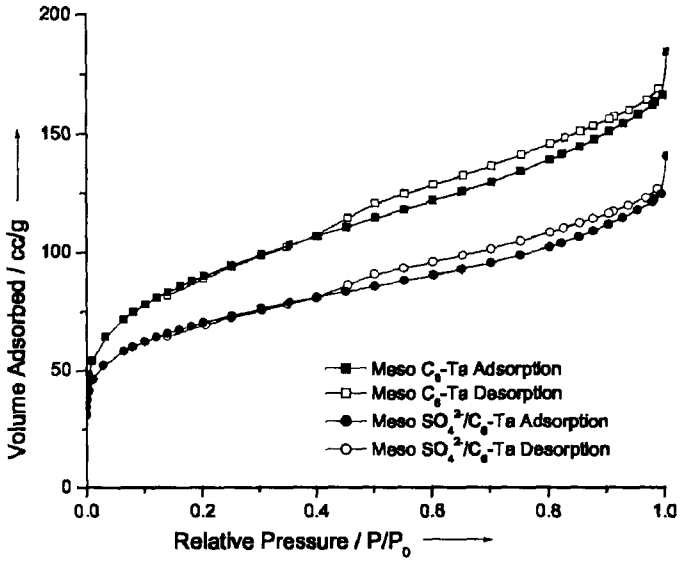

Figure 4.9 N_2 adsorption/desorption isotherms of (a) mesoporous C_6-Ta oxide and (b) sulfated mesoporous C_6-Ta oxide.

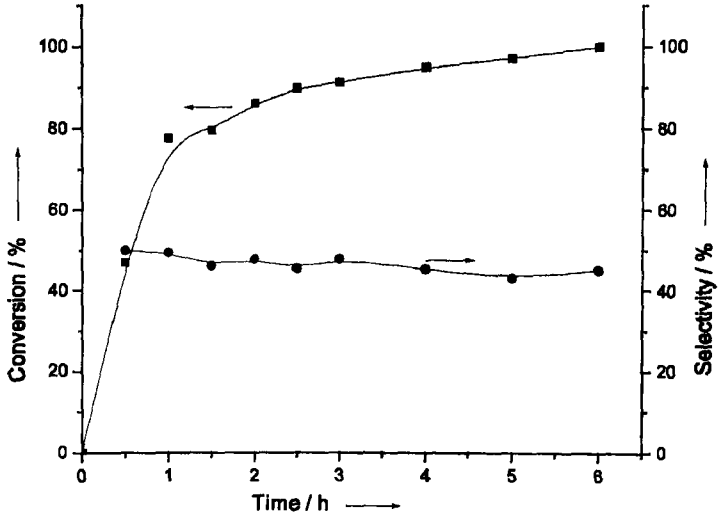

Figure 4.10 1-dodecene conversion and 2-phenyldodecane selectivity over sulfated mesoporous C_6-Ta oxide (Reaction conditions: 80 °C, catalyst loading = 4.0 wt.%)

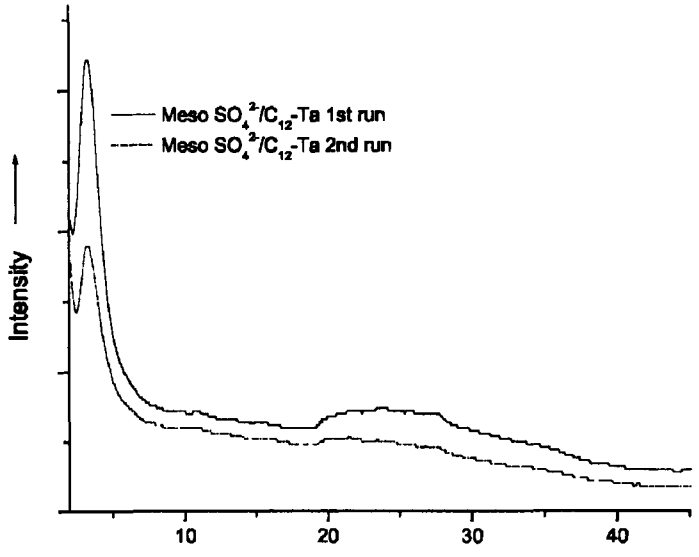

Figure 4.11 X-ray diffraction patterns of sulfated mesoporous C_{12}-Ta oxide after (a) 1 st run and (b) 2nd run.

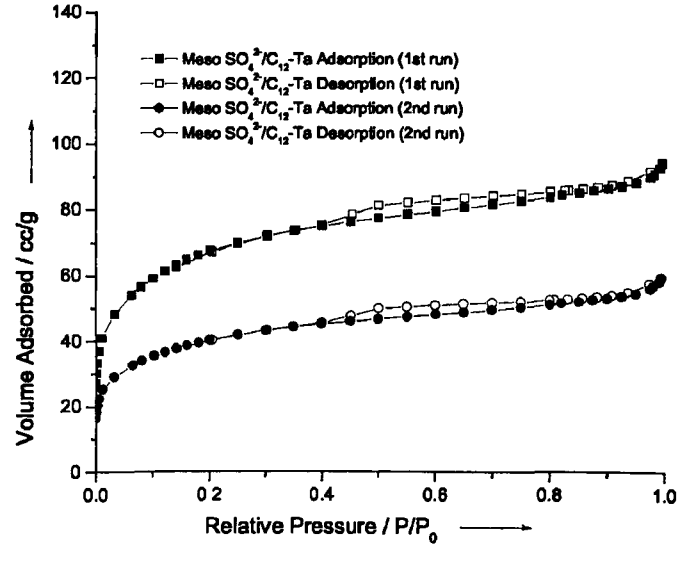

Figure 4.12 N_2 adsorption/desorption isotherms of sulfated mesoporous C_{12}-Ta oxide after (a) 1 st run and (b) 2nd run.

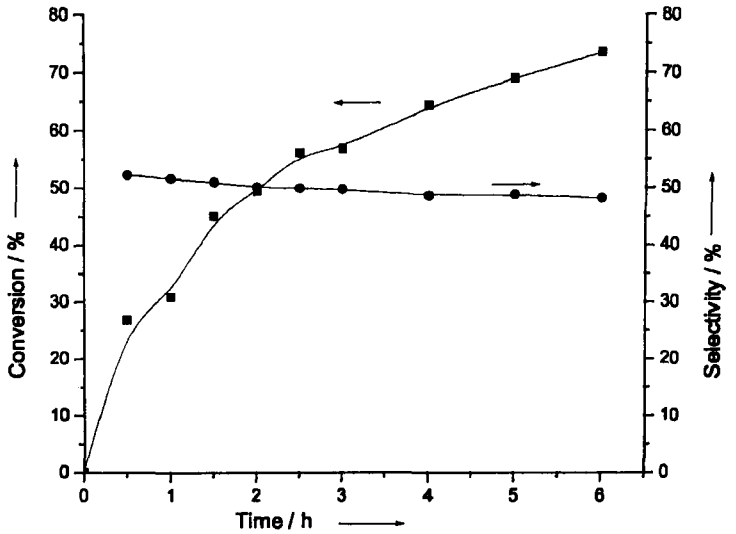

Figure 4.13 1-dodecene conversion and 2-phenyldodecane selectivity over sulfated mesoporous C_{12}-Ta oxide in 2nd run (Reaction conditions: 80 °C, catalyst loading = 4.0 wt.%)

Table 4.4. The internal structure and surface properties of mesoporous Ta and Nb oxide before and after sulfuric acid treatment

	BET surface area [m^2/g]	**Pore volume [cm^3/g]**	**BJH pore size [Å]**
Meso C_6-Ta	253.26	0.1905	17.5
Meso SO_4^{2-}/C_6-Ta	206.40	0.1314	17.0
Meso C_{12}-Ta	582.70	0.3651	18.8
Meso SO_4^{2-}/C_{12}-Ta	292.19	0.0989	18.2
Meso C_{18}-Ta	234.74	0.0538	22.7
Meso SO_4^{2-}/C_{18}-Ta	188.79	0.0347	22.5
Meso C_{12}-Nb	612.02	0.3199	20.6
Meso SO_4^{2-}/C_{12}-Nb	413.97	0.2423	20.5

properties in industrial catalysis. The relatively large pores (12-30 Å) overcome the size constraint of most zeolites, allowing more facile diffusion of bulky substrates, while the very high surface areas (200-1200 m^2/g) create a high concentration of active sites per mass of material. The transition metal centers in the inorganic framework of the mesoporous structure also possess variable oxidation states and empty d-orbitals, properties that allow electron transfer to occur between the reactants and active site during any catalytic process [4a]. Recent work in our group showed that sulfated mesoporous Nb and Ta oxides were effective catalysts for benzylation reaction [5a] due to their combination of strong acidity and large pore size. In this report, we investigate the catalytic properties of mesoporous Ta oxide in the isomerization of 1-hexene and compare the catalytic activities and selectivity with commercially available zeolites [7,8] (HY-zeolite and H-ZSM5) and the ion exchange resin [9] Amberlyst 15. The former are currently the most effective catalysts in catalytic reforming, a process which is important because branched-chain hydrocarbons are better automotive fuels than their straight-chain isomers. This reaction is also widely used by many researchers in both homogeneous [10] and heterogeneous [11] processes as a test of a material's effectiveness as an acid catalyst.

The synthesis of a tantalum oxide molecular sieve (Ta-TSM1) was successfully achieved by using the ligand-assisted templating approach [3] with different chain-length amine surfactants (C_6~C_{18}). The as-synthesized samples were further treated with 1 M sulfuric acid in methanol solution to obtain sulfated mesoporous Ta oxides. The BJH pore sizes slightly decreased after acid treatment, possibly due to the deposit of SO_4^{2-} ions inside their wormhole channels (Table 5.2). The strong reflections (100) at low angle in the XRD pattern showed the retention of the mesoporous structure after acid treatment

(Figure 5.2). This was further confirmed by the type IV isotherm obtained in the nitrogen adsorption/desorption measurements (Figure 5.3), although materials synthesized with the smaller hexylamine displayed a type I isotherm. The pore size of the C_6 material was estimated as 12 Å on the basis of previous work on microporous Nb oxide [5b] and Ti oxide [5c]. These studies used TEM and XRD as a gauge of the pore size, which falls below that of the BJH method using N_2 as an adsorbent.

The FTIR spectrum for C_{12} mesoporous Ta oxide (Figure 5.4) showed a strong peak corresponding to Brønsted acid sites (1538 cm^{-1}), which was enhanced after acid treatment. In contrast, HY-zeolite and H-ZSM5 possess mainly Lewis acid sites (1448 cm^{-1}) with only a weak absorbance observed for Brønsted acid sites. The majority of research indicates that Brønsted acid sites are chiefly involved in isomerization reactions [12]. The Hammett acidity and n-butylamine titration methods were employed to measure acid strength and acid amount of all the samples. The results are summarized in Table 5.1. As is seen from this table, both acid strength and acid amount of the C_{12} mesoporous Ta oxide increased after acid treatment, consistent with previous work on mesoporous Nb oxide [5a].

Table 5.1. Acid Strength and Acid Amount of Solid Acid Catalysts (measured by Hammett Indicators and n-Butylamine Titration)

Sample	Ho	Acid amount (mmol/g)
C_{12} meso Ta	-6.6	0.40
C_{12} H_2SO_4 meso Ta	-8.2	19.8
HY-zeolite	-6.6	1.55
H-ZSM5	-4.4	16.1
Amberlyst 15	N/A	N/A

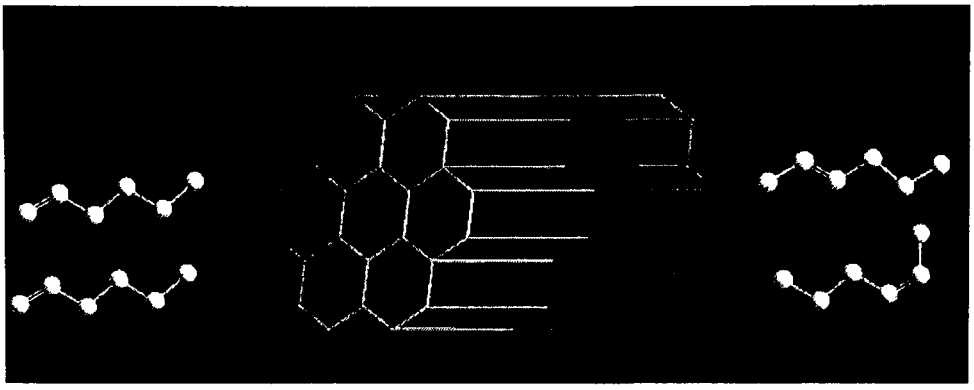

Scheme 5.1 Graphic illustration of 1-hexene isomerization towards *trans* and *cis*-2-hexene over mesoporous Nb oxides

C_{12} H_2SO_4 mesoporous Ta oxide was evaluated in 1-hexene isomerization at reflux temperature (343 K) (Scheme 5.1) and compared to Amberlyst 15, HY-zeolite, and H-ZSM5 (Figure 5.1a). This new material showed much higher activity than HY-zeolite and H-ZSM5 (roughly 10 times greater) and ca. 50% higher activity than Amberlyst 15. In order to investigate the effect of pore size on this reaction, C_6 and C_{18} mesoporous Ta oxides were also synthesized and tested. The results are shown in Figure 5.5. Among these three samples, C_{12} H_2SO_4 mesoporous Ta showed the highest activity (95% in 4 h), which can be attributed to a combination of pore size and its higher BET surface area (292.19 m^2/g, Table 5.2). The C_6 sample has the second highest surface area (206.40 m^2/g), but its smaller pore size leads to the lowest observed activity. The C_{18} sample has the largest pore size (22.5 Å) but the lowest surface area (188.79 m^2/g) and thus displays an activity that falls between that of its two congeners. GC analysis confirmed that *trans*- and *cis*-2-hexene isomers were formed as the only two principal products. Skeletal isomerization, which requires more energy and can only be performed at elevated temperature (>523 K) [13], was not observed at 343 K. C_6 and C_{18} H_2SO_4 mesoporous Ta

oxides showed very similar selectivity, the ratio of trans/cis-2-hexene is less than 1, which is close to the ratios observed from HY-zeolite, H-ZSM5, and Amberlyst 15. However, for the C_{12} sample, the ratio of trans: cis isomers can reach up to 3.7 after 6 h, which is very close to thermodynamic equilibrium (3.37) [14].

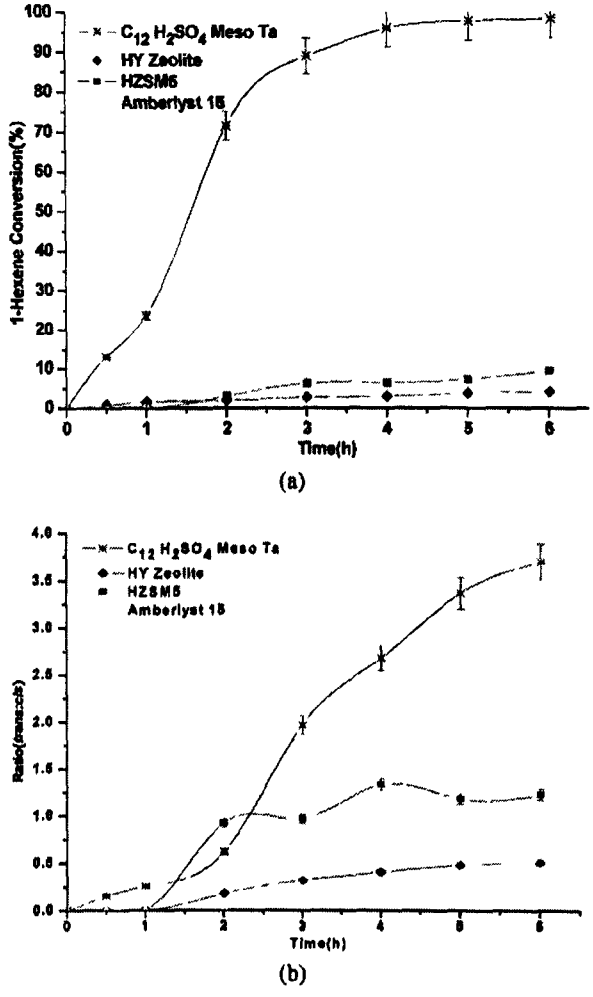

Figure 5.1 1-Hexene isomerization on different catalysts: (a) 1-hexene conversion rate with time; (b) ratio of trans/cis-2-hexene with time.

Tanchoux et al. [15] studied the impact of confinement and nesting effects in the isomerization of 1-hexene by MCM-41, demonstrating that selectivity as well as conversion rate were pore size dependent. This is consistent with the results observed in the present study. The pore size of the C_{12} H_2SO_4 mesoporous Ta oxide is 18.2 Å (Table 5.2), which allows linear trans-2-hexene to pass more easily though its channels than nonlinear cis-2-hexene. Because of the large pore size (22.5 Å) of C_{18} H_2SO_4 mesoporous Ta oxide, both products can be formed inside its channel structure and diffuse out freely, leading to poor selectivity. As for C_6 H_2SO_4 mesoporous Ta oxide, the limitation of its small pore size (12 Å) blocks the penetration of the reactant, allowing most of the reaction to occur on the ektexine of the wall, not inside the pores. This leads to low selectivity. The increase of selectivity over time to the thermodynamic mixture in the case of the C_{12} catalyst can be attributed to the more efficient conversion of *cis*-2-hexene to *trans*-2-hexene by this material relative to the other catalysts in this study. This faster rate of conversion is consistent with Tanchoux's observations on the higher activity of moderate pore size MCM-41 materials in this reaction.

The isomerization of 1-hexene to 2-hexene is a proton transfer process [16]. The initial proton is transferred from the acid sites on the surface of the catalyst to the double bond of 1-hexene, and then the hydride shift along the linear chain produces *cis*-2-hexene and *trans*-2-hexene. To eliminate the potential effect of free H_2SO_4 on selectivity, a separate experiment was performed using a drop of pure sulfuric acid as catalyst (Figure 5.6), the conversion of 1-hexene reached 31.18% after 6 h, and an only slightly higher ratio (1.5) was obtained as compared to the C_6 and C_{18} samples. Nevertheless, this value is still far behind the selectivity of C_{12} H_2SO_4 mesoporous Ta oxide, which establishes

that pore size is crucial to the selectivity in this system.

The reusability of C_{12} H_2SO_4 mesoporous Ta was tested by conducting three continuous runs using the same catalyst. The results showed that its catalytic activity declined linearly, the conversion of 1-hexene decreased from almost 100% conversion for the first run to 76% for the second run, and then to 40% for the third run. This can be attributed to partial pore blockage caused by isomerization products deposited inside the channel, which occupy some of the active sites on the surface and cause the BET surface area to decrease from 292 to 133.25 m^2/g (Figure 5.7). The loss of catalytic activity can also be ascribed to sulfate leaching during each catalytic run. This is demonstrated by the fact that the used catalyst can be partially regenerated to 60% its original activity by treatment with new sulfuric acid. Elemental analysis shows no increase in %C, demonstrating that loss of surface area is not due to build up of polymers.

5.2 Conclusion

In summary, this study provides a straightforward demonstration of the influence of acid sites and confinement effect in 1-hexene isomerization catalyzed over sulfated mesoporous Ta oxides. These catalysts showed higher activities than Amberlyst 15, HY-zeolite, and H-ZSM5. Among the three different pore sizes of sulfated mesoporous Ta oxides studied, C_{12} H_2SO_4 mesoporous Ta showed both the highest activity and selectivity, which can be attributed to its high BET surface area, increased concentration of Brønsted sites on the surface of the mesoporous channels, and optimal pore size for this particular reaction.

5.3 Supporting Information

5.3.1 Synthesis of sulfated mesoporous Tantalum oxide materials

In a typical preparation, Tantalum ethoxide (25g, 61.53mmol) was warmed with either n-hexylamine (1.866g, 18.44mmol), n-dodecylamine (3.42g, 18.45mmol) or n-octadecylamine (4.972g, 18.44mmol) respectively, using a heat gun until a homogeneous colorless solution was obtained. To this solution was added 1L of distilled water with stirring. A white gelatinous precipitate formed immediately. After precipitation occurred, hydrochloric acid (0.1802g, 1.85mmol) was added directly to the solution before the white solid was allowed to sit at room temperature overnight. The mixture was heated at 40°C for 2 days, 60°C for 2 days, 80°C for 2 days, and 95°C for 3 days. After filtration, the solid was dried in an oven at 95°C for 1~2 hours, sealed in a tube, and heated to 110°C for 2 days and 130°C for 2 days. The product was then collected and washed five times with methanol to remove the surfactant. Each washing cycle was conducted for 24 h in a large beaker with vigorous stirring followed by filtration. For the first wash, p-toluene sulfuric acid (7.01g, 36.85mmol) was added to the solution with 100ml diethyl ether. For the second wash, 0.701g p-toluene sulfuric acid was added to methanol solution. The solid was then collected and dried for 24 h at 120°C. The template-free samples were then treated with 1M sulfuric acid (in methanol solution) and filtered to obtain sulfated mesoporous Ta oxides with different pore sizes (C_6~C_{18}).

5.3.2 Characterization

X-ray powder diffraction data were recorded on a Siemens D5000-2diffractmeter

using Cu Kradiation. Nitrogen adsorption and desorption data were collected on a Micromeritics ASAP 2010. FTIR experiments were performed on Bruker Vector 22 FT-IR spectrometer.

5.3.3 Catalytic Runs

A 100mL round-bottom 3-neck flask provided with a reflux condenser was used as a stirred bed reactor to test the catalytic activities of the materials. Nitrogen was introduced into the flask through one of the gas inlets. The second inlet was equipped with a septum for sample removal. 50ml of 1-hexene (97%, Aldrich) were added to the reactor with 0.5g catalysts at each run. The reactant mixture was refluxed with stirring at atmospheric pressure and constant temperature (controlled oil bath temperatures of 80°C). Samples of the reaction mixture were periodically withdrawn and analyzed by using a Varian CP-3800 gas chromatograph equipped with a hydrogen flame ionization detector system and capillary column CP-SIL 5CB (15 m, 0.25 mm ID), the temperature was programmed from 50 to 300 °C (10°C/min) with H_2 1ml/min as carrier gas. Compared with standard sample, the results from GC identified trans-2-hexene and cis-2-hexene as the two main products. Activities were calculated on the basis of percentage conversion 1-hexene in the raw material.

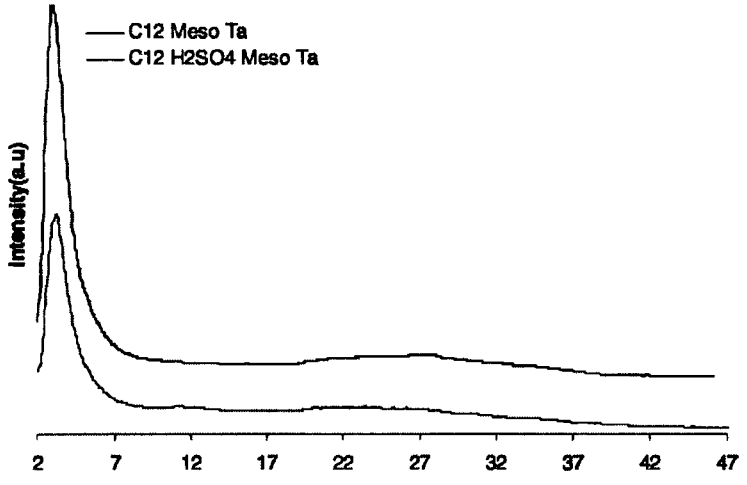

Figure 5.2 X-ray diffraction patterns of Ta-TMS1 samples. a) C_{12} Meso Ta, b) C_{12} H_2SO_4 Meso Ta

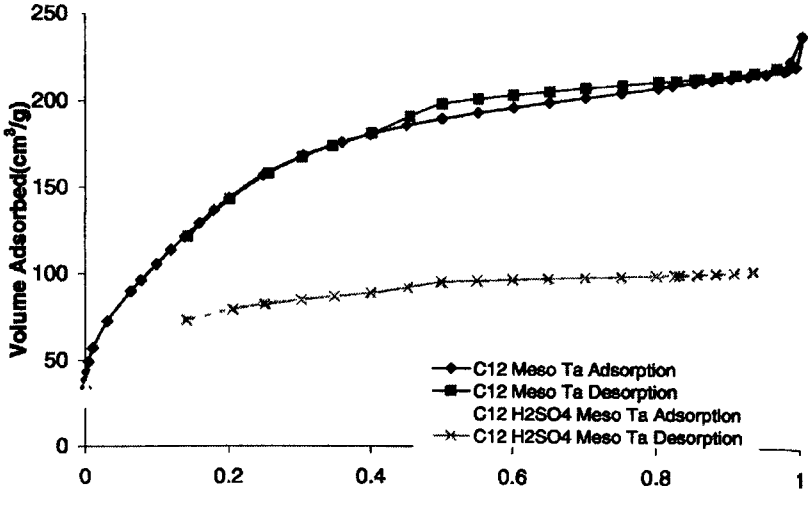

Figure 5.3 N_2 adsorption/desorption isotherms of (a) C_{12} Meso Ta oxide and (b) C_{12} H_2SO_4 Meso Ta oxide

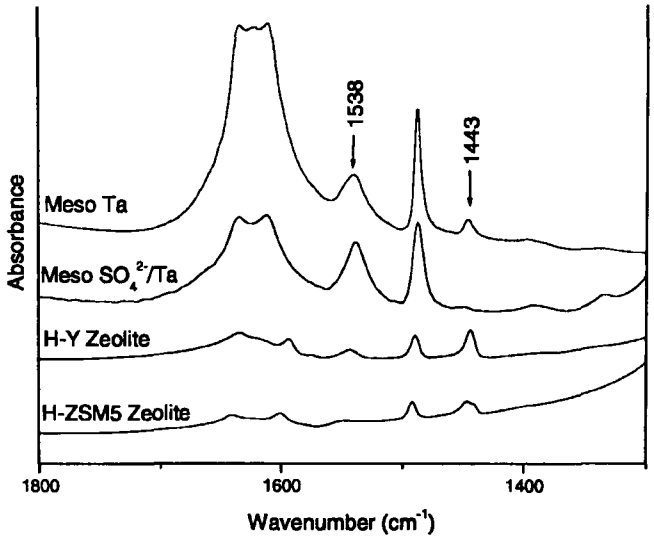

Figure 5.4 FT-IR spectra of pyridine adsorbed on C_{12} Meso Ta, C_{12} H_2SO_4 Meso Ta, HY Zeolite and H-ZSM5 Zeolite.

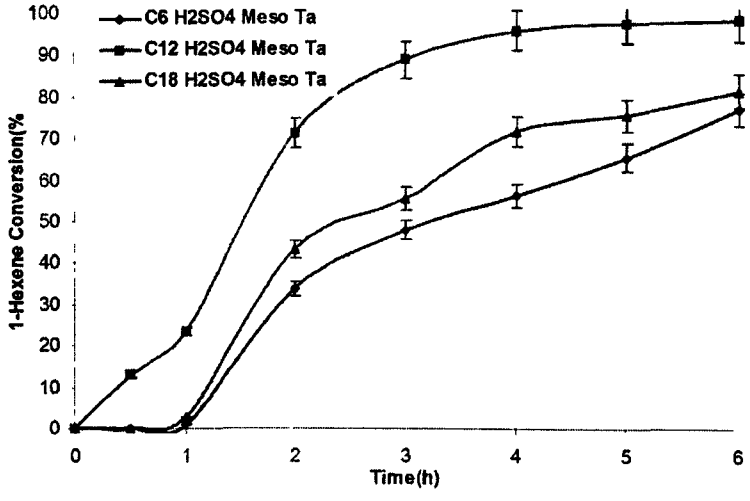

(a)

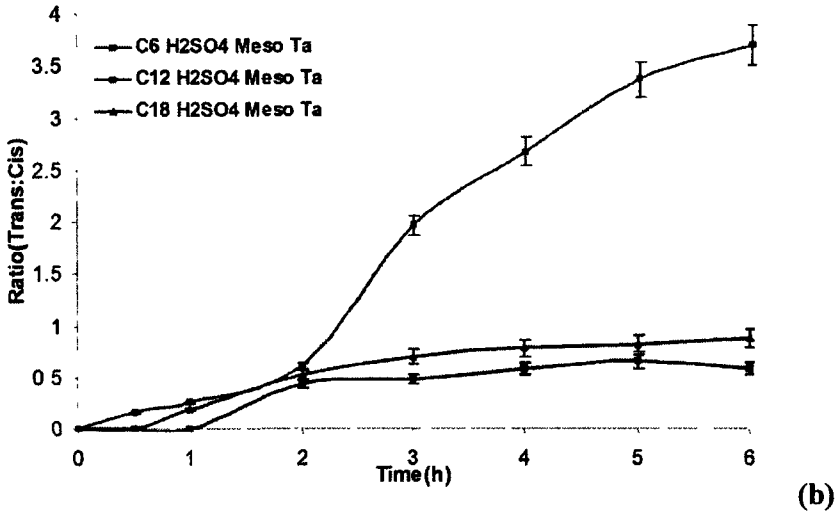

Figure 5.5 1-Hexene isomerization on sulfated mesoporous Ta oxides with different pore sizes. (a) 1-Hexene conversion rate with time (b) Ratio of trans-2-hexene to cis-2-hexene with time

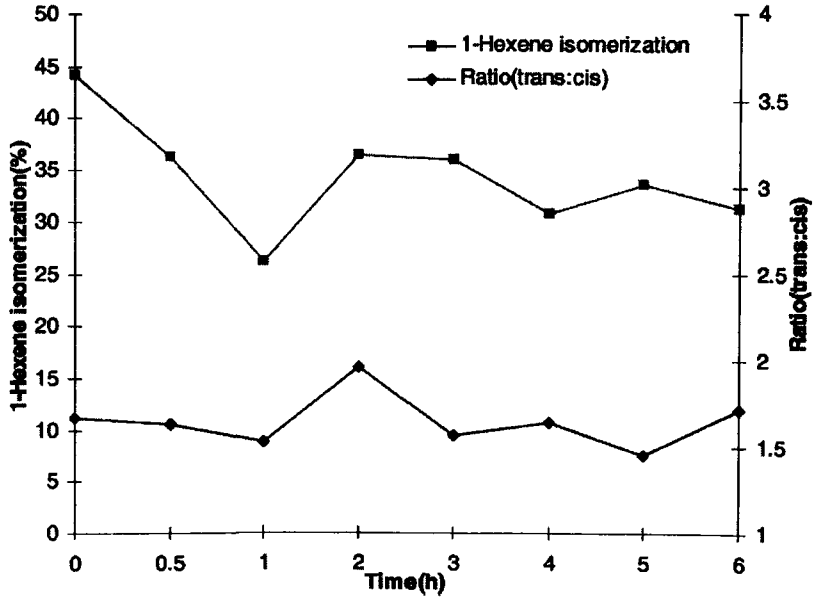

Figure 5.6. Catalytic activity and selectivity of pure sulfuric acid for 1-hexene isomerization. (Catalyst: 0.02g)

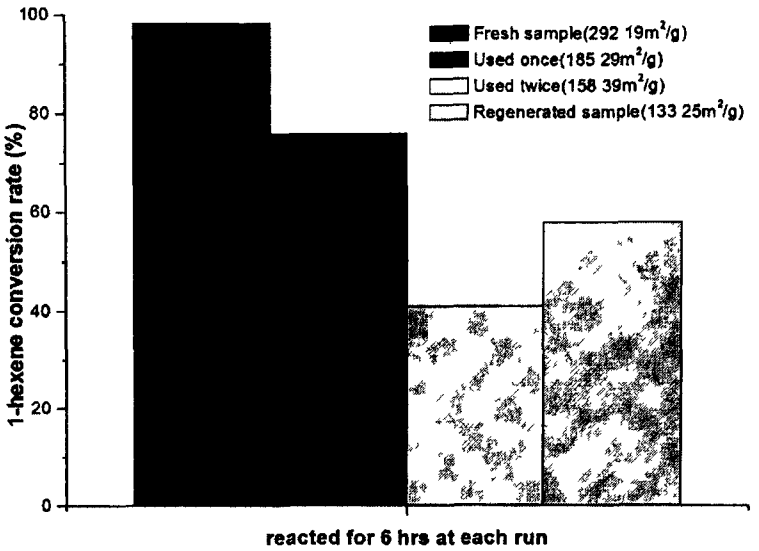

Figure 5.7. Catalytic activity and BET surface areas of C_{12} H_2SO_4 Meso Ta. a) Fresh sample b) Used once c) Used twice d) Regenerated sample

Table 5.2. BET surface area, Pore volume and Pore Size of different catalysts measured by N_2 adsorption at 77K.

Sample	BET (m^2/g)	Pore Volume (cm^3/g)	BJH Pore Size (Å)
C_6 Meso Ta	253.26	0.1905	17.5*
C_{12} Meso Ta	582.70	0.3651	18.8
C_{18} Meso Ta	234.74	0.0538	22.7
C_6 H_2SO_4 Meso Ta	206.40	0.1314	17.0*
C_{12} H_2SO_4 Meso Ta	292.19	0.0989	18.2
C_{18} H_2SO_4 Meso Ta	188.79	0.0347	22.5
HY Zeolite	779.80	0.1160	38.9
H-ZSM5	435.96	0.1076	39.0
Amberlyst 15	51.86	0.3443	303.1

* The pore size was estimated as 12 Å by using more reliable TEM and XRD on previous work [5b].

5.4 References

1. H. Yoshitake, T. Tatsumi, *Chem. Mater.* **2003**, *15*, 1695.
2. (a) M. P. Kapoor, Y. Ichihashi, K. Kuraoka, Y. Matsumura, *J. Mol. Catal. A* **2003**, *198*, 303 (b) Z. R. Tian, W. Tong, J. Y. Wang, N. G. Duan, V. V. Krishnan, S. L. Suib, *Science* **1997**, *276*, 926
3. (a) D. M. Antonelli, Y. J. Ying, *Angew. Chem., Int. Ed. Engl.* **1996**, *35*, 426 (b) D. M. Antonelli, Y. J. Ying, *Chem. Mater.* **1996**, *8*, 874 (c) D. M. Antonelli, A. Nakahira, Y. J. Ying, *Inorg. Chem.* **1996**, *35*, 3126
4. (a) C. Yue, M. L. Trudeau, D. M. Antonelli, *Chem. Commun.* **2006**, 1918 (b) C. Yue, M. L. Trudeau, D. M. Antonelli, *Can. J. Chem.* **2005**, *83*, 308
5. (a) Y. Rao, M. L. Trudeau, D. M. Antonelli, *J. Am. Chem. Soc.* **2006**, *128*, 13997 (b) T. Sun, J. Y. Ying, *Nature* **1997**, *389*, 704 (c) X. Hu, O. B. Skadtchenko, M. Trudeau, D. M. Antonelli, *J. Am. Chem. Soc.* **2006**, *128*, 11740
6. (a) Y. Takahara, J. N. Kondo, D. Lu, K. Domen, *Solid State Ionics* **2002**, *151*, 305. (b) Y. Takahara, J. N. Kondo, T. Takata, D. Lu, K. Domen, *Chem. Mater.* **2001**, *13*, 1194.
7. P. N. Kuznetsov, *J. Catal.* **2003**, *218*, 12
8. D. Li, M. Li, Y. C. Chu, H. Nie, Y. Shi, *Catal. Today* **2003**, *81*, 65 (b) V. Sundaramurthy, N. Lingappan, *J. Mol. Catal. A* **2000**, *160*, 367 (c) C. Yin, R. Zhao, C. Liu, *Fuel* **2005**, *84*, 701
9. (a) M. Mitkova, K. Kurtev, *J. Chin. Chem. Soc.* **2005**, *52*, 1189 (b) P. M. Slomkiewicz, *Appl. Catal. A* **2006**, *301*, 232
10. (a) A. Salvini, P. Frediani, F. Piacenti, *J. Mol. Catal. A* **2000**, *159*, 185. (b) B. Fontal, M. Reyes, T. Suarez, F. Bellandi, N. Ruiz, *J. Mol. Catal. A* **1999**, *149*, 87 (c) K.

Dallmann, R. Buffon, *J. Mol. Catal. A* **2002**, *185*, 187 (d) J. Zhang, H. Gao, Z. Ke, F. Bao, F. Zhu, Q. Wu, *J. Mol. Catal. A* **2005**, *231*, 27 (e) T. Matsumoto, H. Yoshida, *Catal. Lett.* **2001**, *72*, 107 (f) C. J. Yue, Y. Liu, R. He, *J. Mol. Catal. A* **2006**, *259*, 17

11. (a) A. K. Talukdar, K. G. Bhattacharyya, T.; Y. Ono, *Appl. Catal. A* **2001**, *213*, 239 (b) M. Pu, Z. H. Li, Y. J. Gong, D. Wu, Y. H. Sun, *J. Mater. Sci. Lett.* **2003**, *22*, 955 (c) V. Logie, P. Wehrer, A. Katrib, G. Maire, *J. Catal.* **2000**, *189*, 438 (d) J. Wrzyszcz, M. Zawadzki, A. M. Trzeciak, W. Tylus, J. Ziolkowski, *J. Catal. Lett.* **2004**, *93*, 85 (e) P. Wehrer, C. Bigey, L. Hilaire, *Appl. Catal. A* **2003**, *243*, 109 (f) S. Pariente, P. Trens, F. Fajula, F. D. Renzo, N. Tanchoux, *Appl. Catal. A* **2006**, *307*, 51 (g) R. Van Grieken, J. M. Escola, J. Moreno, R. Rodriguez, *Appl. Catal. A* **2006**, *305*, 176
12. (a) C. Bezouhanova, H. Lechert, G. Taralanska, A. Meyer, *React. Kinet. Catal. Lett.* **1989**, *40*, 209 (b) M. Li, Y. Chu, H. Nie, Y. Shi, D. Li, *Stud. Surf. Sci. Catal.* **2003**, *145*, 403 (c) F. DiGregorio, V. Keller, T. DiCostanzo, J. L. Vignes, D. Michel, G. Maire, *Appl Catal. A* **2001**, *218*, 13
13. (a) Z. Wu, Q. Wang, L. Xu, S. Xie, *Stud. Surf. Sci. Catal.* **2002**, 142A (b) I. Eswaramoorthi, V. Sundaramurthy, N. Lingappan, *Stud. Surf. Sci. Catal.* **2001**, 135
14. J. M. Proell, E. E. Mosley, G. L. Powell, T. C. Jenkins, *J. Lipid Res.* **2002**, *43*, 2072
15. S. Pariente, P. Trens, F. Fajula, F. D. Renzo, N. Tanchoux, *Appl. Catal. A* **2006**, *307*, 51
16. (a) J. Abbot, B. W. Wojciechowski, *J. Catal.* **1984**, *90*, 270 (b) J. Abbot, B. W. Wojciechowski, *J. Catal.* **1985**, *92*, 398

Chapter 6

Investigation of The Catalytic Activities of Sulfated Mesoporous Nb and Ta Oxides in 1-Hexene Isomerization

This chapter is organized based on a full paper submitted to *Chemistry of Materials* by **Yuxiang Rao**, Junjie Kang, Michel Trudeau and Dave M. Antonelli

6.1 Introduction

Over the last two decades, there has been a dramatic increase in the synthesis of open-framework micro-and mesoporous inorganic materials of well-defined pore geometry. One of the most important classes of these materials are the M41S family of mesoporous silicates, first synthesized by Mobil Corporation in 1992 [1,2] Since that discovery, there has been considerable interest in exploiting their unique properties, which include controlled pore sizes, high surface area, and high thermal stability, which

are all areas of great importance to catalysis and gas separation [3, 4]. One of the most important potential applications of these materials is in acid catalyzed petroleum and hydrocarbon transformations [5~7], because the larger pores are thought to be an advantage in the suppression of coking. However, mesoporous aluminosilicates do not posses high enough acidities to be useful in many of these reactions. For this reason there has been considerable interest in synthesizing mesoporous materials from highly acidic transition metal oxides and their sulfated analogues. Since the first report of the synthesis of non-silica transition metal oxide mesoporous materials, accomplished using a ligand-assisted templating approach for Nb, Ta, and Ti [8~12], many groups have begun to investigate the catalytic properties of these and related materials. Thus, a wide variety of mesoporous transition metal oxides have been reported as novel catalyst materials [13~14]. Mesoporous transition metal oxides have superior properties in many applications as compared to their traditional silica analogues due to their high acidities and the variable oxidation states afforded by the empty transition metal d orbitals, which allow electron transfer to occur between the reactants and active sites during any given catalytic process [15~16]. Recently we showed that sulfated mesoporous Nb and Ta oxides possess a high concentration of Brønsted acid sites, useful in Friedel Crafts reactions such as benzylation [17] and alkylation [18]. Mesoporous Ta oxide is also an very effective catalyst in the isomerization of 1-hexene, surpassing both zeolite Y and Amberlyst 15 in activity and selectivity [19]. The isomerization of straight-chain hydrocarbons to branched-chain isomers is of great importance in the synthesis of high-octane fuels. In this report, we present a detailed comparative study of the reaction of 1-hexene over a series of sulfated mesoporous Nb and Ta catalysts with different pore sizes and compare their activity to two standard zeolites and Amberlyst 15 ion exchange

resin. The relative activities of the Nb and Ta materials are also studied by temperature programmed desorption of ammonia in order to establish the reason for the much higher activity of the Ta based system in this model reaction.

6.2 Experimental Section

6.2.1 Materials and Equipment

All chemicals unless otherwise stated were obtained from Alfa Aesar without further purification. HY zeolite and HZSM5 were purchased from Zeolyst and Amberlyst 15 was purchased from Aldrich. Nitrogen adsorption and desorption data were collected on a Micromeritics ASAP 2010. X-ray diffraction (XRD) patterns (Cu Ka) were recorded in a sealed glass capillary on a Siemens D-500 θ-2θ diffractometer. High-resolution transmission electron microscopy (HRTEM) images were obtained by using H9000 HR-TEM operated at 300 kV. Scanning electron microscopy (SEM) images were recorded on S-4700 Cold Field Emission SEM from Hitachi. Pyridine adsorption Fourier transform infrared spectroscopy (FTIR) experiments were performed on Bruker Vector 22 FT-IR spectrometer. TGA and DSC data were collected on a TGA/SDTA851 (Mettler Toledo) with Pfeiffer Vacuum Thermostar and DSC822E Differential Scanning Calorimeter (DSC) (Mettler Toledo), respectively, from room temperature to 550 °C at a heating rate of 5 °C min^{-1} TPD experiments were conducted on a ChemBET TPR/TPD instrument from Quantachrome. All elemental analysis data (conducted under an inert atmosphere) were obtained from Galbraith Laboratories, Knoxville, TN.

6.2.2 Thermodynamic Equilibrium Constant Measurement

The thermodynamic equilibrium constant was calculated using the standard Gibbs energy equation

$$\Delta G^{\Phi} = -RT \ln K_{eq} \qquad (1)$$

Where ΔG^{Θ} is the standard Gibbs energy change of reaction, R is the gas constant, and T is the absolute temperature. From reference 20, we know that $G_{cis\text{-}2\text{-}hexene}$ =19.18 kcal/mol and $G_{trans\text{-}2\text{-}hexene}$=18.46 kcal/mol, so for the reaction *cis*-2-hexene → *trans*-2-hexene, $\Delta G<0$. It is therefore a spontaneous reaction and trans-2-hexene is more stable than its cis-isomer. Inputting the numbers into the equation (1), we calculated the equilibrium constant K_{eq}.

6.2.3 Sample Preparation

Synthesis of Sulfated Mesoporous Niobium and Tantalum Oxide Materials with different pore sizes

In a typical preparation, niobium ethoxide (50g, 157.1mmol) was warmed with dodecylamine (8.7372g, 47.13mmol) (n-hexylamine for C_6 Nb and n-octadecylamine for C_{18} Nb) using a heat gun until a homogeneous colorless solution was obtained. To this solution was added 1L of distilled water with stirring. A white gelatinous precipitate formed immediately. After precipitation occurred, hydrochloric acid (37%, 0.1743g, 4.713mmol) was added directly to the solution without agitation before the white solid was allowed to sit at room temperature overnight. The mixture was heated at 40°C for 2 days, 60°C for 2 days, 80°C for 2 days, and 95°C for 4 days. After filtration, the solid was

dried in an oven at 95°C for 1~2 hours, sealed in a tube, and heated to 120°C for 2 days and 140°C for 2 days. The product was then collected and washed five times with 500 ml of methanol to remove the surfactant. Each washing cycle was conducted for 24 hrs in a large Erlenmeyer flask with vigorous stirring followed by filtration. For the first wash, *p*-toluene sulfonic acid (9.8615g, 51.843mmol) was added to the solution with 200ml diethyl ether. For the second washing, 0.8965g *p*-toluene sulfonic acid was added to methanol solution. After 5 washings the solid was collected and dried for 24 hrs at 120°C. The template-free sample was further treated with 1M sulfuric acid solution (in methanol) for 24 hrs and filtered to obtain sulfated mesoporous Nb oxides. The synthesis for mesoporous Ta oxides is identical, except that tantalum ethoxide is used in place of niobium ethoxide.

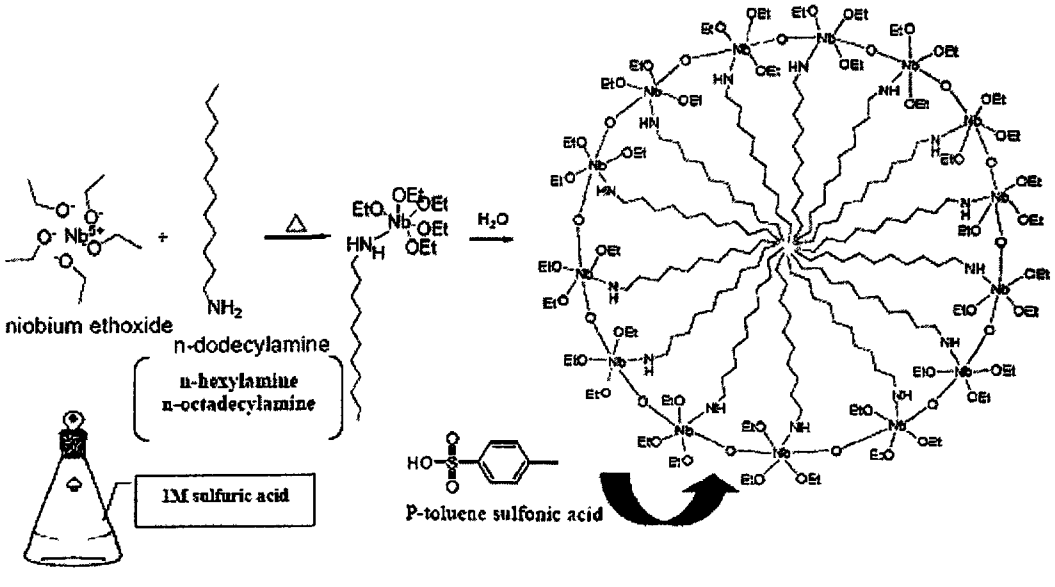

Scheme 6.1 Synthesis of sulfated mesoporous Nb oxide materials with different pore sizes

6.2.4 Catalytic Runs

A 100mL round-bottom 3-neck flask equipped with a reflux condenser was used as a stirred bed reactor to test the catalytic activities of the materials. Nitrogen was introduced into the flask through one of the gas inlets. The second inlet was equipped with a septum for sample removal. 50ml of 1-hexene (97%, Aldrich) were added to the reactor with 0.5g catalysts at each run. The reactant mixture was refluxed with stirring at atmospheric pressure and constant temperature (controlled oil bath temperatures of 343 K). Samples of the reaction mixture were periodically withdrawn and analyzed using a Varian CP-3800 gas chromatograph equipped with a hydrogen flame ionization detector system and capillary column CP-SIL 5CB (15 m, 0.25 mm ID), the temperature was programmed from 50 °C to 300 °C (10°C/min) with H_2 1 ml/min as a carrier gas. Compared with a standard sample, the results from the GC identified *trans*-2-hexene and *cis*-2-hexene as the two main products. Activities were calculated on the basis of percentage conversion of 1-hexene in the starting mixture.

6.3 Results and Discussion

The as-synthesized sulfated Nb and Ta oxide samples were characterized by a series of standard analytical techniques (Nitrogen adsorption and desorption, XRD, TEM, SEM, FTIR, Amine titration, TPD, TG and DSC) prior to use as catalysts for the isomerization of 1-hexene. The results of these studies are detailed below.

6.3.1 XRD and Nitrogen Adsorption

The powder XRD patterns of the Nb and Ta oxide samples before and after acid treatment were obtained to gain information about the mesoporosity and the effect of acid treatment on the stability of the mesoporous structure. While Nb_2O_5 and Ta_2O_5 are extremely robust to acid, the more loose-knit gel structure of the mesostructure walls in these materials is expected to lead to lower kinetic and thermal stabilities. ^{17}O NMR experiments conducted by our group showed that mesoporous Nb oxide possesses almost exclusively 2-coordinate oxygen, with only very small amounts of triply bridging oxygen [21]. This would facilitate any acid-catalyzed hydrolysis reactions that could lead to structural degradation of the walls. Nevertheless, X-ray diffraction (XRD) analysis of the powder samples in Figure 6.1 clearly showed that the mesoporous structures are retained after acid treatment, as the main peak at low angle in each sample representing the strong reflection (100) is almost unchanged. This was further confirmed by the type IV isotherm obtained by the nitrogen adsorption/desorption measurement in Figure 6.2. However, the BET surface area and the BJH pore sizes of mesoporous Nb and Ta oxides decreased after acid treatment (Table 6.1), possibly due to the deposit of SO_4^{2-} ions inside the wormhole channels which would lead to an increase of skeletal density and a concomitant loss of void space, effectively lowering the surface area per gram.

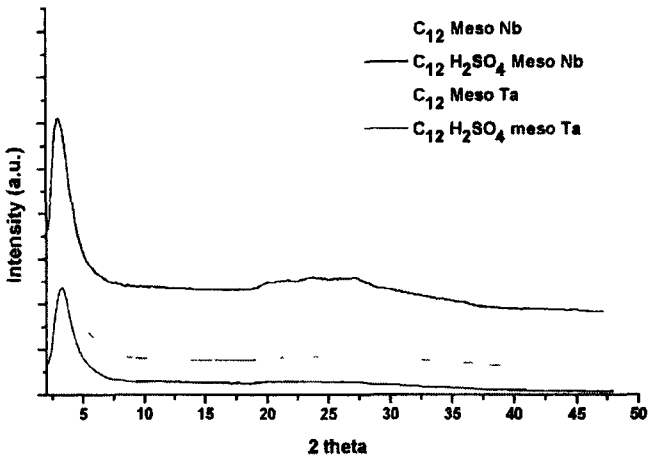

Figure 6.1 Powder X-ray diffraction data for Nb-TSM1 and Ta-TSM1 samples. (From Top to Bottom) a) C_{12} Meso Nb; b) C_{12} H_2SO_4 meso Nb; c) C_{12} Meso Ta; d) C_{12} H_2SO_4 Meso Ta

Table 6.1. BET surface area, Pore volume and Pore Size of different catalysts measured by N_2 adsorption at 77K.

Sample	BET (m^2/g)	Pore Volume (cm^3/g)	BJH Pore Size (Å)
C_6 Meso Nb	519.03	0.4858	17.5
C_{12} Meso Nb	612.02	0.3199	20.6
C_{18} Meso Nb	553.72	0.3595	27.2
C_6 H_2SO_4 Meso Nb	160.35	0.293	16.3
C_{12} H_2SO_4 Meso Nb	413.97	0.2423	20.5
C_{18} H_2SO_4 Meso Nb	282.58	0.2087	25.6
C_6 Meso Ta	253.26	0.1905	17.5*
C_{12} Meso Ta	582.70	0.3651	18.8
C_{18} Meso Ta	234.74	0.0538	22.7
C_6 H_2SO_4 Meso Ta	206.40	0.1314	17.0*
C_{12} H_2SO_4 Meso Ta	292.19	0.0989	18.2
C_{18} H_2SO_4 Meso Ta	188.79	0.0347	22.5
HY Zeolite	779.80	0.1160	38.9
H-ZSM5	435.96	0.1076	39.0
Amberlyst 15	51.86	0.3443	303.1

* The pore size was estimated as 12 Å by using more reliable TEM and XRD on previous work [22].

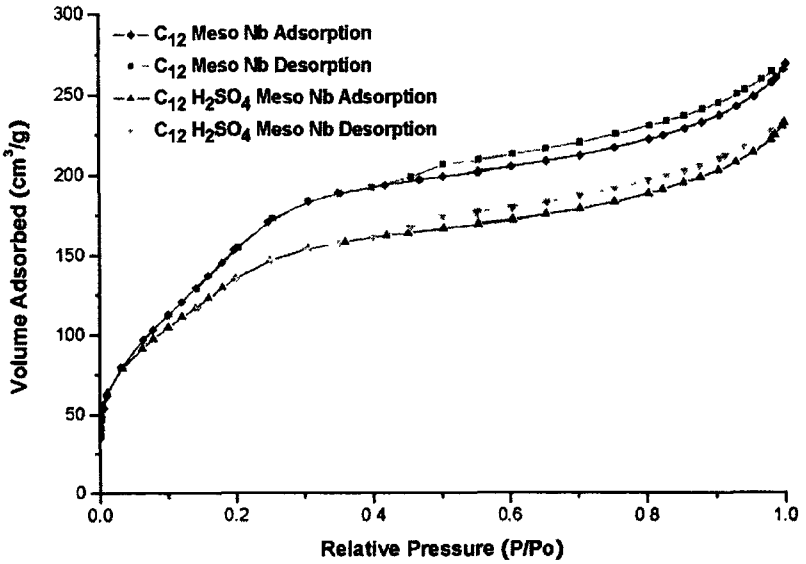

(a)

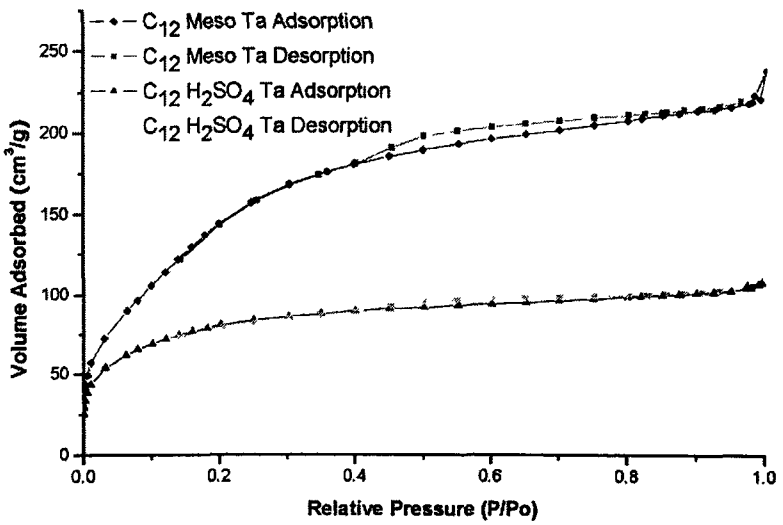

(b)

Figure 6.2. N_2 adsorption/desorption isotherm of a) C_{12} Meso Nb and C_{12} H_2SO_4 Meso Nb; b) C_{12} Meso Ta and C_{12} H_2SO_4 Meso Ta

6.3.2 TEM & SEM Images

TEM and SEM images of C_{12} mesoporous Nb and Ta samples were obtained (Figure 6.3) to elucidate the structure and morphology of these materials.

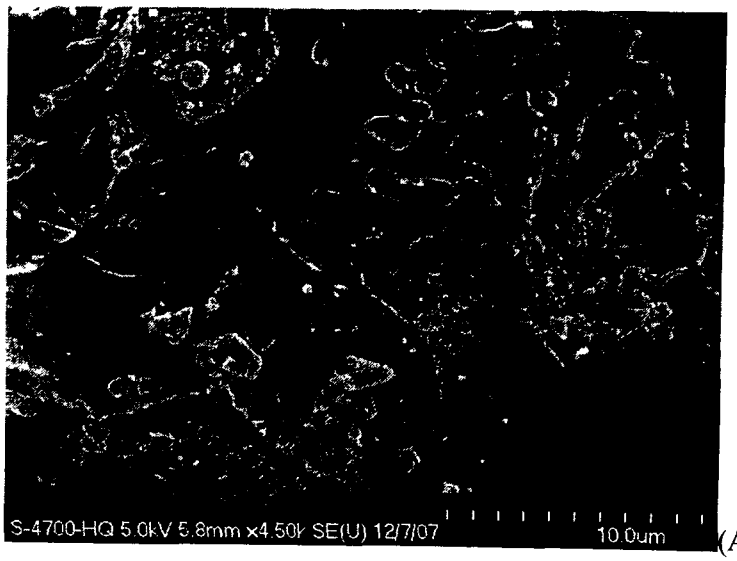

(A)

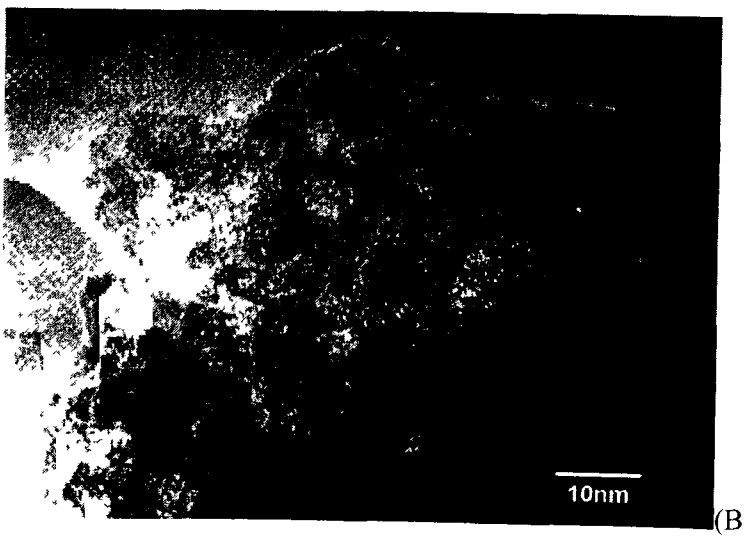

(B)

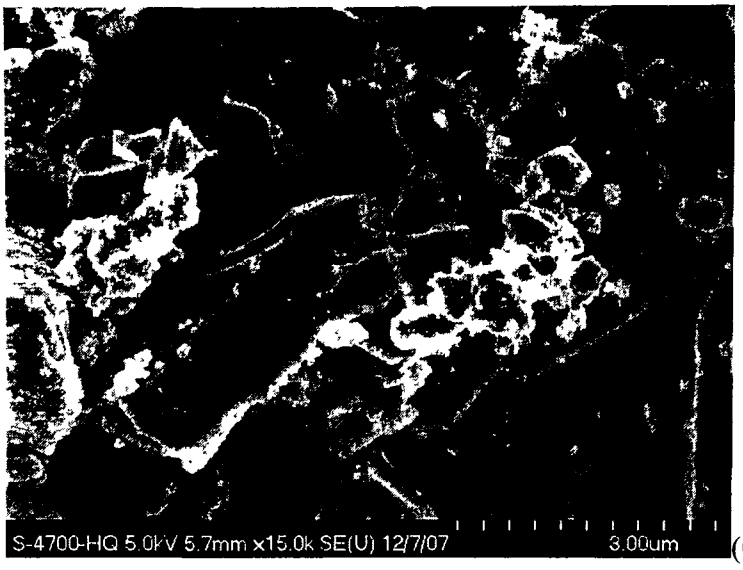

(C)

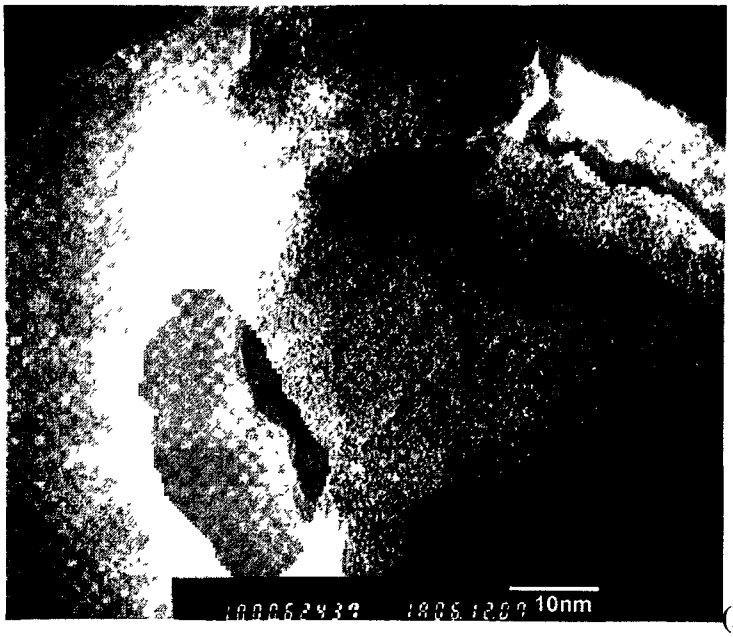

(D)

Figure 6.3 (A) SEM images of the C_{12} H_2SO_4 Meso Nb. (B) TEM image of C_{12} H_2SO_4 Meso Nb. (C) SEM image of the C_{12} H_2SO_4 Meso Ta. (D) TEM image of C_{12} H_2SO_4 Meso Ta

TEM images of Nb and Ta samples (Figure 6.3b and 6.3d) clearly indicate the formation of an ordered mesostructure with a disordered arrangement of mesoporous channels. Both the C_{12} Ta and Nb materials possess powder morphology with a large range of particle sizes from several hundred nanometers over 100 microns. These images are virtually identical to those of unsulfated Nb and Ta materials synthesized by our group and thus confirm that sulfuric acid treatment had little effect on the overall mesostructure or particle morphology of these samples.

6.3.3 FT-IR of pyridine adsorption spectra

The FT-IR (Fourier transform infrared, Figure 6.4) spectrum of C_{12} mesoporous Nb oxide treated with pyridine vapor showed that Brønsted (1540 cm^{-1}) and Lewis (1450 cm^{-1}) acid sites coexist in a roughly 50:50 mixture on the surfaces of the parent material. However, the sulfated Nb and Ta materials both exhibited a strong dominance of Brønsted acid sites, which is the result of sulfuric acid treatment. The FTIR data for mesoporous Ta oxide has been published previously, and shows the same trend in increased Brønsted-acid sites with sulfuric acid treatment [18]. The majority of research indicates that Brønsted-acid sites are chiefly involved in isomerization reactions [23~25], which should give these sulfated Nb and Ta materials a distinct advantage in these reactions. In contrast, HY-Zeolite and H-ZSM5 possess mainly Lewis-acid sites (~1448cm^{-1}) with only a weak absorbance observed for Brønsted-acid sites.

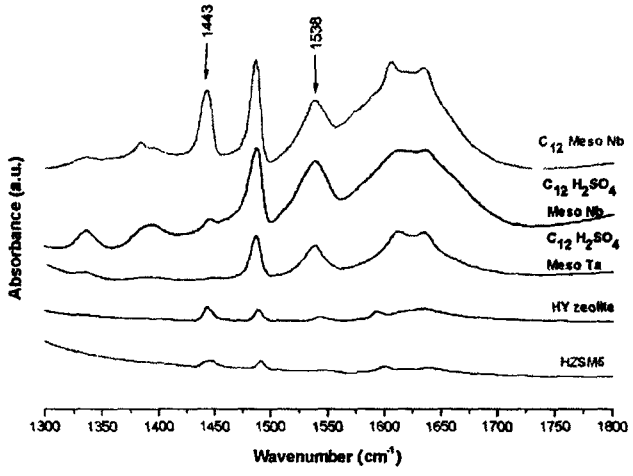

Figure 6.4 FT-IR spectra of pyridine adsorbed on C_{12} Meso Nb, C_{12} H_2SO_4 Meso Nb and Ta, HY Zeolite and H-ZSM5 Zeolite.

6.3.4 Amine titration and TPD experiments

Hammett acidity and n-butylamine titration methods were employed to measure the acid strength and acid amount of all samples. The experimental results are summarized in Table 6.2 As seen from this table, both the acid strength and acid amount of the C_{12} mesoporous Nb and Ta oxides increase dramatically after acid treatment, consistent with previous work on benzylation of toluene and anisole by C_{12} mesoporous Nb oxide [17]. Since sulfated mesoporous Nb and Ta oxides possess similar acid strength (*Ho*~-8.6) and acid amount (31.784 mmol/g for Nb and 19.8 mmol/g for Ta) as determined by this method, more detailed studies are required to account for differences in catalytic activity observed between these two materials in previous studies [19].

Temperature programmed desorption (TPD) is an excellent method to measure the relative strengths of acid sites in a material. Ammonia desorption is routinely used as a

method to measure binding enthalpies and relative amounts for both Lewis and Brønsted sites [26~30], while Ar desorption can be used to measure Lewis acid strength of superacidic materials at low temperature [31~32]. Because of its greater flexibility, we chose to conduct ammonia desorption studies on our materials. For these experiments, sulfated mesoporous Ta and Nb oxides were first treated with ammonia vapor. TPD data for the desorption of ammonia from the C_{12} Nb and Ta catalysts are given in Figure 6.5. The NH_3-TPD curve for C_{12} H_2SO_4 Ta shows one intense and broad peak at 868 K (middle) and two smaller peaks at 802 K (first) and 1023 K (last), corresponding to one strong Brønsted-acid site and two weak Lewis-acid sites, respectively, as reported elsewhere [26~27]. In previous studies on zirconia the intensity of this central Brønsted peak was associated with high activity in acid catalyzed reactions [26~28]. The Nb sample has two main peaks at 840K (Lewis-acid site) and 909K (Brønsted-acid site), the other peak at high temperature (1033 K) is small compared to that in the curve for the Ta analogue. The main Nb Brønsted peak is lower in integrated intensity and also much sharper than that for Ta, typical of desorption from a more highly crystallized surface. Since the walls in mesoporous Nb oxide crystallize at lower temperatures than mesoporous Ta oxide [21], the sharpness of the middle peak on the NH_3-TPD curve for C_{12} H_2SO_4 Meso Nb is most likely due to crystallization during the heating process leading to ammonia desorption from a more highly ordered surface above the crystallization temperature. NH_3-TPD kinetic runs at constant heating rates of 5 °C min^{-1}, 10 °C min^{-1}, and 20 °C min^{-1} gave activation energies of desorption (E_d) of 157.17 KJ/mol and 168.81 KJ/mol, respectively, for the central Brønsted peak in the Ta and Nb curves. These values are in reasonable agreement with those determined by ITPD (intermittent temperature-programmed desorption) study on perovskites reported by

Gaillard [33~34]. Since these values are very close to one another, the greater intensity of the Ta Brønsted peak, and not a difference in p*K*a, likely accounts for the greater activity of the Ta material in reactions involving Brønsted acid sites.

Table 6.2 Acid strength and acid amount of solid acid catalysts (Measured by Hammett indicators and n-butylamine titration)

Sample	*Ho*	Acid amount (mmol/g)
C_{12} Meso Nb	-6.6	2.478
C_{12} H_2SO_4 Meso Nb	-8.2	31.784
C_{12} Meso Ta	-6.6	0.40
C_{12} H_2SO_4 Meso Ta	-8.2	19.8
HY Zeolite	-6.6	1.55
H-ZSM5	-4.4	16.1
Amberlyst 15	N/A	N/A

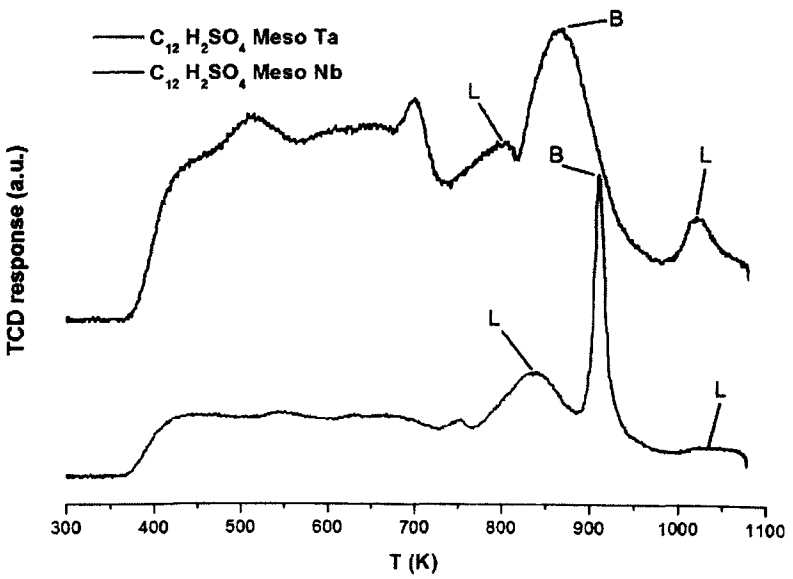

Figure 6.5 NH_3-TPD profiles of sulfated mesoporous Nb and Ta catalysts. Ramp rate: 10K min^{-1}

6.3.5 TGA and DSC experiment

TGA and DSC techniques were applied to study the thermal behaviors of Nb and Ta samples and further elucidate the temperature of crystallization in the Nb sample. The results are shown in Figure 6.6 and Figure 6.7. The first large endothermic peak on both the Nb and Ta DSC curves at around 373 K corresponds to the evaporation of the water. The DSC curve for C_{12} H_2SO_4 Meso Nb shows a large endothermic zone at 454 K~ 491 K. This is not found in the DSC curve for C_{12} H_2SO_4 Meso Ta. This phenomenon is likely the result of endothermic crystallization since the TGA for this sample does not show any corresponding weight loss in this temperature region. This is consistent with both previous XRD and ^{17}O NMR studies on mesoporous Nb oxide [21], and the observation of a very narrow peak in the TPD curve for the Nb sample.

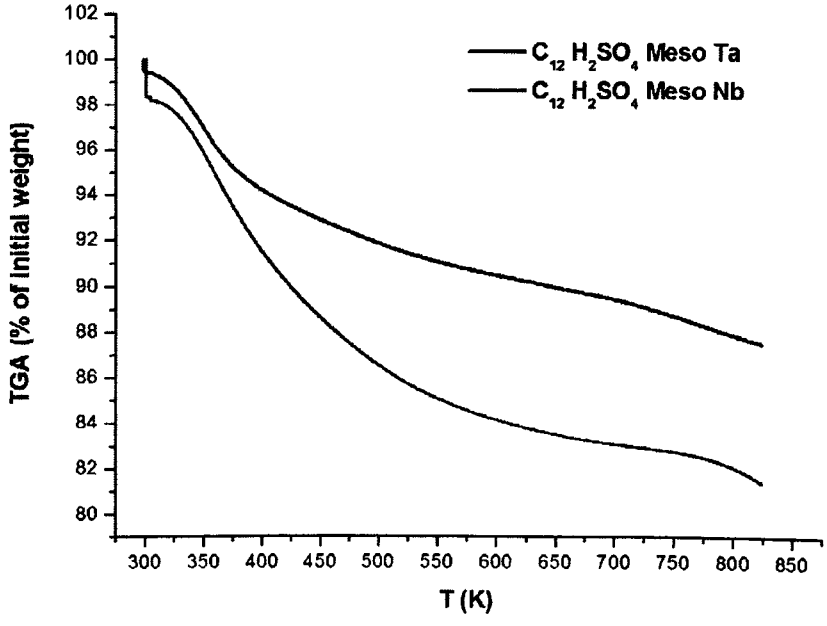

Figure 6.6 TGA curves under N_2 for sulfated mesoporous Nb and Ta catalysts

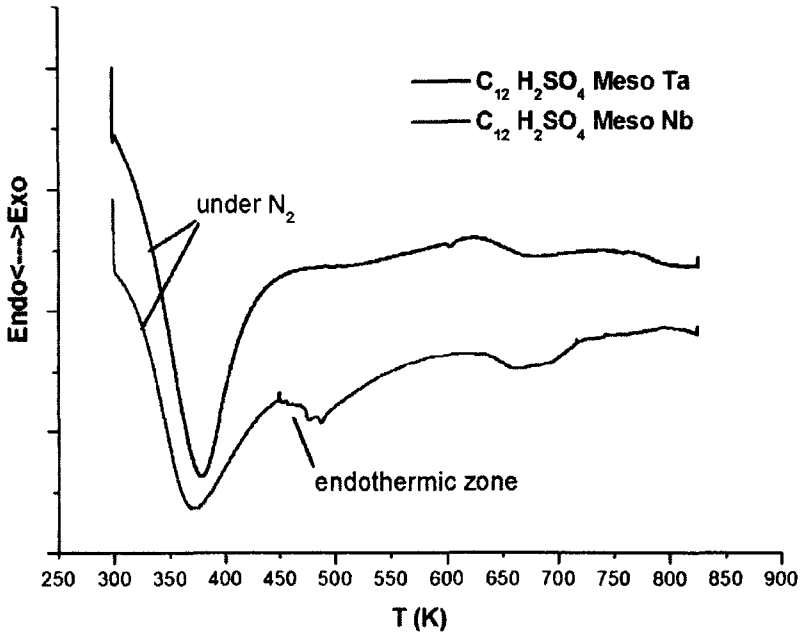

Figure 6.7 DSC curves under N_2 for sulfated mesoporous Nb and Ta catalysts

6.4 Catalysts Evaluation

Previous studies established that sulfated mesoporous Ta oxide was an effective catalyst in the isomerization of 1-hexene to the *cis* and *trans* 2-hexene products. GC analysis confirmed that *trans* and *cis* 2-hexene isomers were the only two products. Skeletal isomerization was not observed at this reaction condition since it requires more energy and can only be performed at elevated temperature (>523 K) [35~37]. In order to investigate the effect of pore size on the activity and selectivity in this reaction, a series of sulfated mesoporous Nb and Ta oxides with different pore sizes (C_6, C_{12}, C_{18}) were synthesized and evaluated at 343 K in a batch reactor. Commercially available zeolites (HY-zeolite and HZSM5) and the ion exchange resin Amberlyst 15 were chosen as reference catalysts. The results are shown in Figure 6.8 and Figure 6.9.

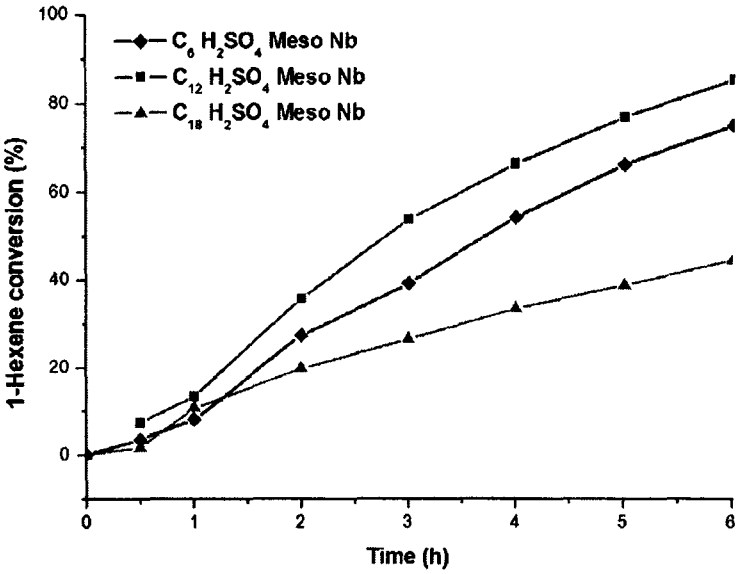
C6 H2SO4 Meso Nb
C12 H2SO4 Meso Nb
C18 H2SO4 Meso Nb
1-Hexene conversion (%)
Time (h)

(A)

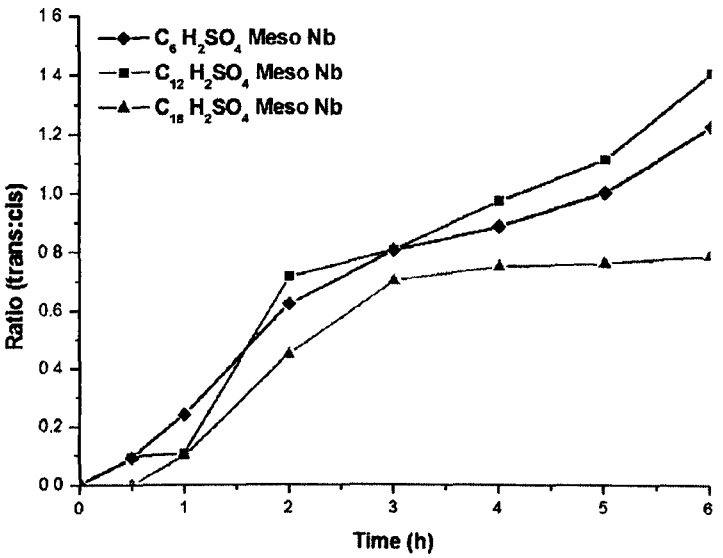
C6 H2SO4 Meso Nb
C12 H2SO4 Meso Nb
C18 H2SO4 Meso Nb
Ratio (trans:cis)
Time (h)

(B)

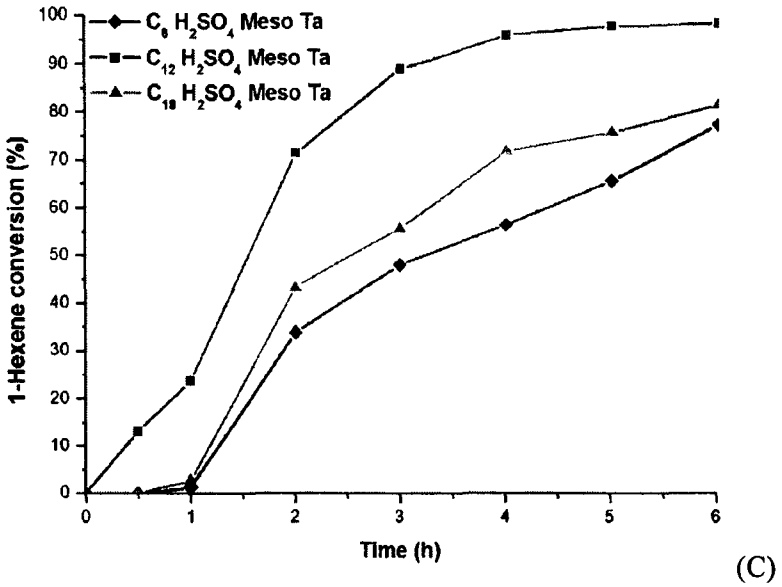

(C)

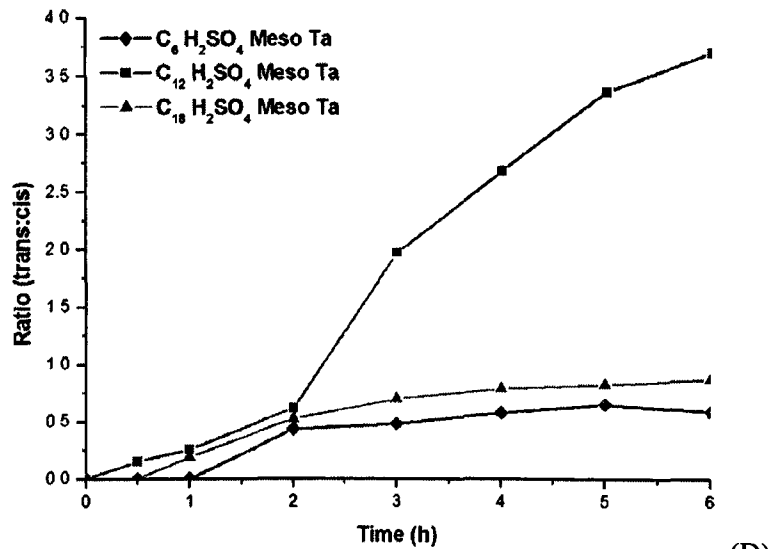

(D)

Figure 6.8 1-hexene isomerization conversion rate and selectivity of different pore size sulfated Nb and Ta oxides (A) activity of different pore size Nb oxides (B) selectivity of different pore size Nb oxides (C) activity of different pore size Ta oxides (D) selectivity of different pore size Ta oxides

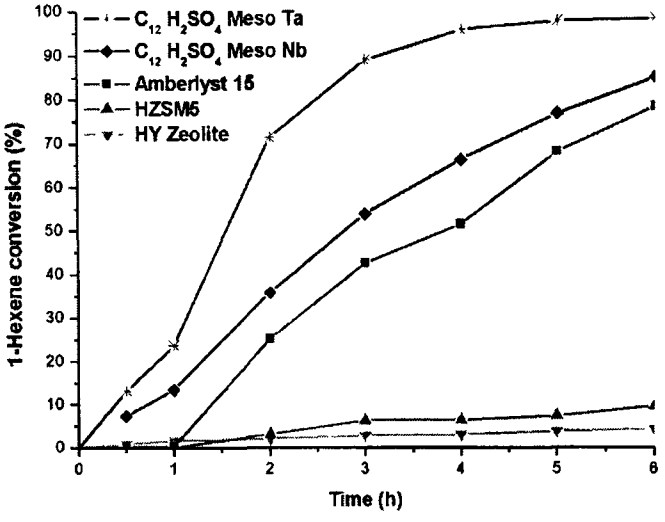

(A)

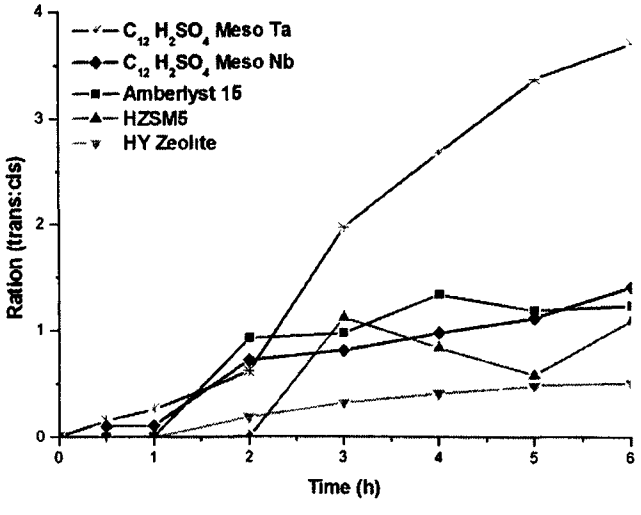

(B)

Figure 6.9 1-hexene isomerization conversion rate (A) and selectivity (B) on different catalysts.

In general, C_{12} samples (Nb and Ta) possess higher activity and selectivity than their C_6 and C_{18} counterparts, which can be attributed to a combination of their relative higher

BET surface area (413.97 m^2/g for C_{12} H_2SO_4 Meso Nb and 292.19 m^2/g for C_{12} H_2SO_4 Meso Ta; Table 6.1) and optimal pore size (18~20 Å). This is consistent with Tanchoux's observations on the higher activity of moderate pore size MCM-41 materials in this same reaction [38]. The author studied the impact of confinement and nesting effects in the isomerization of 1-hexene by MCM-41 and demonstrated that selectivity as well as conversion rate were pore size dependent. The conclusion was that both smaller pores and larger pores were less effective than moderately sized pores in this reaction.

Both the activities and selectivities of the Nb samples follow the order: C_{12} H_2SO_4 Meso Nb>C_{18} H_2SO_4 Meso Nb>C_6 H_2SO_4 Meso Nb, (Figure 6.8a, 6.8b), matching the trend in their BET surface area (413.97 m^2/g >282.58 m^2/g >160.35m^2/g). C_{12} H_2SO_4 Meso Nb has the highest activity and selectivity, but it is only slightly higher than its C_6 counterpart. The conversion of 1-hexene to *trans/cis* 2-isomers reaches roughly 65% in 4 hrs and its *trans/cis* ratio can eventually reach 1.4 in 6 hrs. Although these three Nb samples showed a relatively large difference in activity (ranging from 40% to 85%), they all displayed similar selectivity for this particular reaction. (*Trans/cis* ratio close to 1) The higher activities of all Ta materials relative to their higher surface area Nb counterparts can only be explained by the much more intense and broader distribution of Brønsted acid sites on the surface of Ta oxide relative to Nb oxide measured by TPD of ammonia experiments, as commented on above. (Figure 6.5)

The three Ta oxides samples did not follow the same order. C_6 H_2SO_4 Meso Ta has the smallest pore size (12 Å) and second highest surface area (206.40 m^2/g), but the lowest observed activity and second lowest selectivity. This can be explained by its much smaller pore size, which effectively blocks the penetration of the reactant (1-hexene in

this reaction) and prevents access to the active Brønsted acid sites inside the pore, forcing most of the reaction to occur on the ektexine of the wall. This leads to both low activity and selectivity. In contrast, C_{18} H_2SO_4 Meso Ta possesses the largest pore size (22.5Å), which allows the reactant (1-hexene) and products (both 2-hexene isomers) to diffuse in and out of its large pores without much hindrance. This leads to poor selectivity. Although the large pore size of the C_{18} sample facilitates the diffusion of the reactant to the active site, this sample possess the lowest surface area (188.79 m^2/g), which results in an activity that falls between that of its two congeners. C_{12} H_2SO_4 Meso Ta showed the highest activity (~95% in 4 hrs) and selectivity among these three Ta samples.

The moderate pore size of C_{12} H_2SO_4 Meso Ta oxide (18.2Å, Table 6.1) also allows linear *trans*-2-hexene to pass more easily though its channels than non-linear *cis*-2-hexene. Its *trans/cis* ratio thus reaches 3.7 in 6 hrs, which is much greater than that in the other Nb and Ta samples which level off at a *trans/cis* ratio of close to 1. The *trans/cis* ratio for C_{12} Ta is very close to the thermodynamic equilibrium for this reaction (3.37) calculated using standard Gibbs energy equation. This increase in selectivity over time to the thermodynamic mixture can be attributed to the more efficient conversion of *cis*-2-hexene to *trans*-2-hexene in the pores of this material relative to the other catalysts in this study. So, once the *cis* product is formed it is rapidly converted to the *trans* product, increasing the *trans/cis* ratio. This material thus acts as a bifunctional catalyst, not only speeding up the 1-hexene isomerization conversion rates to the two isomers, but also facilitating the *cis*-2-hexene to *trans*-2-hexene isomerization in these two products. Abbot et al [41~42] systemic studied the isomerization reaction of 1-hexene to 2-hexene and reported that this reaction involves a proton transfer process, the initial proton is

transferred from the acid sites on the surface of the catalyst to the double bond of 1-hexene, and then the hydride shift along the linear chain produces *cis*-2-hexene and *trans*-2-hexene. Further studies are necessary to investigate the confinement effect that results in the facile conversion of the two 2-hexene isomers after initial reaction.

The activity and selectivity of C_{12} Nb and Ta samples are compared with HY zeolite, H-ZSM5 and Amberlyst 15 in Figure 6.9. Both the Nb and Ta materials showed much higher activity than the zeolites (HY zeolite and H-ZSM5) at this low reaction temperature (343 K), roughly 10 times greater and even higher than the well-known ion exchange resin Amberlyst 15, which is regarded as one of the best industrial catalysts for this reaction [39~40]. The selectivity of the C_{12} Ta material (3.7) is again superior to all other samples, which range from 0.5 to 1.1 after 6h. Pure sulfuric acid was used as reference catalyst in a separate experiment to eliminate the potential effect of free H_2SO_4 on selectivity [19]. The conversion of 1-hexene reached 31.18% after 6 hours, and an only slightly higher product ratio (1.5) was obtained as compared to the C_6 and C_{18} Nb and Ta samples. This is still far behind the selectivity of C_{12} H_2SO_4 mesoporous Ta oxide, which establishes once again that pore size is crucial to the selectivity in this system.

To test the reusability of C_{12} H_2SO_4 mesoporous Ta, three continuous runs were conducted using the same catalyst. The results showed that catalytic activity declined linearly, the conversion rate of 1-hexene decreasing from almost 100% to 76%, and then to 40% [19]. This may be attributed to partial pore blockage caused by isomerization products deposited inside the channel. This is consistent with the drop in BET surface area from 292 m^2/g to 133.25 m^2/g. However, elemental analysis shows no increase in

%C, demonstrating that loss of surface area is not due to the build up of carbon species, but some form of structural collapse. The activity of the used catalyst can be partially regenerated to 60% its original activity by treatment with new sulfuric acid, which shows that sulfate leaching during each catalytic run is at least partially responsible for the gradually loss of catalytic activity on recycling.

6.5 Conclusion

This paper provides a clear demonstration of the influence of acid sites and confinement effect in 1-hexene isomerization catalyzed over sulfated mesoporous Nb and Ta oxides. These catalysts showed higher activities and selectivities than Amberlyst 15, HY zeolite and H-ZSM5. Among these different pore size of sulfated mesoporous Nb and Ta oxides studied, C_{12} H_2SO_4 mesoporous Ta showed both the highest activity and selectivity, which can be attributed to its high BET surface area, optimal pore size, and increased concentration of active Brønsted acid sites on the surface of the mesoporous channels, as confirmed by ammonia TPD.

6.6 References

1. C.T. Kresge, M.E. Leonowicz, W.J. Roth, J.C. Vartuli, J.S. Beck, *Nature* **1992**, *359*, 710
2. J.S. Beck, J.C. Vartuli, W.J. Roth, M.E. Lernowicz, C.T. Kresge, K.D. Schmitt, C.T.W. Chu, D.H. Olson, E.W. Sheppard, S.B. Mccullen, J.B. Higgins, J.C. Schlenker, *J. Am. Chem. Soc.* **1992**, *144*, 10834
3. Y Ma, W. Tong, H. Zhou, S. L. Suib, *Microp. Mesop. Mater* **2000**, *37*. 243

4. A.K. Cheetham, G. Fe rey, T. Loiseau, *Angew. Chem. Int. Ed.* **1999**, *38*, 3269

5. A. Corma, *Chem. Rev.***1997**, *97*, 2373

6. D.T. On, D. Desplantier-Giscard, C. Danumah, S. Kaliaguine, *Appl. Catal. A. Gen,* **2003**, *253*, 545

7. A. Taguchi, F Schuth, *Microp. Mesop. Mater.* **2005**, *77*, 1

8. D.M. Antonelli, Y.J. Ying, *Angew. Chem Int. Ed. Engl* **1996**, *35*, 426

9. D.M. Antonelli, Y.J. Ying, *Chem. Mater* **1996**, *8*, 874

10. D.M. Antonelli, A. Nakahira, Y.J. Ying, *Inorg. Chem.* **1996**, *35*, 3126

11. M.S. Wong, D.M. Antonelli, J.Y Ying, *NanoStruct. Mater.* **1997**, *9*, 165

12. D.M. Antonelli, *Microp. Mesop. Mater.* **1999**, *30*, 315

13. Z. Tian, W Tong, J. Wang, N. Duan, V V Krishnan, S.L. Suib, *Science*, **1997**, *276*, 926

14. S. Velu, M.P. Kapoor, S. Inagaki, K. Suzuki, *Appl. Catal. A:Gen.* **2003**, *245*, 317

15. C. Yue, M.L. Trudeau, D.M. Antonelli, *Chem. Commun.* **2006**, 1918

16. C. Yue, M.L. Trudeau, D.M. Antonelli, *Can. J. Chem.* **2005**, *83*, 308

17. Y. Rao, M.L. Trudeau, D.M. Antonelli, *J. Am. Chem. Soc.* **2006**, *128*, 13996

18. J. Kang, Y Rao, M.L. Trudeau, D.M. Antonelli, *Angew. Chem. Int. Ed.* **2008**, *47*, 4896

19. Y. Rao, J. Kang, D.M. Antonelli, *J. Am. Chem. Soc.* **2008**, *130*, 394

20. J.M. Proell, E.E. Mosley, G.L. Powell, T.C. Jenkins, *J. Lipid. Res.* **2002**, *43*, 2072

21. B.O. Skadtchenko, Y Rao, T.F Kemp, P Bhattacharya, P.A. Thomas, M. Trudeau, M.E. Smith, D.M. Antonelli, *Angew. Chem. Int. Ed.* **2007**, *46*, 2635

22. T. Sun, J.Y Ying, *Nature* **1997**, *389*, 704

23. C. Bezouhanova, H. Lechert, G. Taralanska, A. Meyer, *React. Kinet. Catal. Lett.* **1989**, *40*, 209

24. M. Li, Y. Chu, H. Nie, Y Shi, D. Li, *Stud. Surf. Sci. Catal.* **2003**, *145*, 403

25. F Di-Gregorio, V Keller, T. Di-Costanzo, J.L. Vignes, D. Michel, G. Maire, *Appl Catals A- Gen* **2001**, *218*, 13

26. R. Barthos, F Lonyi,; Gy. Onyestyak, J. Valyon, *J. Phys. Chem. B.* **2000**, *104*, 7311

27. R. Barthos, F Lonyi,; Gy. Onyestyak, J. Valyon, *Solid. State. Ionics.* **2001**, *141*, 253

28. W.H. Chen, H.H. Ko, A. Sakthivel, S.J. Huang, S.H. Liu, A.Y Lo, T.C. Tsai, S.B. Liu, *Catal. Today.* **2006**, *116*, 111

29. P Borges, R.R. Pinto, M.A.N.D.A. Lemos, F. Lemos, J.C. Vedrine, E.G. Derouane, F.R. Ribeiro, *J Mol. Catal A-Chem.* **2005**, *229*, 127

30. J.P. Joly, A. Perrard, *Langmuir,* **2001**, *17*, 1538

31. H. Matsuhashi, K. Arata, *Chem. Commun.* **2000**, 387

32. H. Matsuhashi, K. Arata, *Phys. Chem. Chem. Phys.* **2004**, *6*, 2529

33. F Gaillard, J.P Joly, A. Boreave, P. Vernoux, J.P Deloume, *Appl. Surf. Sci.* **2007**, *253*, 5876

34. F. Gaillard, M. Abdat, J.P. Joly, A. Perrard, *Appl. Surf. Sci.* **2004**, *238*, 91

35. Z. Wu, Q. Wang, L. Xu, S. Xie, *Stud. Surf. Sci. Catal.* **2002**, *142*, 747

36. I. Eswaramoorthi, V Sundaramurthy, N. Lingappan, *Microp. Mesop. Mater.* **2004**, *71*, 109.

37. V Logie, G. Maire, D. Michel, J.L. Vignes, *J. Catal.* **1999**, *188*, 90

38. S. Pariente, P. Trens, F Fajula, F.D. Renzo, N. Tanchoux, *Appl. Catal. A- Gen* **2006**, *307*, 51

39. J. Abbot, B.W. Wojciechowski, *J. Catal.* **1984**, *90*, 270.

40. J. Abbot, B.W Wojciechowski, *J. Catal.* **1985**, *92*, 398

41. P. Slomkiewicz, Appl. Catal. A-Gen **2006**, *301*, 232

42. M. Mitkova, K. Kurtev, *J. Chin. Chem. Soc.* **2005**, *52*, 1185

Chapter 7

Mesoporous Transition Metal Oxides: Applications in Heterogeneous Catalysis

This chapter is organized based on an invited highlight paper submitted to *Journal of Materials Chemistry* by **Yuxiang Rao**, and Dave M. Antonelli

7.1 Introduction

In recent years, environmental and economic factors have spurred a strong interest in redesigning commercially important chemical or petrochemical processes so that the use of harmful substances and/or the generation of toxic waste could be avoided. For this reason, heterogeneous catalysts, which do not generate or require harmful or disposable waste materials, are of particular importance. Heterogeneous catalysts are already the most important catalysts in the areas of ammonia production and petroleum refining. One of the most important classes of heterogeneous catalysts is the solid acid. Among the

family of solid acid materials widely used in industry, the best-known examples are zeolites. These are crystalline microporous materials, which have became extremely successful as catalysts for oil refining and petrochemistry due to their high surface areas, high hydrothermal stability, high acidity, narrow and uniform micropore size distribution, especially when dealing with molecules having kinetic diameters below 10 Å. However, zeolites has severe pore size limitations when large reactant molecules are involved, especially in liquid-phase systems as is frequently the case in the synthesis of fine chemicals. Attempts to improve the diffusion of the reactants to the catalytic active sites have focused on increasing the zeolite pore sizes to mesoporous,[1] or on providing an additional mesopore system within the micro porous crystals [2~3].

In 1992, materials scientists in Mobil Oil Corporation first discovered mesoporous silica and aluminosilicates, namely M41S family, which stands for Mobile composition of matter No. 41 [4~5]. This material possesses a highly ordered hexagonal array of unidimensional pores with a narrow pore size distribution. Since this time, mesoporous molecular sieves (MMS) have attracted a great deal of worldwide attention among researchers in the fields of materials synthesis [6~7] and heterogeneous catalysis [8~10] due to their repeat and regular pore structure on the nanometer scale, uniform pore diameter and high surface areas (up to 1600 m^2/g). The adjustable porosity of silica-based MMS allows large molecules to penetrate through their mesoporous structure into the internal void space, to be processed at the active sites on the internal surface and then diffuse out freely as products. This unique property overcomes the pore-size limitation of microporous zeolitic catalysts. During the last two decades, these silica-based mesoporous materials such as MCM-41, FSM-16 and SBA-15, etc., have been well

investigated, their preparation methods and applications have already been covered by several excellent review papers [11~14]. However, siliceous mesoporous materials possess very low acidity due to the silanol groups and lack of crystallinity in their Al-doped counterparts. Less work has been directed toward non-silica transition-metal mesoporous materials although they have great potential in a wide range of catalytic applications [15~19] The advantage of these mesoporous transition-metal oxides over the traditional silica-based materials is that they are capable of existing in various oxidation states because of the empty transition metal d orbitals, which allow electron transfer to occur between the reactants and active sites during a given catalytic process [20~21] Many early transition metal oxides, especially in their sulfated form, possess high acidities, even in their amorphous state. This gives them a strong advantage over aluminosilicates, which must be crystalline to show high surface acidities. This is of special importance because the majority of mesoporous materials are amorphous, especially those with pore sizes less than 30 Å synthesized with surfactant templates rather than block copolymers.

Recent advances in our group showed that mesoporous titanium, niobium and tantalum oxides demonstrated very high activity and selectivity for a wide range of catalytic applications such as dinitrogen activation [22~28], benzylation [29], alkylation [30], and isomerization [31]. The results of these studies are detailed below.

7.2 Dinitrogen Activation

The cleavage and selective functionalization of dinitrogen is one of the most challenging areas of modern catalysis [24~30,32~33]. From a kinetic point of view,

dinitrogen is a notoriously inert gas and difficult to activate. However, the reduction of dinitrogen by hydrogen into ammonia is thermodynamically feasible. The cleavage of the nitrogen triple bond is an extremely rare and important reaction that typically requires very forcing conditions in the solid state, such as high temperature, microwave radiation or argon plasmas etc [34~37]. Commercially, this reaction is carried out with hydrogen at high pressure and temperatures in excess of 400 °C [38]. So far, there are no applicable industrial catalysts have yet been developed for this process that can operate at lower temperatures on a smaller scale such that the selective functionalization of dinitrogen may also be possible. The first example of a molecular sieve mediating this process was reported by our group in 2002 [22~23]. This system relied on a highly reduced mesoporous transition metal center first reducing the dinitrogen, followed in a second step by protonation by residual moisture. The mesoporous niobium and titanium oxide was synthesized by using ligand-assisted liquid crystal templating approach according to literature [39]. The as-synthesized mesoporous niobium and titanium samples were treated with bis(toluene) niobium and bis(toluene) titanium respectively under nitrogen at room temperature, leading to new black materials that exhibited metallic properties. These were the first examples of mesoporous oxides with metallic conductivity. This metallic behavior was attributed to low-valent transition metal existing in the wall of the porous structure.

These materials also reacted spontaneously with dinitrogen. For the Nb sample, this lead to the formation of a thin nitride coat on the surface, which was confirmed by elemental analysis and solid-state ^{15}N NMR experiments. The N content increased from <0.01% to 0.3~1.5%, indicating that up to 8% of the Nb atoms present in the

mesostructure are active in this process as calculated on the basis of the % Nb in the material and assuming a 1:1 N/Nb reaction stoichiometry. When the reaction is conducted with $^{15}N_2$, the solid-state ^{15}N NMR spectrum exhibits two overlapping peaks at –356.3 ppm and –381.2 ppm, confirming that dinitrogen is indeed the source of these nitride species. The facility of nitrogen activation in this oxide-based system was attributed to the high fraction of exposed low-coordinate Nb^{II} centers on the inner surface of the material. Also, the controlled porosity, high surface areas and large concentration of surface defects in the amorphous walls of the mesostructure may have played an important role in this stoichiometric process. The nitride coat rapidly reacts with moisture to produce ammonia as evidenced by XPS. This contrasts to many metal nitrides, which are normally inert towards proton sources. This high reactivity was attributed the large number of defects and amorphous nature of the surface of the nitrided mesostructure.

The extension of this chemistry to Ti-based systems was successfully achieved afterwards and represented a significant step [22], since bis(toluene) niobium is extremely difficult to synthesize and Ti is a much less expensive metal than Nb. An analogous reaction towards dinitrogen was observed in this system. The conversion of dinitrogen to nitride most likely occurs by cleavage of dinitrogen by low valent Ti centers on the surface of the mesostructure. However, IR and solid-state ^{15}N CPMAS NMR experiments demonstrated that the initially formed nitride species had already further reacted with moisture imbedded in the walls of the mesostructure and produced surface ammonia. Since Ti (II) does not have enough electrons to reduce dinitrogen, several adjacent Ti centers must be involved in this process.

These reactions were very interesting because they represented rare examples of the spontaneous conversion of dinitrogen to ammonia at room temperature. The question was how to make this system catalytic. In order to accomplish this, it is important to make the mesoporous catalysts as stable as possible. Mesoporous titanium oxide begins to collapse at only 300 °C, while mesoporous niobium oxide shows a slightly higher thermal stability, collapsing at 400 °C [40]. The stability of these materials under operating conditions for long periods of time is likely to be even lower. To this regard, mesoporous tantalum oxide, with thermal stability in excess of 500 °C, is probably the best candidate for a catalytic support material out of these three systems [24]. However, reducing this material with corresponding bis(toluene) tantalum is unfeasible due to the lack of effective routes to synthesis this compound. For this reason, the surface of mesoporous tantalum was reduced with much cheaper and widely available bis(toluene) titanium prepared by metal vapor synthesis [32]. This leaves a low valent coat of Ti on the surface of the mesoporous Ta oxide. This Ti-Ta system also allows for more clear XPS observation of the Ti oxidation states than the Ti-Ti system studied above since these two elements have different XPS emission regions. Thus any Ti in the Ti-Ta system comes from bis(toluene) titanium, while there is ambiguity as to the origin and overlapping of emissions in the Ti-Ti system. As in the case of the Ti-Ti and Nb-Nb systems, the activation of dinitrogen and complete conversion of nitride to ammonia proceeds smoothly at room temperature with excess moisture, as confirmed by the appearance of a dominant N-H stretch in the IR spectrum.

Our first attempts to develop a truly catalytic conversion of dinitrogen to ammonia over mesoporous Ta oxide involved photocatalysis and the use of water as the reductant

and proton source. Schrauzer et al. demonstrated that electron-hole separation on Fe-doped titania led to highly reactive sites on the surface, which could trap and reduce dinitrogen [26]. Oxidation of water by the hole provided a source of protons and electrons to complete the cycle and make the process catalytic. The doping of the metal oxide was found to be a necessary step for the high activity for reasons that are still not clear, but may be related to the creation of a permanent space-charge region in the materials. Since these materials are based on oxides that normally display photocatalytic activity in the bulk phase (ie Ti, Ta), it appears that the development of a related mesoporous transition metal oxide photocatalysts may indeed be feasible. Based on this assumption, pure mesoporous tantalum oxide, Fe^{3+}-doped mesoporous tantalum oxide and bis(toluene) titanium reduced mesoporous tantalum oxide were used for the first time as Schrauzer-type photocatalysts [25] using a dinitrogen and water mixture as the feeding source. These materials were characterized by XRD, TEM, XPS, and nitrogen absorption before and after each catalytic run.

Pure mesoporous tantalum oxide without any treatment only shows low activity of 0.263 μmol/g/h. Thermal treatment at 300 °C for 3 h improves the activity to 0.683 μmol/g/h. Prolonged heating decreased the activity to 0.47 μmol/g/h. The improved activity on heat treatment is not unexpected because this process increases local crystallization of materials, which often leads to more efficient migration of electrons and holes through the lattice to the surface. This is consisted with Schrauzer and Guth's work [26] on the conversion of the anatase phase to the rutile phase where modification by heat treatment at 1000 °C was a prerequisite for the high activity. However, in the case of mesoporous Ta oxide, prolonged calcinations at 400 °C causes a diminution of the active

surface in addition to an increasing loss of surface metal hydroxide groups, both contributing to a decrease of photocatalytic activity. Crystallization of the walls to the bulk oxide occurs upon exhaustive thermal treatment, resulting in a collapse of the mesostructure. To get higher activities, a series of Fe^{3+}-doped Ta oxides with different loading levels (from 0.3% to 2%) were prepared. The highest activities appeared on the 1-wt% Fe^{3+}-doped sample. The reason for this Fe-induced enhancement of activity is not completely clear, but it may be related to a modification of the band-gap region and (or) formation of a permanent space charge region in the walls. The organometallic sandwich compound bis(toluene) titanium was used as reducing agent to improve the surface conductivity of mesoporous tantalum oxide, which may be useful in promoting electron-hole separation and thus increase the activity. Surprisingly, this bis(toluene) Ti reduced mesoporous Ta oxide catalyst did not give better results than pure tantalum oxide. The most likely explanation for this is that although bis(toluene) titanium increases the surface conductivity and creates sites capable of splitting dinitrogen, this surface coat is very air sensitive and likely degrades as O_2 is formed over the course of the reaction.

While this photocatalytic route did produce some ammonia, the activities were very low. For this reason we decided to develop catalysts that used a precious metal electrode on a mesoporous Ta oxide surface to convert hydrogen into protons and electrons for the cleavage and subsequent protonation of dinitrogen. Since Ru has been proved effective in a wide variety of Haber systems [41~44] a series of Ru-doped mesoporous Ta oxides employing $Ru_3(CO)_{12}$ as a Ru source and barium nitrate as the promoter were synthesized in our group as catalysts for nitrogen activation and ammonia synthesis [27]. This experiment was conducted under a stream of 1:3 N_2+H_2 at 350 °C. The catalyst has a high

initial activity of 163 x 10^{-6} $molg^{-1}h^{-1}$ in the first hour, but then the rate drops off dramatically in the second hour and continues at a rate of 1~2 x 10^{-6} $molg^{-1}h^{-1}$ The initial rate is over 100 times greater than that previous reported bis(toluene) Ti reduced mesoporous Ta oxide photocatalyst. The drop off in rate after the first hour is not understood but may be related to a combination of surface deactivation and thermally induced loss of structure, as the XRD shows a further loss of mesoscopic order and the BET surface area drops to 229 m^2g^{-1} While some of the NH_3 formed in the initial hour may come from residual nitrate, in order to verify that the catalyst is actually producing new ammonia in the second hour and the apparent activity does not come from ammonia adsorbed on the surface in the first hour, the catalyst after 1 h of initial activity at 350 °C was placed under vacuum at 10^{-3} Torr and 350 °C for 1 h before the temperature was lowered to ambient and catalysis resumed. The activity value obtained is 2~5 x 10^{-6} $molg^{-1}h^{-1}$, virtually the same as those obtained without the vacuum step, which rules out ammonia formation from any residual source. The activation energy (E_a) calculated from this plot is 9.3 $kJmol^{-1}$, roughly 10% of that calculated by the same methods for Ru-doped catalysts on other supports (E_a for Ru-Ba-MCM-41 is 90 kJ mol^{-1}; Ru-Ba-MgO is76 kJ mol^{-1}) in which dinitrogen cleavage is known to occur at the Ru clusters. This value suggests that the cleavage of N_2 occurs on reduced Ta sites in our system (as observed in many organometallic systems) and may be diffusion controlled. Since pure mesoporous Ta oxide does not react with H_2 under this condition, the Ru dopant must act as a hydrogen electrode thus lowering the activation barrier to the reduction of Ta species. A new mechanism for conversion of dinitrogen to ammonia was propose based on these observation in which the Ru acts as an interface to transfer electrons from hydrogen to the neighboring Ta sites on the oxide support and dinitrogen cleavage occurs on the reduced

Ta center and not the precious metal surface as in traditional Ru-Haber systems. In the final step the nitride generated at the Ta reacts with the protons liberated from the hydrogen at Ru. (Scheme 1) XPS studies on catalysts at various stages of the process revealed reduced Ta sites, adding further support to this mechanism. Since reduced Nb and reduced Ti cleaves dinitrogen on the surface of the corresponding mesoporous oxide, such a proposal seemed feasible. The role of the Ba promoter in our system is not yet clear.

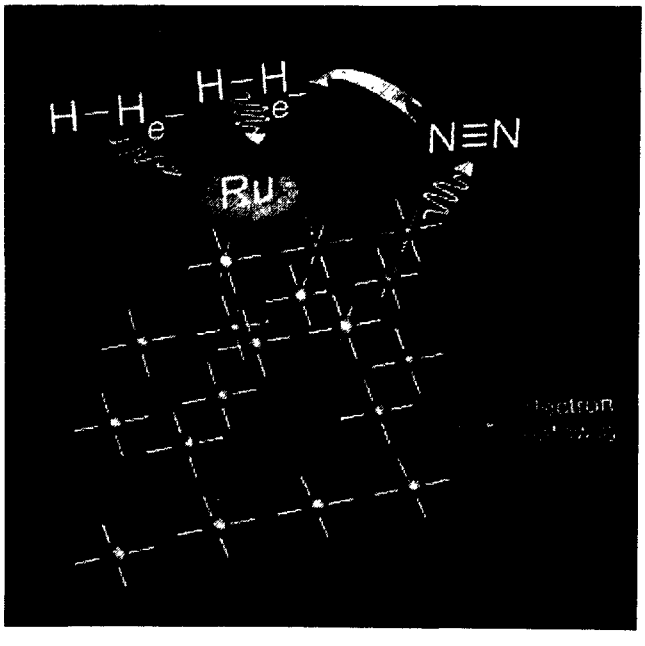

Scheme 7.1 Possible mechanism for ammonia formation on Ru-doped mesoporous Ta oxide materials showing reduced Ta sites in dark blue. Adapted from ref.27 © 2006 with permission from The Royal Society of Chemistry

To better understand this new system, the dependence of the activities on the type of Ru precursor, Ru loading levels, precious metal dopant other than Ru (i.e., Pd, Pt, Rh), promoter metal, promoter precursor, promoter loading levels, and hydrogen activation

temperature were investigated. A series of early metal-promoted Ru-, Pd-, Pt-, and Rh-doped mesoporous tantalum oxide catalysts thus were synthesized using a variety of dopant ratios and dopant precursors [28]. The effects of these parameters on the catalytic activity of NH_3 synthesis from H_2 and N_2 were explored. The results showed that Ba is a better promoter then Cs or La and that the nitrate is a superior precursor for Ba than the isopropoxide or the hydroxide. ^{15}N labeling studies demonstrated that residual nitrate functions as the major ammonia source in the first hour but it does not account for the ammonia produced after the nitrate is completely consumed. $Ru_3(CO)_{12}$ proved to be a better Ru precursor than $RuCl_3$ H_2O and an almost linear increase in activity with increasing Ru loading level was observed at 350 °C (623K). Pd functioned with a comparable rate to Ru, while Pt and Rh functioned far less efficiently. This surprising activities for the Pd-doped catalysts, coupled with XPS evidence for low-valent Ta in this catalyst system, further support the above mechanism in which cleavage of N-N triple bond occurs on reduced Ta center rather than the precious metal because the Ea value (~250 kJ mol^{-1}) for N-N cleavage on Pd is 2.5 times greater than that for Ru (76~90 kJ $mol^{-1)}$ These numbers are far beyond the 9.3 kJ mol^{-1} Ea value measured previously for the Ru system [27], which provides evidence that N-N triple bond cleavage cannot occur on the Ru or Pd surface under the conditions of our study. $Ba(NO_3)_2$ was found to be the best promoter in almost all studied Ru catalyst system [45]. The simplest explanation is that it facilitates electron transfer between the Ru and the Ta by modifying the Fermi level of the Ru, but this neglects possible direct interactions between Ba and Ta, Ba and O, or other factors mentioned above.

7.3 Benzylation

In 1996, Ying first reported the successful synthesis of mesoporous niobium oxide molecular sieves by using ligand-assisted liquid crystal templating approach [39~40].The catalytic properties of this novel material have not been systematic studied until recently [29]. Since phosphated and sulfated Nb oxides are known to have acid properties useful in hydrocarbon coupling and rearrangement reactions, we decided to explore the applications of mesoporous Nb oxide in these areas. So, as-synthesized pure mesoporous Nb samples were treated with 1M sulfuric acid or phosphoric acid (both in methanol solution) separately to enhance their surface acidities. The catalytic activities of these materials were then evaluated using the model reaction of benzylation of anisole or toluene with benzyl alcohol in the liquid phase at reflux temperature [46]. The untreated mesoporous Nb oxide possesses an activity of ca. 8 times (80% in 9h) that of the sulfated bulk material (10% in 9 h), while the phosphated mesoporous Nb sample possess an activity almost 20 times higher than this value. The best results were achieved with the sulfated mesoporous Nb oxide, which showed 100% conversion in only 30 mins. This activity is ca. 200 times greater than that of the sulfated bulk Nb oxide. To explore the unusually high reactivity of sulfated mesoporous Nb oxide, a series of modern analytical techniques including XRD, N_2 adsorption, TEM, FT-IR and amine titration method were adopted to probe its structure and surface properties before and after reaction.

The strong reflection in the XRD patterns in all samples (pure mesoporous Nb oxide, sulfated and phosphated Nb oxides) demonstrated the retention of the mesoporous structures after acid treatment. This was further confirmed by the type IV isotherm

obtained by nitrogen adsorption/desorption measurements [29]. This stability to acid is surprising considering that mesoporous silica and alumina lose their pore structure under low pH conditions. The average pore size of sulfated mesoporous Nb oxide estimated from the TEM image is around 20 Å. The FTIR (Fourier transform infrared) analysis of the spectra of pyridine adsorption (Figure 7.1) showed that Brønsted (1540 cm^{-1}) and Lewis (1450 cm^{-1}) acid sites coexist in a roughly 50:50 mixture on the surfaces of the parent materials and that the sulfated and phosphated materials exhibited a strong dominance of Brønsted acid sites.

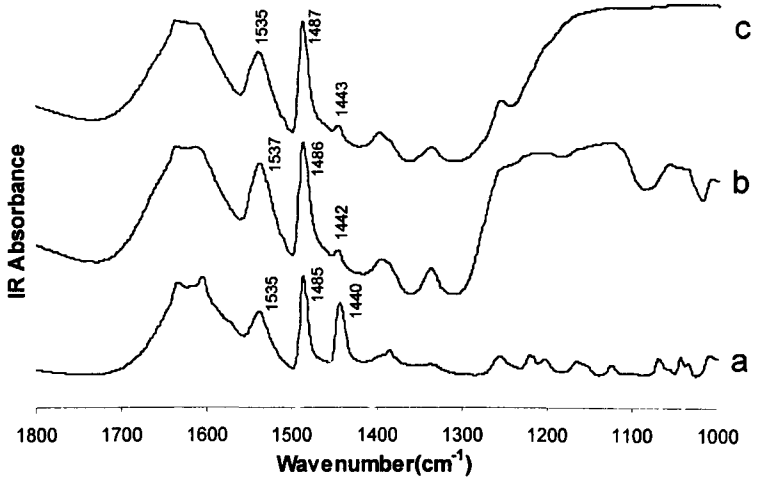

Figure 7.1 The FTIR spectra of different meso Nb oxides after pyridine vapor adsorption. a) Meso Nb, b) H_2SO_4/Meso Nb, c) H_3PO_4/Meso Nb. Adapted from ref.29 © 2006 with permission from the American Chemical Society

The Hammett acidity and n-butylamine titration methods were also employed to further probe the surface acidity of these mesoporous Nb oxides. These were also compared with commercially available bulk niobium pentoxide to gauge the effect of the

mesoporous structure on acidity. (Table 7.1, 7.2) The results clearly demonstrated that bulk niobia possess only weak acidic sites on the surface (pKa=+3.3), even for the sulfated and phosphated Nb samples (pKa=-3.0). In contrast, pure mesoporous Nb oxide has a surprisingly acidic Ho<-6.6, and after treatment with 1M sulfuric or phosphoric acid, its *Ho* value drops to –8.2, equal to 90% sulfuric acid. The n-butylamine titration experiments showed that sulfated mesoporous Nb possess 10 times more total Lewis and Brønsted acid sites (31.78 mmol/g) than the parent (2.478 mmol/g) or phosphated (3.086 mmol/g) mesoporous Nb oxides, and almost 100 times more acid sites than the bulk samples (0.024-0.338 mmol/g). Based on the observed results mentioned above, it is reasonable to assume that the extremely high activity of sulfated mesoporous Nb oxide is attributable to its high BET surface area, suitable mesoporosity, strong acid strength and increased concentration of Brønsted acid sites on the surface of the mesoporous channels.

Table 7.1 Distribution of the acidic strength with Hammett indicators. Adapted from ref.29

Indicator	**pKa**	**Nb_2O_5**	**H_2SO4 /Nb_2O_5**	**H_3PO_4 /Nb_2O_5**	**Meso Nb**	**H_2SO_4 /Meso Nb**	**H_3PO_4 /Meso Nb**
Methyl red	+5.0	+	+	+	+	+	+
Methyl yellow	+3.3	+	+	+	+	+	+
Crystal Violet	+0.8	-	+	+	+	+	+
Dicinnamalacetone	-3.0	-	+	+	+	+	+
2,4-Dinitroaniline	-4.4	-	-	-	+	+	+
Benzalacetophenone	5.6	-	-	-	+	+	+

2-Bromo-4,6-dinitroaniline	-6.6	-	-	-	+	+	+
9,10-Anthraquinone	-8.2	-	-	-	-	+	+
3-Nitrotoluene	-11.99	-	-	-	-	-	-
1-chloro-4-Nitrobenzene	-12.70	-	-	-	-	-	-
2,4-Dinitrofluorobenzene	-14.52	-	-	-	-	-	-

"+": color changed "-": color unchanged

Table 7.2. The amount of acids as mmol g^{-1}as calculated from n-butylamine titration. Adapted from ref.29 © 2006 with permission from the American Chemical Society.

Indicator	Nb_2O_5	H_2SO_4/ Nb_2O_5	H_3PO_4/ Nb_2O_5	Meso Nb	H_2SO_4/ Meso Nb	H_3PO_4/ Meso Nb
Methyl yellow	0.024	0.338	0.317	2.478	31.784	3.086

7.4 Alkylation

Friedel-Crafts reactions, including alkylation, are always performed in liquid phase with homogenous acid catalysts like $AlCl_3$ and H_2SO_4. However, this process lacks selectivity toward the desired products and also causes severe environmental problems. MMS thus offer the opportunity to apply heterogeneous catalysis to these organic reactions for bulky substrates, while maintaining easy product diffusion to the catalytically active sites. For instance, linear alkylbenzenes (LAB), the primary intermediates in detergent industry, are commercially manufactured by the alkylation of benzene with C_{10-14} n-alkenes [47]. Among LAB isomers, 2-phenyl isomers are the most favorable starting materials for the production of ecofriendly domestic and industrial

detergents because of their high solubility and biodegradability [48]. However, when traditional homogeneous catalysts such as HF or $AlCl_3$ are used, a thermodynamic mixture of LAB isomers is always obtained. Furthermore, the use of highly corrosive and toxic HF or $AlCl_3$ poses disposal problems. So the development of environmentally friendly solid acid catalysts with a high selectivity to 2-pheyl isomers in benzene alkylation is an area of great interest.

Due to their high thermal stability and acidity, a series of mesoporous Ta oxides with different pore sizes were prepared using the ligand-assisted templating approach [39]. Treating the template free mesoporous Ta oxides with 1M sulfuric acid produced the sulfated samples. The confined mesoporous structure in the sulfated sample was also confirmed by XRD and the N_2 adsorption/desorption isotherm. The BET surface area dropped from 582.7 m^2/g to 292.2 m^2/g after acid treatment.

The catalytic properties of sulfated mesoporous Ta oxides were evaluated in terms of olefin conversion and the selectivity towards 2-phenyl isomers. At 80°C and a benzene/olefin molar ratio of 10:1, 100% 1-dodecene conversion was achieved within 0.5h. More interestingly, the pore size optimum depends strongly on the dimensions of the molecules of reagents. When 1-tetradecene was used, the conversion was only 17.5%. This is not unexpected since the longer the olefin chain, the more difficult it is for the olefin molecules to access the active sites in the mesopores. Therefore, activity decreased with an increase in olefin chain length. In order to further clarify the effect of pore structure on activity, this reaction was also carried out over sulfated C_6 and C_{18} mesoporous Ta oxide prepared by using 1-hexylamine and 1-octadecylamine as templates. The results showed a lower activity of 46.9% for the C_6 sample and 2.3% for the C_{18}

sample. The lower activity of sulfated C_6 Ta oxide is attributed to the strong diffusion resistance offered by the pore blocking in smaller pores [49]. As for the sulfated C_{18} Ta oxide, the low 1-dodecene conversion rate may be caused by its relatively low surface area and extremely low pore volume. H-Y zeolite, H-ZSM5 and Amberlyst 15 solid acid catalysts were also tested for comparison. H-Y zeolite showed similar activity with sulfated C_{12} Ta oxide and gave 100% 1-dodecene conversion at 80 °C within 0.5h, but only half the selectivity (25.31%) at a 1-dodecene conversion of ca. 60% towards 2-phenyldodecane compared to 49.19% for sulfated C_{12} Ta oxide. H-ZSM5 has not activity at all for this alkylation reaction, possible due to the diffusion limitation into the channels with smaller pore windows. Although it possesses strong acid sites, Amberlyst 15 only has moderate activity and selectivity (38.31%), which may be explained by its low surface area (55.1 m^2g^{-1}) and thus smaller amount of active sites on the internal surface of pores. The high selectivity of sulfated C_{12} Ta oxide can be attributed to "confinement effect", which indicates that selectivity as well as conversion rate are pore size dependent [50]. Jaenicke et al. reported the shape-selective [51] catalysts prepared by immobilizing $AlCl_3$ onto a series of MCM-41 mesoporous silicas with different pore sizes. They found that the selectivity towards the monoalkylation product in the synthesis of linear alkyl benzenes could be controlled by changing the pore size of the MCM-41 supports. The mesoporous structure in our sulfated Ta oxide may offer a similar confined space for the establishment of shape selective reactions.

7.5 Isomerization

The isomerization of straight-chain hydrocarbons to branched-chain isomers is of

great importance in the synthesis of high-octane fuels. This reaction is also widely used by many researchers in both homogeneous [52,53] and heterogeneous [50,54~55] process as a test of a material's effectiveness as an acid catalyst. Due to its quite mild reaction condition (343 K) and simple monomolecular reaction process, 1-hexene isomerization was chosen as model system to evaluate the activity and selectivity of sulfated mesoporous Ta oxides with different pore sizes [31]. H-Y zeolite, H-ZSM5 and Amberlyst 15 solid acid catalysts were also tested for comparison.

The results are shown in Figure 7.2. C_{12} H_2SO_4 Meso Ta has the highest activity (~95% in 4h) and selectivity (~3.7) towards *trans*-2-hexene, far beyond its competitors such as zeolites and Amberlyst ion exchange resin [31], which can be attributed to a combination of its pore size optimum and highest surface area (292.19 m^2/g). The selectivity (ratio of *trans:cis*) of C_{12} Ta is around 3.7, close to its theoretical thermodynamic equilibrium constant as calculated using the standard Gibbs energy equation [eqn (1)].

$$\Delta G^{\Phi} = -RT \ln K_{eq} \qquad (1)$$

Where ΔG^{Θ} is the standard Gibbs energy change of reaction, R is the gas constant, and T is the absolute temperature. This conspicuously high selectivity and short reaction time was not detected with the Ta materials synthesized with C_6 or C_{18} template, confirming that confinement effects are at work. This phenomenon is consistent with the results we observed in our previous work on alkylation [30]. The pore size of the C_{12} H_2SO_4 Meso Ta oxide is 18.2Å, which allows linear *trans*-2-hexene to pass more easily though its channels than nonlinear *cis*-2-hexene. The larger pore size (22.5Å) in the C_{18} Ta sample

allows both isomers (*trans* and *cis*) to be formed inside its channel structure and diffuse out freely, leading to poor selectivity. As for the C_6 Ta sample, the limitation of its small pore size (12Å) blocks the penetration of the reagent, forcing most of the reaction to occur on the ektexine of the wall and not inside the pores. This leads to low selectivity as well.

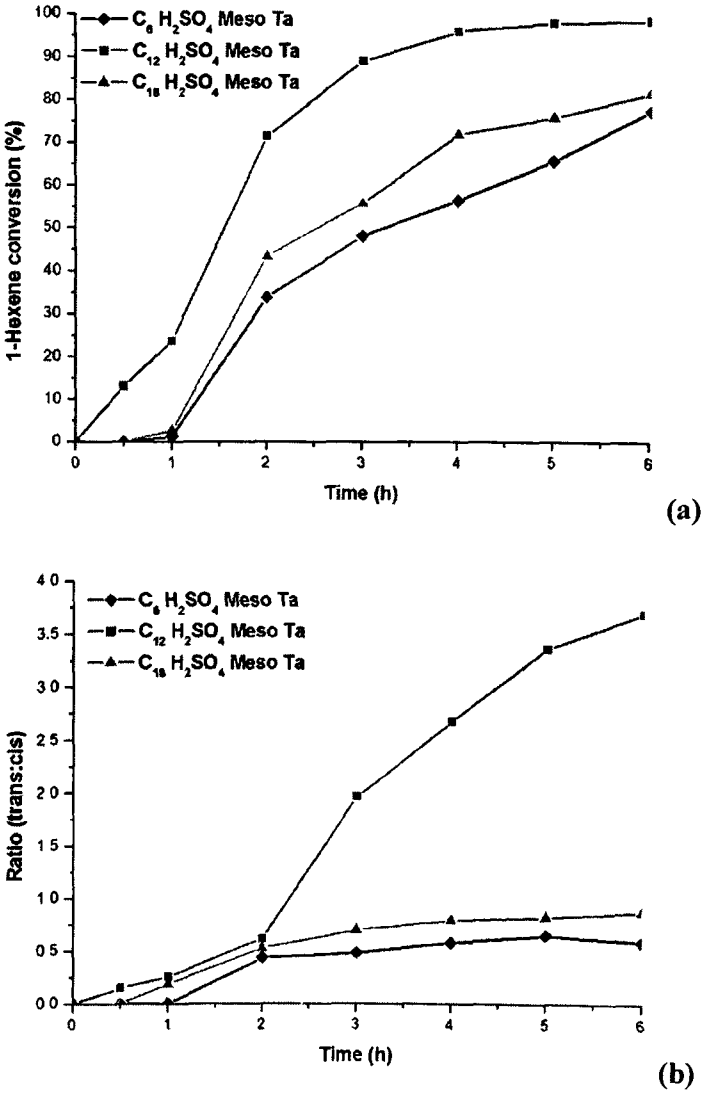

Figure 7.2 1-Hexene isomerization on sulfated mesoporous Ta oxides with different pore sizes. (a) 1-Hexene conversion rate with time (b) Ratio of trans-2-hexene to

cis-2-hexene with time. Adapted from ref.57 © 2008 with permission from the American Chemical Society.

To eliminate the potential effect of free H_2SO_4 on selectivity, a separate experiment was performed using a drop of pure sulfuric acid as catalyst, the conversion of 1-hexene reached 31.18% after 6 h, and an only slightly higher ratio (1.5) was obtained. This value is still far behind the selectivity of C_{12} H_2SO_4 Meso Ta oxide, which establishes that pore size is crucial to the selectivity in this system.

7.6 Conclusions

The narrow and uniform pore size of mesoporous transition metal oxide materials (M = Ti, Nb, Ta) with variable oxidation states and high surface area holds much promise for the development of novel catalysts in areas requiring high surface acidity or variable oxidation states of the support. Already a novel process for ammonia formation from dinitrogen and a new family of extremely active and selective solid acid catalysts that surpass the industry standard have been realized. The wide pore openings of the mesoporous catalysts minimize mass transfer problems posed by bulky reactants and products that often cause diffusion problems in zeolitic systems. Confinement effects were found in this study and seem to be the basis of the very high selectivities observed in the many of the reactions. These findings highlight the high potential of these mesoporous materials in a wide range of heterogeneous processes.

7.7 References

1. M. E. Davis, C. Saldarriaga, C. Montes, J. Garces, C. Crowder, *Nature*, **1988**, *331*, 698.
2. B. J. Schoeman, J. Sterte, J. E. Otterstedt, *J. Chem. Soc. Chem.Commun.* **1993**, 994.
3. A. H. Janssen, A. J. Koster and K. P. de Jong, *Angew. Chem. Int. Ed.* **2001**, *40*, 1102.
4. C. T. Kresge, M. E. Leonowicz, W. J. Roth, J. C. Vartuli, J. S. Beck, *Nature* **1992**, *359*, 710.
5. J. S. Beck, J. C. Vartuli, W. J. Roth, M. E. Lernowicz, C. T. Kresge, K. D. Schmitt, C. T. W. Chu, D. H. Olson, E.W. Sheppard, S. B. Mccullen, J. B. Higgins, J. C. Schlenker, *J. Am. Chem. Soc.* **1992**, *144*, 10834
6. Q. Huo, R. Leo'n, P. M. Petroff, G. D. Stucky, *Science* **1995**, *268*, 1324.
7. D. Zhao, J. Feng, Q. Huo, N. Melosh, G. H. Fredrickson, B. F. Chmelka, G. D. Stucky, *Science* **1998**, *279*, 548.
8. A. Taguchi, F Schuth, *Micro. Meso. Mater.* **2005**, *77*, 1
9. F. A. Twaiq, A. R. Mohamed, S. Bhatia, *Micro. Meso. Mater.* **2003**, *64*, 95
10. E. Byambajav, Y. Ohtuska, *Fuel* **2003**, *82*, 1571
11. N.K. Raman, M.T. Anderson, C.J. Brinker, *Chem. Mater.* **1996**, *8*, 1682
12. A. Sayari, P. Liu, *Micropor. Mater.* **1997**, *12*, 149
13. A. Corma, *Chem. Rev.* **1997**, *97*, 2373
14. J. Y. Ying, C. P. Mehnert, M. S. Wong, *Angew. Chem. Int. Ed*, **1999**, *38*, 56
15. H. Yoshitake, T. Tatsumi, *Chem. Mater.* **2003**, *15*, 1695
16. M. P. Kapoor, Y. Ichihashi, K. Kuraoka, Y. Matsumura, *J. Mol. Catal. A: Chem* **2003**, *198*, 303

17. S. Velu, M. P. Kapoor, S. Inagaki, K. Suzuki, *Appl. Catal. A: Gen.* **2003**, *245*, 317

18. J. Yan, C. F Blanford, B. T. Holland, W. H. Smyrl, A. Stein, *Chem. Mater.* **2000**, *12*, 1134

19. M. A. Al-Daous, A. Stein, *Chem. Mater.* **2003**, *15*, 2638

20. D. M. Antonelli, *Microp. Mesop. Mater.* **1999**, *30*, 315

21. Z. Tian, W. Tong, J. Wang, N. Duan, V. V. Krishnan, S. L. Suib, *Science,* **1997**, *276*, 926

22. M. Vettraino, M. Trudeau, A. Y. H. Lo, R. W. Schurko, D. M. Antonelli, *J. Am. Chem. Soc.* **2002**, *124*, 9567

23. M. Vettraino, X. He, M. Trudeau, J. E. Drake, D. M. Antonelli, *Adv. Funct. Mater.* **2002**, *12*, 174

24. A. Lezau, B. Skadtchenko, M. L. Trudeau, D. M. Antonelli, *Dalton Trans.* **2003**, 4115

25. C. Yue, M. L. Trudeau and D. M. Antonelli, *Can. J. Chem.* **2005**, *83*, 308.

26. G. N. Schrauzer and T. D. Guth, *J. Am. Chem. Soc.* **1977**, *99*, 7189

27 C. Yue, M. L. Trudeau, D. M. Antonelli, *Chem. Commun.* **2006**, 1918.

28. C. Yue, L. Qiu, M. L. Trudeau, D. M. Antonelli, *Inorg. Chem.* **2007**, *46*, 5084

29. Y. Rao, M. L. Trudeau and D. M. Antonelli, *J. Am. Chem. Soc.* **2006**, *128*, 13996

30. J. Kang, Y. Rao, M. L. Trudeau, D. M. Antonelli, *Angew. Chem. Int. Ed. Engl.* **2008**, *47*, 4896

31. Y. Rao, J. Kang, M. L. Trudeau, D. M. Antonelli, *J. Am. Chem. Soc.* **2008**, *130*, 394

32. F. G. N. Cloke, *Chem. Soc. Rev.,* **1993**, 17

33. D. V. Yandulov, R. R. Schrock, *Science*, **2003**, *301*, 76

34. N. Niewa, H. Jacobs, *Chem. Rev.* **1996**, *96*, 2053

35. N. Niewa, F. J. Disalvo *Chem. Mater.* **1998**, *10*, 2733

36. R. Asahi, T. Morikawa, T. Ohwaki, K. Aoki, Y. Taga, *Science,* **2001**, *293*, 269

37 N. C. Saha, H. G. Tompkins *J. Appl. Phys.*, **1992**, *72*, 3072

38. J. Kubota, K. Aika, *J. Phys. Chem.*, **1994**, *98*, 11293

39. D. M. Antonelli, J. A. Ying, *Angew. Chem. Int. Ed. Engl.* **1996**, *35*, 426

40. D. M. Antonelli, A. Nakahira, J. Y. Ying, *Inorg. Chem.*, **1996**, *35*, 3126

41. S. Murata, K. I. Aika, *J. Catal.*, **1992,** *136*, 110

42. H. Bielawa, O. Hinrichsen, A. Birkner, M. Muhler, *Angew. Chem. Int. Ed.*, **2001**, *40*, 1061

43. C. T. Fishel, R. J. Davis, J. M. Garces, *J. Catal.* **1996**, *163*, 148

44. F. Rosowski, A. Hornung, O. Hinrichson, D. Herein, M. Muhler, G. Ertl, *Appl. Catal.* **1997**, *151*, 443

45. I. E. Wachs, Y. Chen, J. M. Jehng, L. E. Briand, T. Tanaka, *Catal. Today.* **2003**, *78*, 13.

46. M. Morais, E. F. Torres, L. M. P. M. Carmo, N. M. R. Pastura, W. A. Gonzalez, A. C. B. dos Santos, E. R. Lachter, *Catal. Today* **1996**, *28*, 17.

47 J. A. Kocal, B. V. Vora, T. Imai, *Appl. Catal. A* **2001**, *221*, 295

48. R. J. Larson, T. M. Rothgeb, R. J. Shimp, T. E. Ward, R. M. Ventullo, *J. Am. Oil. Chem. Soc.* **1993**, *70*, 645

49. X. Hu, B. O. Skadtchenko, M. Trudeau, D. M. Antonelli, *J. Am. Chem. Soc.* **2006**, *128*, 11740

50. S. Pariente, P. Trens, F. Fajula, F.D. Renzo, N. Tanchoux, *Appl. Catal. A* **2006**, *307*, 51

51. X. Hu, M. L. Foo, G. K. Chuah, S. Jaenicke, *J. Catal.* **2000**, *195*, 412

52. C. J. Yue, Y. Liu, R. He, *J. Mol. Catal. A* **2006**, *259*, 17

53. T. Matsumoto, H. Yoshida, *Catal. Lett.* **2001**, *72*, 107

54. R. Van Grieken, J. M. Escola, J. Moreno, R. Rodriguez, *Appl. Catal. A* **2006**, *305*, 176

55. J. Wrzyszcz, M. Zawadzki, A. M. Trzeciak, W. Tylus, J. J. Ziolkowski, *Catal. Lett.* **2004**, *93*, 85

Chapter 8

^{17}O and ^{15}N Solid State NMR Studies on Ligand-Assisted Templating and Oxygen Coordination in the Walls of Mesoporous Nb, Ta and Ti Oxides

This chapter is organized based on a paper submitted to Journal of the American Chemistry Society by **Yuxiang Rao**, Tom F. Kemp, Michel Trudeau, Mark E. Smith, and Dave M. Antonelli

8.1 Introduction

Since the first report of M41S mesoporous molecular sieves by Mobil Oil Corporation researchers in 1992, interest in mesoporous materials has been growing [1,2]. These materials possess a hexagonal arrangement of uniformly sized meso-pores in the range from 20 to 100 Å and large surface areas of up to 1400 m^2/g, which makes them attractive in a wide variety of applications such as small molecule adsorption [3] and

catalysis [4]. The mechanism of formation of these materials has also been an area of great interest and has been explored by a wide variety of techniques including ^{29}Si and ^{15}N NMR [5-7]. The first successful synthesis of thermally stable mesoporous transition metal oxide analogues of MCM-41 were reported by Ying *et al.* in 1995 and 1996 [8,9]. These titanium oxide [8] and niobium oxide [9] materials (Ti-TMS1 and Nb-TMS1) were synthesized via a novel mechanism in which a long-chain amine surfactant is believed to be covalently bonded to the metal alkoxide precursor through an M-N dative bond on the basis of ^{15}N NMR solution shifts of the precursor mixture prior to hydrolysis, as well as after condensation and aging. The interaction between the amine head group and the metal atom has not been completely elucidated by spectroscopy. Tanev *et al* [10] reported a closely related neutral templating route for preparing mesoporous silica molecular sieves (HMS) in 1995 using the same amine template. The authors proposed a hydrogen-bonding interaction mechanism between the neutral primary amine surfactant (S^o) and the neutral inorganic precursor (I^o). ^{14}N NMR further verified that templating in this mesoporous material occurs primarily by the assembly of neutral amine surfactants, and not tetrahedral ammonium species. There are no other reports in the literature focusing on the interaction between the head group and the wall in these systems, although there are numerous NMR studies on the templating mechanism of mesoporous oxides synthesized with cationic trimethylammonium surfactants [11]. While there is some evidence of a Nb-N bond in the templating of Nb-TMS1, the results of this earlier study [9] are not strong enough to preclude the possibility that Nb-TMS1 and HMS are formed via a similar templating mechanism. M-TMS1 (M=Nb, Ti, Ta) materials are of increasing interest due to the wide range of physical properties accessible due to the variable-oxidation-state-capacity of the walls [12] and their high surface acidities. These

unique properties have already led to applications in hydrogen storage [13], nitrogen activation [14], Friedel- Crafts alkylations [15,16], and hydrocarbon skeletal rearrangements [17], and therefore warrant a more detailed study of the synthesis mechanism and wall structure.

Solid-state NMR spectroscopy is an extremely useful and informative tool in identifying and characterizing local environments in materials, even in those that lack long-range order [18]. Oxygen is a key chemical element and solid state ^{17}O NMR can provide unique insight into the local environment and its structural role in a wide range of materials and molecules [19-21]. The large chemical shift range of ^{17}O produces high sensitivity to even subtle differences in the structure [18-21]. The major problem with ^{17}O NMR is the low natural abundance of the NMR-active ^{17}O isotope (0.037%) and subsequent poor sensitivity, which can be overcome by even modest enrichment of the material (e.g. using 20 at% in the precursor material) [19,20]. A recent ^{17}O NMR study on Nb-TMS1 [22] showed its walls are exclusively constructed of ONb_2 linkages, which is very unusual as all other ^{17}O NMR data reported on niobia have shown a mixture of ONb_2 and ONb_3 environments [22,23]. This suggests that the amine template may play a role in suppressing the formation of ONb_3 units, which would represent an unprecedented example of a structure directing agent not only templating the formation of a pore structure, but also the discrete local structure. There are numerous papers concerning ^{29}Si MAS NMR of mesoporous silicas, there are few if any studies using ^{17}O, apart from in the precursor solutions [24]. To further investigate the surfactant organization mechanism in these mesoporous materials, a detailed NMR study on the mechanism of formation and wall structure of doubly labeled (^{15}N and ^{17}O) M-TMS1 (M = Nb, Ta, Ti) materials is

presented. The thermal stability of the template-formed wall structure is examined by following changes of the local structure with heat treatment. These NMR results are compared to these same oxides prepared in bulk form, as well as dodecylamine-templated HMS silica. NMR results are also reported from ^{15}N, along with some double resonance experiments that include ^{15}N-^{93}Nb and ^{15}N-^{17}O REAPDOR [25,26]. This series of NMR experiments provides insight into how the nitrogen in the template is bound to the walls of the different mesoporous oxides and the effect of this templating interaction on the structure of these walls.

8.2 Experimental Section

8.2.1 Sample Preparation

Mesoporous Nb and Ta samples were prepared using the ligand-assisted templating approach with long-chain ^{15}N dodecylamine surfactant as described previously [9, 27]. In a typical procedure, 10 g of niobium ethoxide or tantalum ethoxide was treated with 0.3 molar equivalents of 100% enriched [^{15}N]-dodecylamine. The resulting clear solutions were further treated with 100 ml deionized water, and a white gelatinous precipitate formed immediately. These samples were then aged from 30-110 °C over 10 days with gradual temperature ramping. The samples were then collected by filtration and dried in air in an oven at 95 °C for 2 hrs. Mesoporous titania samples were prepared in an analogous fashion, except that the samples were aged in water from 30-80 °C for 7 days followed by filtration and further aging of the dried sample at 110 °C in the absence of water for 2 days [28]. Mesoporous silica samples were prepared by the method of Tanev *et al* [10]. The ^{17}O enrichment of these as-synthesized samples was carried out by heating

the mesoporous metal oxides and [^{17}O] water (20% enriched) together in a sealed vessel under an inert atmosphere at 80 °C overnight and then at 120 °C for 24 h. For all template-free samples, the template was removed by stirring the sample in methanol for 24 h with 1.1 equivalents of p-toluenesulfonic acid with respect to the amine. This was followed by filtration and four additional cycles of stirring the sample in methanol for 24 h followed by filtration. The samples were then dried in an oven at 95 °C for 24 h. ^{17}O-labelling of these template-free samples was done after template removal using the same method as noted above for the as-synthesized materials.

8.2.2 Characterization

X-ray diffraction (XRD) patterns (see supplementary information Fig. 8.4) were recorded with $Cu_{K\alpha}$ radiation on a Siemens D500 θ/2θ diffractometer to confirm the mesostructure of all the samples

^{15}N magic angle spinning (MAS) NMR was conducted on a Chemagnetics Infinity Plus spectrometer equipped with a 7.05 T magnet at 30.41 MHz, using a 4 mm Doty probe spinning at 12 kHz. A 2.5 μs 90° excitation pulse was used, followed by a 1 ms ramped cross-polarization (CP) pulse and 65 kHz of TPPM decoupling. Using a 3 s recycle delay, between 2000 and 28000 acquisitions was obtained depending on the sample. Referencing was conducted using ^{15}N-enriched glycine at -347.4 ppm, relative to CH_3NO_2. ^{17}O NMR was conducted on a Chemagnetics Infinity spectrometer equipped with a 7.05 T magnet at 40.67 MHz using a 4 mm Bruker probe spinning at 10 kHz. To increase the signal Rotor Assisted Population Transfer (RAPT) [29-31] was used, which consisted of 17 cycles of the RAPT sequence using 1.5 μs pulses. A recycle delay of 3 s

was also used and approximately 25000 acquisitions were obtained. Referencing was against H_2O at 0 ppm.

^{15}N-^{17}O Rotational-Echo Adiabatic Passage Double Resonance (REAPDOR) [24,25] was conducted on a Bruker Avance II^+ spectrometer equipped with a 14.1 T magnet using a 3.2 mm Bruker HXY probe spinning at 5 kHz. The detection nucleus was ^{15}N (at 60.81 MHz) with CP from ^1H (at 600.09 MHz) with a contact time of 1 ms. 40000 acquisitions were required with a 3 s recycle delay. The recouping pulse was applied to ^{17}O (at 81.39 MHz). A Spinal64 decoupling pulse sequence [32] was used on ^1H during the REAPDOR and acquisition period, the B_1 field used for this was 100 kHz. The B_1 field used for the REAPDOR pulse sequence was 50 kHz. ^{15}N-^{93}Nb REAPDOR was conducted on the same spectrometer system using a 4 mm Varian T3 probe spinning at 5 kHz. 288 repetitions were acquired per increment with a recycle delay of 2 s. The recoupling pulse was applied to ^{93}Nb (at 146.72 MHz). The same pulse sequence as for ^{15}N-^{17}O REAPDOR was employed except that during the REAPDOR and acquisition period, the B_1 field used was 50 kHz.

8.3 Results

The ^{17}O MAS NMR spectra from the as-formed templated mesoporous oxides are shown in Fig. 8.1. It can be seen that in all these cases, a relatively broad ^{17}O resonance is observed, much broader than expected for crystalline samples of the more ionically bonded materials, titania, tantala and niobia [18,19]. It is also worth noting that in all cases only a single major resonance is observed, with any other resonances present only having minor intensity in comparison. There is also some low intensity spinning

sidebands. Mesoporous niobia, titania and tantala, all show a major Gaussian-like resonance, peaking at ~518, 690 and 432 ppm respectively, which probably correspond to ONb_2, OTi_2 and OTa_2. The spectrum from mesoporous silica also shows a single resonance, although there is some structure due to second-order quadrupolar broadening [31] from the larger quadrupolar interaction that is experienced in this more covalently bonded system. Simulation of this lineshape using an in-house computer program [33] gives interaction parameters of χ_Q = 5 MHz and η = 0 (the quadrupole coupling constant and asymmetry parameter respectively [34]) and the isotropic chemical shift, δ_{iso} = 33 ppm. This is as expected from an Si-O-Si environment [18,19]. The data also shows that there is no indication of Si-OH species being present as have been reported from silica gel samples [35].

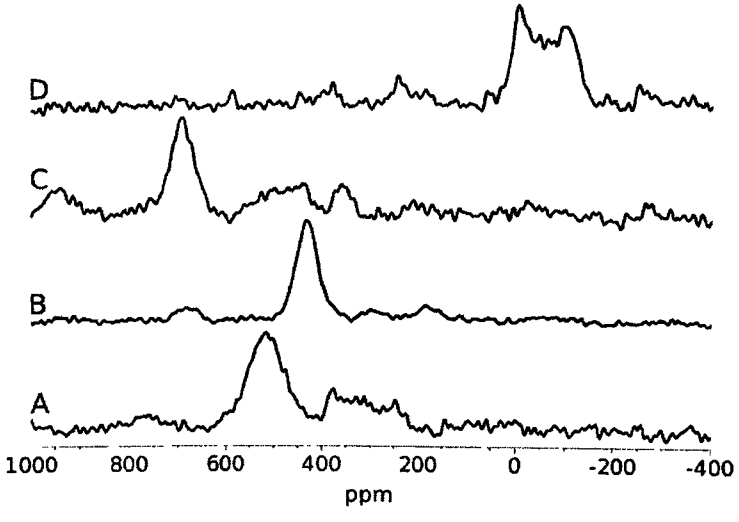

Figure 8.1 ^{17}O MAS NMR spectra of mesoporous oxides with amine template in place. (A) niobia, (B) tantala, (C)titania and (D) silica.

The evolution of the ^{17}O MAS NMR spectra with removal of the template and

subsequent heat treatment are shown for TiO_2 (Fig. 8.2(a)) and Ta_2O_5 (Fig. 8.2(b)). There is a clear change in the spectra which start off from the single coordination observed in the initial templated oxide. For TiO_2 there are two observed peaks at 562 and 380 ppm, with linewidths of ~2 kHz (Table 8.1). This probably corresponds to there being a mixture of OTi_3 and OTi_4 coordinations. It worth noting the very large change from the surfactant-containing sample, suggesting a very strong effect of the templating interaction on the wall, that is not stable with respect to template removal. With increasing heat treatment there is increasing OTi_4 content and it becomes the dominant coordination above 500 °C. For all cases these ^{17}O resonances remain broad with the width probably indicating a spread of environments from a range of chemical shifts. For the case of tantala the initial spectrum after the template has been removed shows a dominant resonance at 459 ppm (Table 8.1) corresponding to OTa_2 and a smaller peak at 306 ppm arising from OTa_3. These peaks exhibit linewidths of ~1.2 kHz and the OTa_2 resonance does have significant spinning sidebands. Then with heat treatment the relative intensity of the OTa_3 peak increases and becomes dominant in the 750 °C heat-treated sample, although there is still significant intensity in both sites. These two sets of spectra make an interesting comparison with our recently reported ^{17}O MAS NMR data from mesoporous niobia [22]. In the case of niobia the one dominant ONb_2 resonance observed in the as-formed material persists in the heat treated samples, but with a remarkable difference to the transition metal oxides reported here in the observed linewidth of only ~200 Hz once the template is removed. The linewidth remains small at all heat treatment temperatures, with an increase to 340 Hz at 500 °C and then two distinct ONb_2 resonances at 750 °C at 590 and 557 ppm [22].

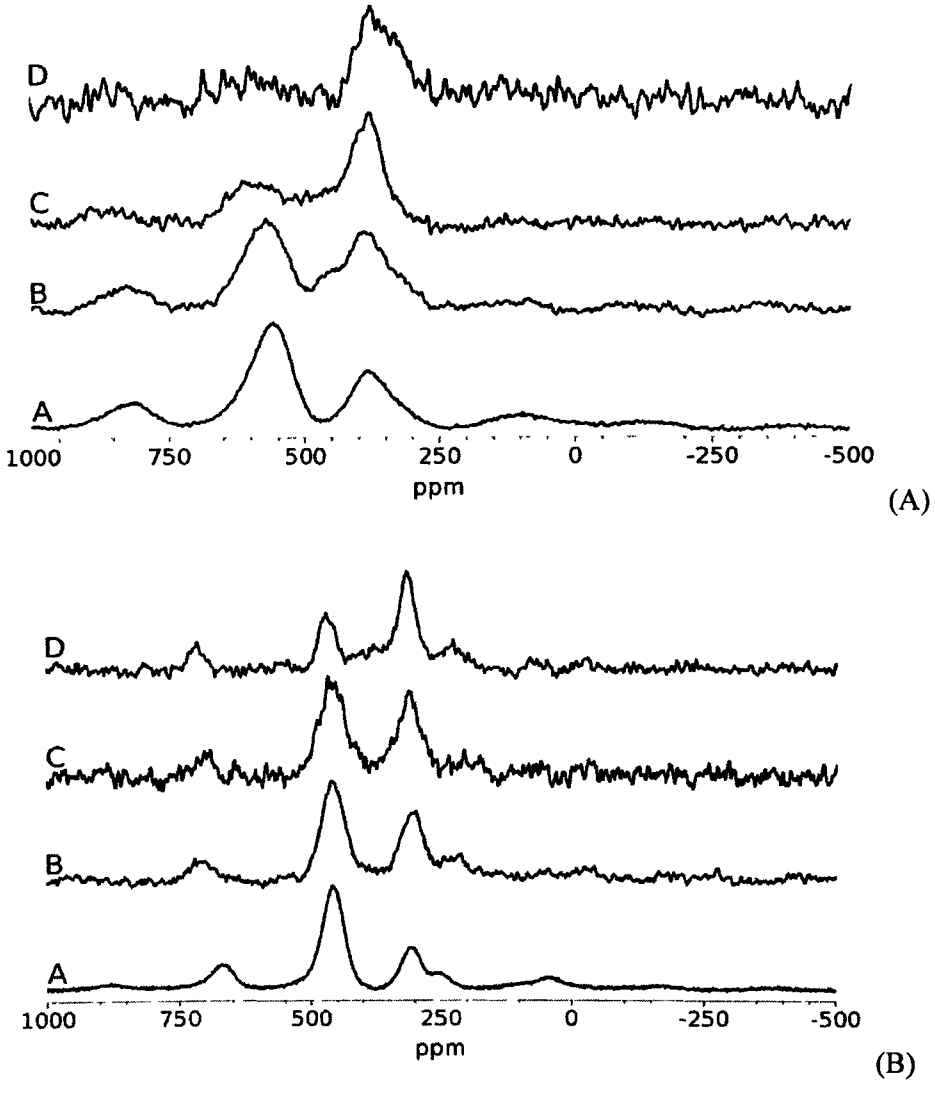

Figure 8.2 ^{17}O MAS NMR spectra of mesoporous (a) titania and (b) tantala with the template removed after (A) no extra heat treatment, (B) heating to 250 °C, (C) heating to 500 °C and (D) heating to 750 °C.

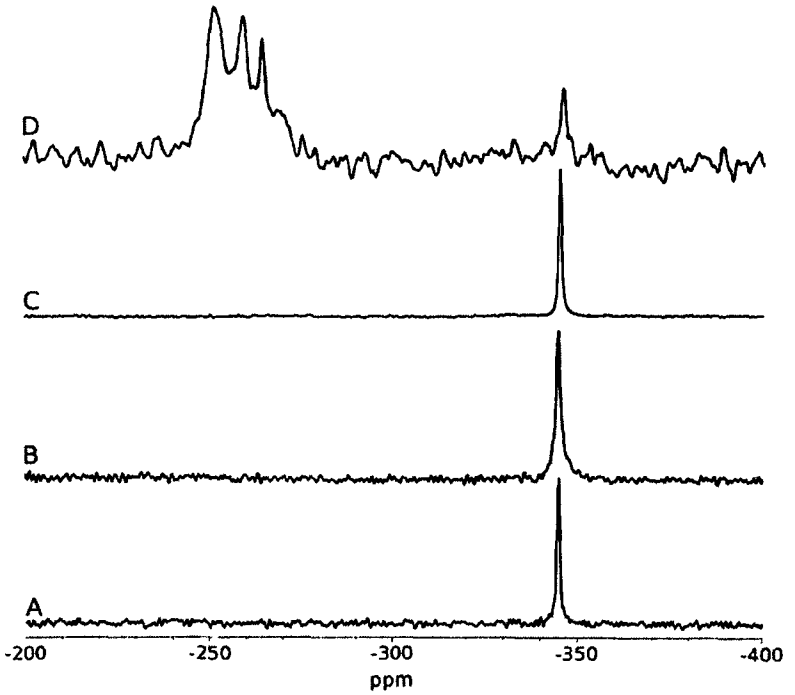

Figure 8.3 ^{15}N MAS NMR spectra of mesoporous oxides with the amine in place in (A) niobia, (B) tantala, (C) titania and (D) silica.

To better understand the interaction between the wall and the template, ^{15}N CP MAS NMR spectra were collected from all the initial samples. Spectra with good signal-to-noise were obtained from all samples. The mesoporous titania, niobia and tantala show a single peak in the range -343.6 to -345 ppm, with the corresponding linewidth increasing 28, 36 to 45 Hz. A peak at similar resonance frequency was observed in previous solid-state ^{15}N NMR studies on Nb-TMS1 [9]. These peaks are in the range expected for amines. In the mesoporous silica although there is a small peak in this region at -346 ppm with a width of 80 Hz, there are several much stronger peaks in the NH region. A simulation of the ^{15}N spectrum in this region indicates 4 inequivalent nitrogen sites (see supplementary material, Figure. 8.5). This spectrum can be interpreted as the

amine [36,37] becoming protonated by the acidic Si-OH groups and forming a series of tertiary amines bonded in different, but chemically similar places in the structure. From ^{15}N NMR it is known that protonation causes a deshielding of the proton [37]. In solid state NMR a whole series of experiments have been devised that reintroduce dipolar couplings so as to assist in identification of different sites. The methods work on the principle of a comparison between two sequences, with the only difference being produced by dipolar coupling if there is spatial proximity between different nuclei. Many of these sequences were originally designed for spin-½ nuclei. However the REAPDOR experiment is specifically designed to involve at least one quadrupolar nucleus and in fact does not work on systems containing only spin-½ nuclei. These MAS-based experiments rely on the modulation of the heteronuclear dipolar coupling to prevent an echo from refocusing, with the modulation in the REAPDOR experiment is provided by a train of rotor-synchronized 180° pulses applied to the spin-½ nucleus, spaced half a rotor period apart. With faster MAS the limitations placed on the sequence by the T_2 decay of the quadrupolar nucleus is alleviated. The decay of the ^{15}N-^{93}Nb REAPDOR signal was observed (Table 8.1). Although the effect is relatively weak given the strong T_2 dephasing of ^{93}Nb detecting any effect is significant and clearly shows that there are definite dipolar couplings between the nitrogen and the niobium. ^{15}N-^{17}O REAPDOR on the mesoporous templated silica shows no difference indicating effectively no interaction between the oxygen and the nitrogen.

Table 8.1 Summary of the ^{17}O NMR spectral characteristics of mesoporous oxides with and without the template and then heated after template removal.

		TiO_2		Ta_2O_5		Nb_2O_5	
		δ_p (ppm)	Δ (Hz)	δ_p (ppm)	Δ (Hz)	δ_p (ppm)	Δ (Hz)
Template in place		690±10	2400±50	432±5	2220±30	518±10	3900±50
Template Removed	**Unheated**	380±2 562±2	2080±10 2130±10	306±3 459±3	1200±10 1270±10	566±2	290±10
	250°C	387±3 574±2	2500±20 2705±20	306±3 460±3	1480±10 1380±10	558±2	210±10
	500°C	387±2 594±5	1640±20 2650±50	310±3 460±3	1330±10 1520±10	554±2	340±10
	750°C	363±5 599±10	2610±50 4270±100	314±3 469±3	970±10 1110±10	557±2 591±2	200±10 220±10

Δ =full width at half maximum, δ_p= peak position. Nb_2O_5 data taken from ref. 22

8.4 Discussion

The ^{15}N NMR results demonstrate that nitrogen from the template exists probably in the form of a protonated ammonium species for the silica and as neutral amines for the titania, tantala and niobia. In the case of the silica the majority of the template is held in the structure by a RNH_3^+ $^-$O-Si- hydrogen-bonding interaction with the walls, which is clearly strong enough that it can no longer be described as an NH_2-HOSi hydrogen-bonding interaction. The presence of a small amount of free amine in this material is expected on the basis of the weak acid-base equilibrium between these two structures. The different fully protonated ammonium species most likely arise from interactions with 0, 1, 2 or 3 SiO^- groups in the walls. The shift observed here between the

silica and the other species is larger than often observed for simple protonation of an amine or ammonia observed in solution [37]. However being constrained in the mesopores and interacting with the wall, as well as being in the solid state could lead to a significantly different and larger shift. The lack of a signal in previous solution state ^{14}N NMR study of a mixture has been taken to indicate neutral templating occurred [10,38]. The quadrupole spin-1 nature of ^{14}N complicates interpretation of NMR spectra [18], both in the solution mixture and for solids. The state of the sample here is different from previous studies, i.e. in the solid state and not the solution mixture. Here the template interacting with the wall in the solid state after any liquid phase has been removed. For Nb-TMS1, the ^{15}N-^{93}Nb REAPDOR shows that there is a measurable interaction between the template and the Nb centers in the wall indicative of dative bonding. There is also a range of linewidth in the ^{15}N MAS NMR of the three transition metal samples with the narrower line from the titania probably indicating a weaker interaction with the wall (hence leading to weaker constraint by the wall). The interaction of the template with the wall can also be judged by how easily the template can be washed out. In the case of silica the template is removed by simple washing in ethanol. Titania shows a stronger interaction, as the template cannot be washed out by ethanol, but leaches out at 90°C during aging in water. The interaction is stronger still and in tantala/niobia where the template remains within the structure even after heating at 180°C in an aqueous environment. For all the transition metal oxides the template must be protonated with p-toluenesulfonic acid followed by repeated methanol washings to ensure complete template removal.

The ^{17}O MAS NMR data immediately indicates a very significant difference between these mesoporous templated oxides and their bulk analogues. For mesoporous

silica the oxygen is in the expected Si-O-Si linkages (i.e.OSi_2) with the NMR interaction parameters typical of such linkages within bulk tetrahedrally coordinated silica phases. However, for the transition metal oxides examined here their bulk crystalline forms have well defined local oxygen coordination, which are respectively OTi_3 for TiO_2, ONb_2 and ONb_3 for Nb_2O_5 and OTa_2 and OTa_3 for Ta_2O_5. It is very clear that in *all* cases in the mesoporous templated samples the oxygen is only coordinated by two metal centers (i.e. M-O-M). Hence it is unequivocal that the templating must have a strong effect and force the wall to assume an unusual local coordination with only two-fold oxygen environments. Stated differently, the ligand-assisted templating effect uses a dative N-M interaction, which suppresses higher coordinate oxygen by blocking the Lewis acidic metal sites, which would otherwise be coordinated to the O ligands. Essentially the template not only directs the structure of the mesophase, but also influences the local coordination environment in the walls. There are also very different stabilities and degrees of order within the mesoporous walls as the sample is heated after template removal. Our previously reported ^{17}O MAS NMR data on mesoporous niobia [22] indicates that the wall retains its unusual single ONb_2 coordination and it takes on a remarkably ordered structure once the template is removed, with both these factors remaining after all heat treatments even up to 750 °C. This behaviour is very different from bulk niobia where crystallization of a gel leads to various mixtures of ONb_2 and ONb_3 as the temperature is varied [22]. For mesoporous tantala the OTa_2 environment is immediately converted to a mixture of OTa_2 and OTa_3. The linewidth remains similar as to that observed in the initial oxide indicating resonances where the linewidths are determined by chemical shift dispersion, i.e. a range of environments exist. Hence a significant change of structure occurs on removal of the template. This is possibly brought about by the creation of open coordination sites at the

metal upon removal of the N-donating template, and/or the paratoluenesulphonic acid acting as a network enhancer to promote crystallization and a higher degree of local ordering. The OTa_2 environment also clearly changes with a chemical shift difference of ~30 ppm (strictly the peak position, but with the small χ_Qs that are typical for such an ionic system this can be closely identified with a chemical shift difference [18]). This can be compared with gel formation of bulk tantala [39], which has two peaks at 430 ppm (OTa_2) and 270 ppm (OTa_3). On heat treatment the mixture of two coordinations remains approximately constant until the highest temperature of 750 °C where the OTa_3 becomes dominant. The variations observed in this heat-treated mesoporous tantala show that OTa_3 starts off as the less populated coordination, but gradually becomes the more intense signal, although OTa_2 and OTa_3 remain throughout.

TiO_2 shows the largest change of all the oxides studied here in going from the templated oxide to the sample when the template has been removed. The OTi_2 coordination at 690 ppm is immediately replaced by two peaks at 562 and 380 ppm which can be attributed to OTi_3 and OTi_4 respectively. In bulk sol-gel produced TiO_2, the initial oxide has an approximately equal concentration of OTi_3 and OTi_4, with the OTi_3 concentration increasing with heat treatment until just before crystallization at 300°C there is a large excess of the OTi_3, with virtually all the OTi_4 removed on crystallization [40]. There is also a large decrease in the linewidth of the OTi_3 resonance at this point as well, an indication of the much higher order on crystallization. This again is very different in the mesoporous titania since initially OTi_3 starts off as the dominant coordination which on heat treatment decreases in intensity with respect to the OTi_4 which becomes the dominant coordination after heat treatment at 750 °C. At all temperatures the linewidth remains typically at ~2 kHz

(see Table 8.1) which is comparable to that seen in amorphous, bulk gels at 3.5 kHz.

8.5 Conclusion

Amine-templated mesoporous silica, niobia, tantala and titania materials were synthesized and studied by solid state NMR. ^{15}N NMR studies revealed that the amine template was bound in the structures as hydrogen-bonded ammonium species in tha case of Si, and in amine form for Nb, Ta, and Ti. However REAPDOR experiments revealed a substantial direct Nb-N interaction in the niobia material, confirming a N-M dative bonded ligand interaction, as previously hypothesized. ^{17}O NMR studies on the Nb, Ta and Ti materials showed that the amine template suppresses the formation of higher coordinate oxygen, ubiquitous in oxide gels for these metals. This is most likely due to the influence of the template head group on the local structure of the wall via ligand interaction where the amine occupies a coordination site that would otherwise be taken by triply coordinated oxygen. Thus, the amine surfactant plays an unprecedented dual role of templating the mesostructure while also directing the oxygen coordination in the walls. In the template-free samples there are more open metal Lewis acid sites at the metal and more basic oxygen lone pairs present as compared to the corresponding oxide gels where the lone pairs of the oxygen block most open metal sites. This configuration should have several advantages in catalysis and other applications such as gas separation.

8.6 Supporting Information

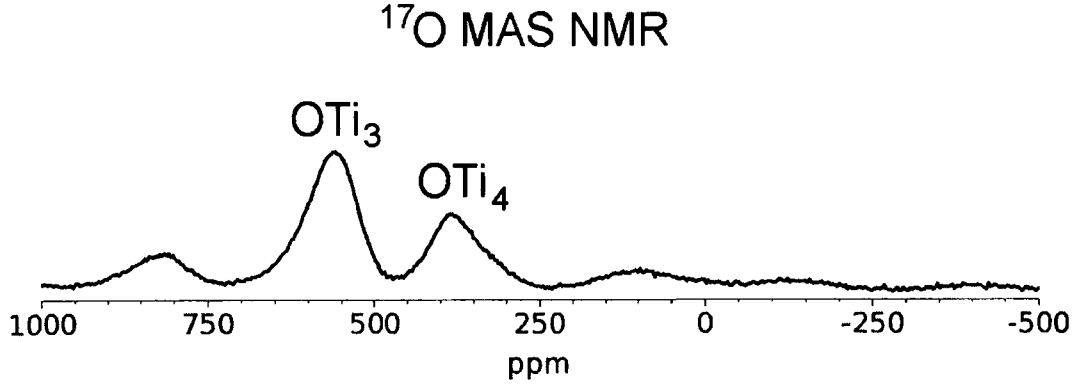

TOC

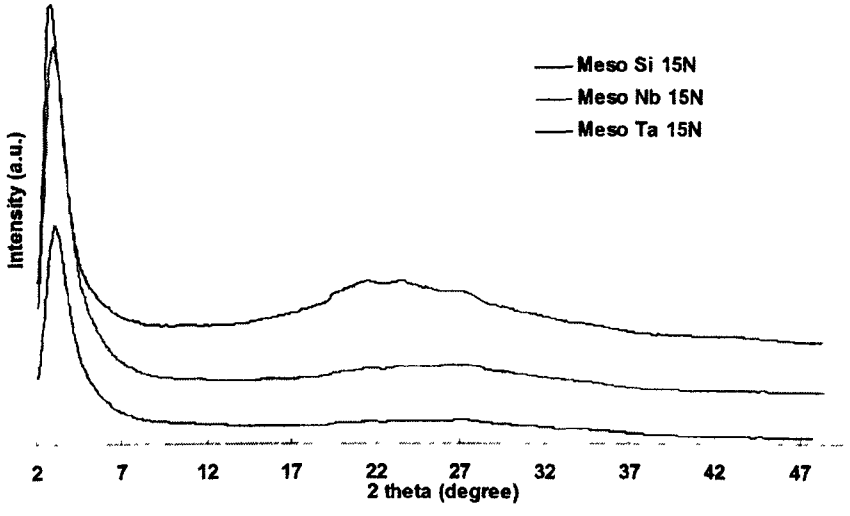

Figure 8.4 XRD plot of mesoporous oxides with the amine template in place.

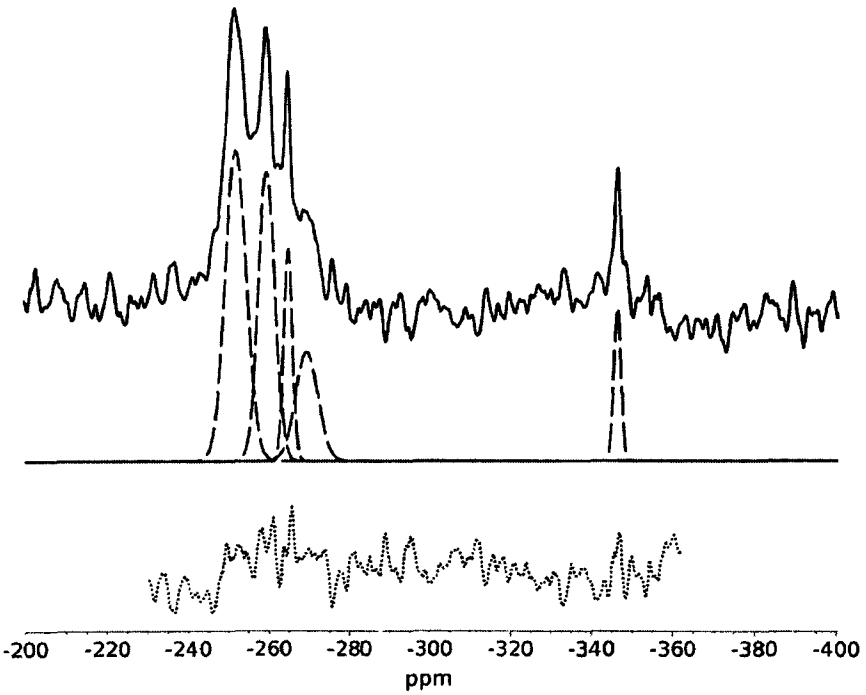

Figure 8.5 Simulation of ^{15}N MAS NMR spectra of mesoporous silica. Solid line is the spectra, dashed line is the simulation and the dotted line is the difference.

8.7 References

1. C.T. Kresge, M.E. Leonowics, W.J. Roth, J.C. Vartali, J.S. Beck, *Nature*, **1992**, *359*, 710
2. J.S. Beck, J.C. Vartuli, W.J. Roth, M.E Leonowicz, C.T. Kresge, K.D. Schmitt, C.T.W. Chu, D.H. Olson, E.W. Sheppard, S.B. McCullen, J.B. Higgins, J.L. Schlenker, *J. Am. Chem. Soc.*, **1992**, *114*, 10834
3. A. Hamaed, M. Trudeau, D. M. Antonelli, *J. Am. Chem. Soc.* **2008**, *130*, 6992
4. C. P Mehnert, M. S. Wong, J. Y. Ying, *Angew. Chem. Int. Ed.* **1999**, *38*, 56
5. C. Chen, H. Li, M. E. Davis, *Micro. Mater.* **1993**, *2*, 17

6. I.G. Shenderovich, D. Mauder, D. Akcakayiran, G. Buntkowsky, H.H. Limbach, G.H. Findenegg, *J. Phys. Chem. B* **2007**, *111*, 12088

7. A. Firouzi, D. Kumar, L.M. Bull, *Science*, **1995**, *267*, 1138

8. D.M. Antonelli, J.Y. Ying, *Angew. Chem. Int. Ed.* **1995**, *34*, 2014

9. D.M. Antonelli, J.Y. Ying, *Angew. Chem. Int. Ed.* **1996**, *35*, 426

10. P.T. Tanev, T.J. Pinnavaia, *Science*, **1995**, *267*, 865

11. R. Simonutti, A. Comotti, S. Bracco,; Sozzani, P.; *Chem. Mater.* **2001**, *13*, 771

12. X. He, D. M. Antonelli, *Angew. Chem. Int. Ed.* **2002** *41*, 214

13. X. Hu, B. O. Skadtchenko, M. Trudeau, D. M. Antonelli, *J. Am. Chem. Soc.* **2006**, *128*, 11740

14. C. Yue, M. Trudeau, D. M. Antonelli, *Chem. Comm.* **2006**, 1918.

15. Y. Rao, M. Trudeau, D. M. Antonelli, *J. Am. Chem. Soc.* **2006**, *128*, 13996.

16. J. Kang, Y. Rao, M. Trudeau, D. M. Antonelli, *Angew. Chem. Int. Ed.* **2008**, *47*, 4896

17. Y. Rao, J. Kang, Antonelli, D. M. *J. Am. Chem. Soc.* **2008**, *130*, 394

18. K.J.D. Mackenzie, M.E. Smith, *Multinuclear Solid State NMR of Inorganic Materials*, Pergamon, Oxford, **2002**

19. S.E. Ashbrook, M.E. Smith, *Chem. Soc. Rev.*, **2006**, *35*, 718

20. V. Lemaitre, M.E. Smith, A. Watts, *Solid State Nucl. Magn. Reson.*, **2004**, *26*, 215

21. G. Wu, *Prog. Nucl. Magn. Reson. Spectrosc.*, **2008**, *52*, 118

22. B.O. Skadtchenko, Y. Rao, T.F. Kemp, P. Bhattacharaya, P.A. Thomas, M. Trudeau, M.E. Smith, D.M. Antonelli, *Angew. Chem. Int. Ed.* **2007**, *46*, 2635

23. B. Julián, C. Gervais, E. Cordoncillo, P. Escribano, F. Babonneau, C. Sanchez, *Chem. Mater*, **2003**, *15*, 3026

24. J.D. Epping, B.F Chmelka, *Curr. Opinion Coll. Interfac. Sci.*, **2006**, *11*, 81.

25. T. Gullion, *Chem. Phys. Lett.* **1995**, *246*, 325.

26. T. Gullion, *J. Magn. Reson. A*, **1996**, *117*, 326

27. D. M. Antonelli, J. Y. Ying, *Chem. Mater.* **1996**, *8*, 874

28. D. M. Antonelli, *Micro. Meso. Mater.* **1999**, *30*, 315

29. Z. Yao, H.T. Kwak, D. Sakellariou, L. Emsley, P.J. Grandinetti, *Chem. Phys. Lett.* **2000,** *327*, 85.

30. A. Goldbourt, P.K. Madhu, S. Vega,*Chem. Phys. Lett.* **2000**, *320*, 448

31. P.K. Madhu, K.J. Pike, R. Dupree, M.H. Levitt, M.E. Smith, *Chem. Phys. Lett.* **2003** *367*, 150

32. B.M. Fung, A.K. Khitrin, K. Ermolaev, *J. Magn. Reson.* **2000,** *142*, 97.

33. T.F. Kemp, M.E. Smith, *Solid State Nucl. Magn. Reson.*, Submitted for publication.

34. M.E. Smith, E.R.H. van Eck, *Prog. Nucl. Magn. Reson. Spectrosc.* **1999,** *34*, 159.

35. S.C. Kohn, E.R.H. van Eck, M.E. Smith, *Solid State Nucl. Magn. Reson.* **1999,** 15, 181.

36. G.C. Levy, R.L. Lichter, Nitrogen-15 Nuclear Magnetic Resonance Spectroscopy; J.Wiley **1979**

37. J. Mason, In *Encyclopedia of Nuclear Magnetic Resonance*; Grant, D. M., Harris, R. K., Eds. Wiley: Chichester, **1996**; Vol. 5, p 3222.

38. A. Steel, S.W. Carr, M.W. Anderson, *Chem. Commun.* **1994,** 1571.

39. D.M. Pickup, G. Mountjoy, M.A Holland, G.W. Wallidge, R.J. Newport, M.E. Smith, *J. Mater. Chem.*, **2000,** *10*, 1887.

40. T.J. Bastow, A.F Moodie, M.E. Smith, H.J. Whitfield, *J. Mater. Chem.*, **1993,** *3*, 697.

Chapter 9

Conclusion and Future Work

9.1 Research contribution of thesis work.

The narrow and uniform pore size of mesoporous materials with extremely high surface areas holds much promise for the development of novel solid catalysts. There are many strategies for the design and preparation of mesoporous catalysts. Varying oxidation states in the wall, capacity for doping with other metals, as well as surface coating or treatment with sulfuric acid or phosphoric acid can result in the formation of new properties. As far as we are aware, there are no other examples in which the same type of materials can be modified in so many different ways. This re-emphasizes the high potential of these mesoporous materials.

The study reported herein is a continuation of previous work in our group on the synthesis of mesoporous Ta oxide based catalysts and the study of their reactivity in nitrogen activation at mild conditions. Previous work in our group showed that Ru acts as

an interface to transfer electron density from hydrogen to neighboring Ta sites on the mesoporous Ta oxide support, which in the reduced form is then able to cleave dinitrogen. This thesis work has made significant contributions to the area of preparation and modification of Group V mesoporous transition metal oxides (Nb and Ta), as well as the extension of their applications into the area of strong acid catalysis. The major research contributions of this thesis work are summarized below.

In this dissertation, a series of pristine and acid-treated mesoporous niobium and tantalum oxides materials with different pore sizes (from 12Å to 30Å) were synthesized by the ligand assisted amine template method, characterized by solid-state NMR, nitrogen adsorption, XRD, TEM, SEM, FT-IR, TPD of ammonia, TG and DSC techniques and investigated for their catalytic applications in benzylation, alkylation and isomerization. In Chapter 2, amorphous mesoporous niobium oxide was synthesized by using the amine-template approach as described previously. In order to get more information about the coordination geometry of the Nb atom with the oxygen and compare this to sol-gel produced bulk niobium oxide, solid-state ^{17}O NMR experiments were conducted at different heating stages (From room temperature to 1000 °C). This technique has proved to be an extremely useful tool in identifying and characterizing local environments on the nanometer scale since the large chemical-shift of ^{17}O provides high sensitivity to even subtle differences in the structure in both amorphous and crystalline solids. The only problem with ^{17}O NMR spectroscopy is the low natural abundance of ^{17}O (0.037%), but this can be overcome by ^{17}O enrichment using [^{17}O] water (20% enriched). The results of this study revealed an unprecedented, highly ordered oxygen structure in the mesoporous niobia walls, the oxygen exclusively present as ONb_2. This was confirmed by a single

sharp resonance at δ=565.5 ppm. The wall of this material was not in the form of an ONb_2 and ONb_3 mixture as observed in the conventional Nb_2O_5. This phenomenon was not observed in other samples of niobia gels, nor in samples of mesoporous titanium and tantalum oxides prepared through the same route. The reason that the walls of the mesoporous niobium oxide adopt this highly ordered structure is presently unknown, but maybe related to the action of the amine surfactant during the self-assembly process leading to the formation of mesostructure.

To explore this unique property of mesoporous niobium oxide and its potential application in catalysis, this material was synthesized and further treated with sulfuric acid or phosphoric acid to enhance its surface acidity. The acid modified materials were used as solid acid catalysts for the benzylation of anisole and toluene with benzyl alcohol, as reported in Chapter 3. XRD patterns of pure Nb oxide, sulfated and phosphated Nb oxides demonstrated the retention of the mesoporous structure after acid treatment. This was further confirmed by a typical type IV isotherm recorded by nitrogen adsorption analysis. FT-IR analysis of the material treated with pyridine showed that Bronsted and Lewis acid sites coexist in a roughly 50:50 mixture on the surface of the parent material with a strong dominance of Bronsted acid sites on the acid-treated samples. To further probe the surface acidity and quantify the acid amount of these mesoporous materials, Hammett acid indicators and the n-butylamine titration method were adopted. Bulk niobium pentoxides were also evaluated as standards to gauge the effect of mesostructure on acidity. The results showed that bulk niobia possess only weak acidic sites on its surface (pKa = +3.3, 0.024 mmol/g) compared to mesoporous niobium (pKa = -6.6, 2.478 mmol/g), even for the sulfated and phosphated bulk samples. (pKa = -3.0, 0.3 mmol/g).

After acid treatment, the acid amount on the surface of mesoporous niobium oxide can reach an amazing 31.784 mmol/g (treated with sulfuric acid), far beyond the untreated sample and the sample treated with phosphoric acid (3.086 mmol/g). It is thus quite clear that sulfate is more effective than phosphate in generating surface acid sites. Other acids like nitric acid and hydrochloric acid are not chosen here since they are less effective in this process as reported somewhere else.

The much higher observed catalytic activity of mesoporous Nb oxide compared to bulk Nb_2O_5 clearly demonstrates the diffusion advantages of the mesoporous system, which can be attributed to its high BET surface area (612.63 m^2/g) and high mesoporosity. The best results were achieved with sulfated mesoporous Nb oxide, which showed 100% conversion in only 30 min. Since the phosphated and sulfated samples possess similar surface area and acid strength, the greater activity of the latter over the former must due to the greater number of acid sites.

Mesoporous Ta oxide is more thermally stable then mesoporous Nb oxide, its mesoporous structure does not begin to collapse until 500 °C, which makes it more suitable as a catalyst for industrial application. In Chapter 4, mesoporous Ta oxides with different pore sizes were prepared using the ligand-assisted templating approach and were then further treated with 1M sulfuric acid to enhance the surface acidities. After that, these materials were evaluated for their catalytic activities in the shape selective synthesis of linear alkyl benzene (LAB). At 80 °C and a benzene/olefin molar ratio of 10:1, no oligomerization of 1-dodecene was observed and only monoalkylated phenyldodecenes were detected. 100% 1-dodecene conversion was achieved within 0.5h over the sulfated mesoporous C_{12} Ta sample. However, the conversion was only 1.2% over sulfated

mesoporous C_{12} Nb at 0.5h. The reason for this is not understood, but maybe related to the unique highly ordered structure in the wall of this material as discussed in Chapter 1.

The activity of sulfated mesoporous Ta oxide is also affected by the size of reactants. When larger 1-tetradecene was used instead of 1-dodecene, the activity of sulfated mesoporous Ta oxide decreased dramatically from 100% to 17.5% in 0.5h, which clearly indicates that the longer the olefin chain, the more difficult it is for the olefin molecule to access the active sites in mesopores. In order to further clarify the effect of pore structure on activity, the alkylation reaction was also carried out over sulfated mesoporous C_6 and C_{18} Ta oxides prepared using 1-hexylamine and 1-octadecylamine as templates. The results showed that C_{12} Ta oxide has the highest activity and selectivity towards 2-phenyldodecane among the three Ta oxides, and even better than widely used HY-Zeolte, H-ZSM5 and Amberlyst 15. This can be partly attributed to its high surface area (292.2 m^2/g) and optimal pore size (23.3Å), which offers a large amount of active acid sites and a diffusion advantage over the other samples.

In order to probe further into the impact of confinement effects in catalysis for reactants confined in small mesopores, we extended our study to isomerization.of 1-hexene over sulfated mesoporous Nb and Ta oxides with different pore sizes (Chapter 5 and Chapter 6). Double bond isomerization of 1-hexene at 343 K was chosen as a model reaction because (i) it is a monomolecular reaction; (ii) this catalytic reaction can be performed without any solvent; (iii) the reaction conditions are quite mild (< 100 °C) and do not require an expensive high pressure auotoclave. The isomerization of 1-hexene to 2-hexene is a proton transfer process. The initial proton is transferred from the acid site on the surface of the catalyst to the double bond of 1-hexene, and then the hydride shift

along the linear chain produces *cis*-2-hexene or *trans*-2-hexene. GC analysis confirmed that those two isomers are formed as the only two principal products. Skeletal isomerization was not observed in these reaction conditions since it requires more energy and can only be performed at elevated temperature (> 523K). The experimental results showed that the selectivity as well as conversion rate were pore size dependent. Sulfated C_{12} samples (both Nb and Ta) demonstrated the highest activity (~95% for C_{12} Ta and ~70% for C_{12} Nb in 4 hrs) as well as selectivity (*Trans/Cis* ratio reach 3.7 for C_{12} Ta and 1.4 for C_{12} Nb in 6 hrs) among all three corresponding samples (C_6, C_{12}, C_{18}). This is consistent with the results observed in the previous study in Chapter 4.

In general, Ta samples always have higher activity than the Nb samples although they possess lower surface areas compared to the Nb counterparts. To explain this, TPD of ammonia was conducted and the results clearly showed a greater intensity of the peak corresponding to Bronsted acid site on the surface of the Ta samples than that of Nb samples. This must account for its greater activity in reactions involving Bronsted acid sites, such as isomerization. Unlike other catalysts, which produce a trans/cis ratio, close to 1, C_{12} H_2SO_4 Meso Ta demonstrates a dramatically increasing selectivity over time approaching a value close to its thermodynamic equilibrium (3.37). Thus it appears that this material acts as a bifunctional catalyst, not only speeding up the 1-hexene isomerization conversion rates to the two isomers, but also facilitating the *cis*-2-hexene to *trans*-2-hexene isomerization.

In Chapter 7, we reviewed the preparation and characterization of mesoporous materials containing transition metal oxides (Ti, Nb and Ta), and their potential applications in heterogeneous catalysis. In general, these mesoporous molecular sieves

(MMS) can be readily modified by doping with other elements, reduction or acid treatment to extend their applications in catalysis. We also reported some of the recent finding from our group focusing on the modification of existing mesoporous transition metal oxides, characterization of these new mesoporous structures and their respective surface properties, and the exploration of their potential catalytic applications in areas such as dinitrogen activation, benzylation, alkylation and isomerization. Confinement effects and mesoporosity, which are known to strongly affect diffusion and catalytic properties, resulting in the existence of an optimal catalytic efficiency depending on pore size and internal surface area, are also discussed.

Finally, in the last Chapter (Chapter 8), a multinuclear solid state NMR approach was applied to four templated mesoporous oxides (Si, Ti, Nb and Ta), including ^{15}N and ^{17}O magic angle spinning (MAS) NMR and double resonance ^{15}N-^{93}Nb, ^{17}O REAPDOR experiments. ^{15}N MAS NMR shows that the surfactant is only present in the amine form in TiO_2, Nb_2O_5 and Ta_2O_5. In SiO_2, amines are only present in minor amounts, but there are several strong ammonium ^{15}N resonances. The REAPDOR experiments show unequivocally that the nitrogen interacts with niobium, confirming a ligand interaction between the Nb and N, as previously believed. In the case of silica the amine is quaternized and there is apparently no interaction with the Si, suggesting a RNH_3-O-Si-hydrogen-bond interaction with the walls. ^{17}O MAS NMR provides the clearest indication of the local wall structure. In the aged, templated samples in all cases only OM_2 coordinations are present which is very different from the pure bulk oxides (apart from SiO_2) and must be due to the effects of amine coordination at the metal centers. On removal of the template these oxides behave differently, with Ta_2O_5 showing a mixture of

OTa_2 and OTa_3, which is similar to the coordination found in the bulk oxide. The previously reported ^{17}O MAS NMR data from heat-treated mesoporous niobia shows only ONb_2, which is very highly ordered. In contrast, for titania the OTi_2 coordination is immediately lost on removal of the template to be replaced by a mixture of OTi_3 and OTi_4, with the OTi_4 becoming dominant, very different from the corresponding bulk oxide. In summary, this NMR study shows that the local oxygen coordination in amine-templated mesoporous transition metal oxides is present as OM_2, which is relatively rare in bulk oxides. The template interaction is largely controlled by the N-M dative bond to the wall, suppressing higher oxygen coordination numbers. The strength of this interaction varies greatly in the different mesoporous oxides.

9.2 Recommendation for future research

In recent years, there has been great concern over many serious environmental problems on a global scale. The increase in world population and industrial development have led to accelerated release of chemical waste into the air and water, especially in developing countries like China and India, which raises havoc in the ecosystem in the form of global warming and pollution-related diseases. So it is urgent to develop clean and safe chemical technologies with a low cost and an affordable operation expense.

The application of pollution-free photocatalysis techniques by using transition metal oxide semiconductors as catalysts has great potential to control aqueous organic contaminates or air pollutions. This technique has several advantages over conventional oxidation processes as follows. (1) Use of near-UV or solar light as energy source; (2) no addition of other chemicals; (3) operation at near room temperature; (4) low cost. Among

the diverse semiconductor oxides commonly used today, TiO_2 is the most widely studied due to its abundance on the earth (beach sand), non-toxicity, chemical stability and relatively high reactivity under ultraviolet (UV) light [wavelength (λ)<387nm]. The photocatalytic activity of TiO_2 can be further improved by doping transition metal ions into its structure to replace Ti ions or nonmetal anions, such as B, C, N, F, S, Cl and Br into TiO_2 to replace O ions.

Compared with conventional bulk TiO_2 photocatalysts, mesoporous TiO_2 with large surface area and porosity may provide higher activity. Research of the application of modified mesoporous TiO_2 materials in photocatalysis is fairly new and a better understanding of the influence of surface area, pore sizes and wall thickness and doping level on its photocatalytic activity is needed.

The focus of the future research plan is to use different preparation methods, in combination with powder-XRD, nitrogen-adsorption, TEM, SEM, ED techniques, to investigate the influence of surface area, pore size, wall thickness, doping element, doping level, calcination temperature and time to the structure, morphology and crystallization of pure mesoporous TiO_2 nanomaterials and those modified by doping with metal or nonmetal elements. The photocatalytic activity of pure and modified materials will be evaluated using photocatalytic oxidation of phenol as a model reaction. The objectives of the research project are as follows:

1) *Preparation of mesoporous Titanium photocatalysts using the triblock copolymer method.*

The preparation of mesoporous TiO_2 is not entirely new. Yang and stucky have

reported the preparation of mesoporous TiO_2 by using amphiphilic poly (alkylene oxide) block copolymers as a structure-directing agent in non-aqueous solution. Crystallized mesoporous TiO_2 was obtained after removing the surfactant species by calcinating the as made samples at 400 °C for 5 h in air.

2) *Preparation of mesoporous Titanium photocatalysts by modified sol-gel method combined with silica coating pore wall reinforcement technology.*

Mesoporous TiO_2 prepared by the triblock copolymer method possess relative large pore size (65Å) and wall thickness (51 Å) as well as a low surface area (205 m^2/g), which are undesirable for photocatalysis. To investigate the influence of pore size, wall thickness and surface area on its photocatalytic activity, the modified sol-gel method will be adopted to prepare mesoporous TiO_2 with small pore size and thin walls. However, the as-synthesized mesoporous TiO_2 has mainly amorphous pore detected by powder XRD, which offer poor thermal and mechanical stability, and restrict the range of application of these materials. Recently, Kondo and Domen reported a novel silica-coating pore wall reinforcement method for crystallizing amorphous mesoporous metal oxides. The crystallization of an amorphous inorganic network of mesoporous metal oxides is successfully achieved while maintaining the original ordered mesoporous structure. Based on this technology, we can synthesize crystallized anatase mesoporous TiO_2 with high surface area, small pore size and thin walls, which are ideal for photocatalysis.

(3) Modification of mesoporous TiO_2 by doping with metal or nonmetal elements.

The photocatalytic activity of pure mesoporous TiO_2 prepared by the above two methods will be evaluated using photocatalytic degradation of phenol. The disappearance

of phenol will be monitored using a Varian Gas Chromatograph CP-3800 equipped with a FID detector. The optimal parameters such as pore size; wall thickness, surface area and crystalline phase will be determinated. The best sample of pure mesoporous TiO_2 materials will be doped with .a series of transition metals (V, Cr, Mn, Fe, Co, Ni, Cu) or nonmetal elements (C, S, N, F, Cl) respectively to further improve its performance for this model reaction. The modified mesoporous TiO_2 will also be analyzed by the same techniques mentioned above.

In summary, the proposed research will have a major impact in gaining a better understanding of the potential application of mesoporous TiO_2 in photocatalysis and the effect of pore size, wall thickness, crystalline phase and the optimal modification parameters such as metal or nonmetal doping element and doping level on its photocatalysis activity. Furthermore, the combination of methodology used in this study may encourage the employment of silica coating pore wall reinforcement technology to improve the properties of other amorphous mesoporous metal oxides that have not been crystallized before.

Appendices

Copyrights

American Chemical Society's Policy on Theses and Dissertations

If your university requires a signed copy of this letter see contact information below.

Thank you for your request for permission to include **your** paper(s) or portions of text from **your** paper(s) in your thesis. Permission is now automatically granted; please pay special attention to the implications paragraph below. The Copyright Subcommittee of the Joint Board/Council Committees on Publications approved the following:

> Copyright permission for published and submitted material from theses and dissertations
> ACS extends blanket permission to students to include in their theses and dissertations their own articles, or portions thereof, that have been published in ACS journals or submitted to ACS journals for publication, provided that the ACS copyright credit line is noted on the appropriate page(s).
>
> Publishing implications of electronic publication of theses and dissertation material
> Students and their mentors should be aware that posting of theses and dissertation material on the Web prior to submission of material from that thesis or dissertation to an ACS journal may affect publication in that journal. Whether Web posting is considered prior publication may be evaluated on a case-by-case basis by the journal's editor. If an ACS journal editor considers Web posting to be "prior publication", the paper will not be accepted for publication in that journal. If you intend to submit your unpublished paper to ACS for publication, check with the appropriate editor prior to posting your manuscript electronically.

If your paper has **not** yet been published by ACS, we have no objection to your including the text or portions of the text in your thesis/dissertation in **print and microfilm formats**; please note, however, that electronic distribution or Web posting of the unpublished paper as part of your thesis in electronic formats might jeopardize publication of your paper by ACS. Please print the following credit line on the first page of your article: "Reproduced (or 'Reproduced in part') with permission from [JOURNAL NAME], in press (or 'submitted for publication'). Unpublished work copyright [CURRENT YEAR] American Chemical Society." Include appropriate information.

If your paper has already been published by ACS and you want to include the text or portions of the text in your thesis/dissertation in **print or microfilm formats**, please print the ACS copyright credit line on the first page of your article: "Reproduced (or 'Reproduced in part') with permission from [FULL REFERENCE CITATION.] Copyright [YEAR] American Chemical Society." Include appropriate information.

Submission to a Dissertation Distributor: If you plan to submit your thesis to UMI or to another dissertation distributor, you should not include the unpublished ACS paper in your thesis if the thesis will be disseminated electronically, until ACS has published your paper. After publication of the paper by ACS, you may release the entire thesis (**not the individual ACS article by itself**) for electronic dissemination through the distributor; ACS's copyright credit line should be printed on the first page of the ACS paper.

Use on an Intranet: The inclusion of your ACS unpublished or published manuscript is permitted in your thesis in print and microfilm formats. If ACS has published your paper you may include the manuscript in your thesis on an intranet that is not publicly available. Your ACS article cannot be posted electronically on a publicly available medium (i.e. one that is not password protected), such as but not limited to, electronic archives, Internet, library server, etc. The only material from your paper that can be posted on a public electronic medium is the article abstract, figures, and tables, and you may link to the article's DOI or post the article's author-directed URL link provided by ACS. This paragraph does not pertain to the dissertation distributor paragraph above.

Questions? Call +1 202/872-4368/4367. Send e-mail to copyright@acs.org or fax to +1 202-776-8112. 10/10/03, 01/15/04, 06/07/06

From: kangjj@uwindsor ca
Subject: Re REQUEST FOR PERMISSION TO USE COPYRIGHTED MATERIAL
Date: Mon, 11 Aug 2008 13 57 17 -0400
To: rao7@webmail1 uwindsor ca

Dear Dr. Yuxiang Rao,

I am writing to response to your request for permission to reprint in your dissertation from the following: Angewandte Chemie International Edition 2008, 47, 4896-4899.

The copyright might already be transfered to Angewandte Chemie International Edition when it was accepted. However, if I still have the mentioned copyright, I am very pleased to give you the permission to use it, covering future revisions and editions of your dissertation and the prospective archiving and publication of your dissertation by the University of Windsor library and Library and Archives Canada through UMI.

Please make sure if you have to get permission from Angewandte Chemie International Edition before using materials in it.

Sincerely,

Junjie Kang
Department of Chemistry & Biochemistry
University of Windsor

-----"Rao Y" <rao7@uwindsor.ca> wrote: -----

To: kangjj@uwindsor.ca
From: "Rao Y" <rao7@uwindsor.ca>
Date: 08/10/2008 04:33PM
Subject: REQUEST FOR PERMISSION TO USE COPYRIGHTED MATERIAL

<!--[if !supportEmptyParas]-->

Dear Dr. Junjie Kang:

I am completing a doctoral dissertation at the University of Windsor entitled "Mesoporous Nb and Ta Oxides: Synthesis, Characterization and Applications in Heterogeneous Catalysis " I would like your permission to reprint in my dissertation from the following:

Angewandte. Chemie. International. Edition. 2008, 47, 4896-4899

The requested permission covers future revisions and editions of my dissertation and the prospective archiving and publication of my dissertation by the University of Windsor library and Library and Archives Canada through UMI. Your agreement will verify that you owns the copyright to the above material(s). Please supply a statement granting me permission to use the work.

<!--[if !supportEmptyParas]-->

Thank you very much for your attention to this matter.

Sincerely,

Yuxiang Rao

Ph.D. candidate,

Department of Chemistry and Biochemistry

University of Windsor

373-1 Essex Hall

401 Sunset Ave

Windsor, ON, Canada

N9B 3P4

Phone: 1(519)-253-3000 ext 1423

Fax: 1(519)-973-7098

E-mail: rao7@uwindsor.ca

From: "Skadtchenko Boris" <skadtch@uwindsor.ca>
Subject: Re: REQUEST FOR PERMISSION TO USE COPYRIGHTED MATERIAL
Date: Tue, 12 Aug 2008 10:03:34 -0400
To: "Rao Y" <rao7@uwindsor.ca>

Rao,

You can go ahead and re-print what you requested with appropriate referencing. Good luck with the defence.

Cheers,

Boris

On Sun, 10 Aug 2008 16:39:39 -0400 "Rao Y" wrote:
>
>
>
>
>
>
>
>
>
>
>
>
>
> Dear Dr. Boris O. Skadtchenko:
>
> I am completing a doctoral dissertation at the University of Windsor entitled "Mesoporous Nb
> and Ta Oxides: Synthesis, Characterization and Applications in Heterogeneous Catalysis " I
> would like your permission to reprint in my dissertation from the following:
> Angewandte Chemie International Edition, 2007, 46, 2635-2638
> The requested permission covers future revisions and editions of my dissertation and the
> prospective archiving and publication of my dissertation by the University of Windsor library
> and Library and Archives Canada through UMI. Your agreement will verify that you owns the
> copyright to the above material(s). Please supply a statement granting me permission to use
> the work.
>
> Thank you very much for your attention to this matter.
> Sincerely,
> Yuxiang Rao
> Ph.D. candidate,
> Department of Chemistry and Biochemistry
> University of Windsor
> 373-1 Essex Hall
> 401 Sunset Ave
> Windsor, ON, Canada
> N9B 3P4
> Phone: 1(519)-253-3000 ext 1423
> Fax: 1(519)-973-7098
> E-mail: rao7@uwindsor.ca
>
>
> Yuxiang(Tony) Rao, Ph.D candidate
> Department of Chemistry, University of Windsor
> 373-1 Essex Hall, 401 Sunset Ave
> Windsor,Ontario,Canada
> N9B 3P4
> Phone: (519)253-3000 ext 1423
>

From: VCH-RIGHTS-and-LICENCES <RIGHTS-and-LICENCES@wiley-vch.de>
Subject: Antwort WG REQUEST FOR PERMISSION TO USE COPYRIGHTED MATERIAL
Date: Tue, 19 Aug 2008 08 37 13 +0200
To: rao7@uwindsor ca

Dear Customer,

Thank you for your email.

We hereby grant permission for the requested use expected that due credit is given to the original source.

Please note that we only grant rights for a printed version, but not the rights for an electronic/ online/ web/ microfiche publication, but you are free to create a link to the article in question which is posted on our website (http://www3.interscience.wiley.com)

If material appears within our work with credit to another source, authorisation from that source must be obtained.

Credit must include the following components:
- Books: Author(s)/ Editor(s) Name(s): Title of the Book. Page(s) Publication year. Copyright Wiley-VCH Verlag GmbH & Co. KGaA. Reproduced with permission.

- Journals: Author(s) Name(s): Title of the Article. Name of the Journal. Publication year. Volume. Page(s) Copyright Wiley-VCH Verlag GmbH & Co. KGaA. Reproduced with permission.

With kind regards

Bettina Loycke
****
Bettina Loycke
Copyright & Licensing Manager
Wiley-VCH Verlag GmbH & Co. KGaA
Boschstr. 12
69469 Weinheim
Germany

Phone: +49 (0) 62 01- 606 - 280
Fax: +49 (0) 62 01 - 606 - 332
Email: rights@wiley-vch.de

----- Forwarded by Rachel Coffey/Canada/Wiley on 08/18/2008 01:19 PM -----

"Rao Y" <rao7@uwindsor.ca> 08/10/2008 04 10 PM

To: racoffey@wiley.com

cc:

Subject: REQUEST FOR PERMISSION TO USE COPYRIGHTED MATERIAL

To Whom It May Concern:

Dear Sir/Madam:

I am completing a doctoral dissertation at the University of Windsor entitled "Mesoporous Nb and Ta Oxides: Synthesis, Characterization and Applications in Heterogeneous Catalysis " I would like your permission to reprint in my dissertation excerpt(s) from the following:

Angewandte Chemie International Edition, 2007, 46, 2635-2638

Angewandte. Chemie. International. Edition. 2008, 47, 4896-4899

The requested permission covers future revisions and editions of my dissertation and the prospective archiving and publication of my dissertation by the University of Windsor library and Library and Archives Canada through UMI. Your agreement will verify that your company owns the copyright to the above material(s) Please supply a statement granting me permission to use the work.

Thank you very much for your attention to this matter.

Sincerely,

Yuxiang Rao

Ph.D. candidate,

Department of Chemistry and Biochemistry
University of Windsor
373-1 Essex Hall
401 Sunset Ave
Windsor, ON, Canada
N9B 3P4
Phone: 1(519)-253-3000 ext 1423
Fax: 1(519)-973-7098
E-mail: rao7@uwindsor.ca

Yuxiang(Tony) Rao, Ph.D candidate
Department of Chemistry, University of Windsor
373-1 Essex Hall, 401 Sunset Ave
Windsor,Ontario,Canada
N9B 3P4
Phone: (519)253-3000 ext 1423

VITA AUCTORIS

Name: Yuxiang(Tony) Rao

Place of Birth: Jiangxi, China

Year of Birth: 1981

Education: Tianjin University, China

1997-2001 B. Sc.

Tianjin University, China

2001-2004 M. Eng

University of Windsor, Canada

2004-2008 Ph.D.

LIST OF PUBLICATIONS

(1) **Y Rao,** J. Kang, D.M. Antonelli,"Investigation of synthesis and characterization of mesoporous Nb and Ta oxide and application in 1-Hexene isomerization", submitted to *Journal of Materials Chemistry*, **2008**

(2) **Y. Rao,** T.F. Kemp, M. Trudeau, M.E. Smith, D.M. Antonelli, "^{17}O and ^{15}N Solid State NMR Studies on Ligand-Assisted Templating and Oxygen Coordination in the Walls of Mesoporous Nb, Ta and Ti Oxides", accepted by *Journal of American Chemistry Society*, **2008**

(3) **Y. Rao,** D.M. Antonelli, "Mesoporous transition metal oxides: characterization and applications in heterogeneous catalysis", submitted to *Journal of Materials Chemistry*, **2008**

(4) J. Kang, **Y Rao,** D.M. Antonelli, "Sulfated Mesoporous Ta Oxides in the Shape Selective Synthesis of Linear Alkyl Benzene", *Angewandte Chemie International Edition* **2008**, *47*:1-5

(5) **Y. Rao,** J. Kang, D.M. Antonelli, "1-Hexene Isomerization Over Sulfated Mesoporous Ta Oxide: The effects of activie site and confinement", *Journal of the American Chemical Society* **2008**, *130* (2): 394-395

(6) B.O. Skadtchenko, **Y Rao,** T.F Kemp, P Bhattacharya, P.A. Thomas, M. Trudeau, M.E. Smith, D.M. Antonelli, "A Solid-State ^{17}O NMR Study of Local Order and

Crystallinity in Amine-Templated Mesoporous Nb Oxide", *Angewandte Chemie International Edition.* **2007**, *46*:2635-2638

(7) **Y. Rao,** M. Trudeau, D.M. Antonelli, "Sulfated and Phosphated Mesoporous Nb Oxide in the Benzylation of Anisole and Toluene by Benzyl Alcohol" *Journal of the American Chemical Society* **2006**, *128* (43): 13996-13997

PROFESSIONAL ACTIVITIES

(1) **Y. Rao**, J. Kang, D.M. Antonelli, "1-Hexene Isomerization over Sulfated Mesoporous Nb and Ta Oxides: The effects of active site and confinement", 20th Canadian Symposium on Catalysis, Kingston, ON, Canada, June 15~18, 2008 (national conference, poster presentations)

(2) **Y. Rao**, J. Kang, D.M. Antonelli, "1-Hexene Isomerization over Sulfated Mesoporous Nb and Ta Oxides: The effects of active site and confinement", 234th American Chemical Society National Meeting & Exposition, Boston, MI, USA, August 19~23, 2007 (national conference, oral presentations)

(3) **Y. Rao**, D.M. Antonelli, "Sulfated and Phosphated Mesoporous Nb Oxide in the Benzylation of Anisole and Toluene by Benzyl Alcohol", 9th Annual Chemistry and Biochemistry Graduate Research Conference (CBGRC), Montreal, Canada, November 24~25, 2006(national conference, poster presentation)

(4) **Y. Rao**, D.M. Antonelli, "Acidic Properties and Catalytic Activities of Mesoporous Niobium Oxides by the Benzylation of Anisole and Toluene with Benzyl Alcohol", 89th Canadian Chemistry Conference and Exhibition, Halifax, NS, Canada, May 27~31. 2006, (national conference, oral presentation)